

NASA Technical Memorandum 81221

Experimental Unsteady Aerodynamics of Conventional and Supercritical Airfoils

Sanford S. Davis and Gerald N. Malcolm

(NASA-TM-81221) EXPERIMENTAL UNSTEADY
AERODYNAMICS OF CONVENTIONAL AND
SUPERCritical AIRFOILS (NASA) 100 P
HC A04/MF A01

N80-33345

CSCCL 01A

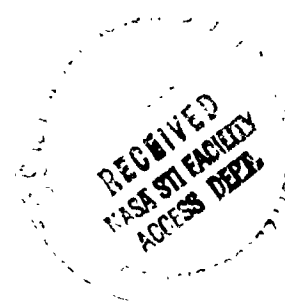
Unclass

G3/02 28772

August 1980



National Aeronautics and
Space Administration



Experimental Unsteady Aerodynamics of Conventional and Supercritical Airfoils

Sanford S. Davis and Gerald N. Malcolm
Ames Research Center, NASA, Moffett Field, California



National Aeronautics and
Space Administration

Ames Research Center
Moffett Field, California 94035

TABLE OF CONTENTS

	<u>Page</u>
NOMENCLATURE	v
SUMMARY	1
1. INTRODUCTION	1
2. TEST HARDWARE	2
11- by 11-Foot Transonic Wind Tunnel	3
Splitter Plates	3
Wings and Push-Pull Rods	4
Motion Generators	6
Pretest Verification of System Components	7
3. DATA ACQUISITION SYSTEM	7
Dynamic Data Acquisition	8
Static Data Acquisition	9
4. TEST PROGRAM	9
5. DATA REDUCTION AND PRESENTATION	10
Static-Pressure Coefficients	10
Integrated Static Pressures	11
Dynamic Pressure Complex Amplitudes	11
Integrated Dynamic Pressures	12
6. SUMMARY OF RESULTS	12
APPENDIX A: METHODS FOR INTEGRATING EXPERIMENTAL PRESSURE DISTRIBUTIONS	14
APPENDIX B	16
REFERENCES	17
TABLES	19
FIGURES	44

PRECEDING PAGE BLANK FOR REASON

NOMENCLATURE

A	complex amplitude of the unsteady airfoil motion: for pitching, A = oscillatory angle of attack in radians; for plunging, A = displacement normalized by half-chord. The physical motion is $\text{Re}(Ae^{i\omega t})$
ALPHA	mean angle of attack, deg
C	chord of airfoil, m
CL	mean lift coefficient, + up
CL,A	normalized unsteady lift coefficient, + up
CM	mean moment coefficient at leading edge, + nose up
CM,A	normalized unsteady moment coefficient at leading edge, + nose up
CPU,A(CPL,A)	complex amplitude of the unsteady upper (lower) surface
CPU(CPL)	mean value of upper (lower) surface pressure coefficient, $\frac{PU(PL) - P_{INF}}{Q_{INF}}$
$\exp(i\omega t)$	$\cos \omega t + i \sin \omega t$
f, FREQ	frequency, Hz, $\frac{1}{T}$
IU,A(Q) (IL,A(Q))	Qth moment of the complex amplitude of the unsteady upper (lower) surface pressure coefficient
IU(Q) (IL(Q))	Qth moment of the mean value of upper (lower) surface pressure coefficient
k,K	reduced frequency, $\frac{\omega C}{2U}$
M_{∞}	free-stream Mach number
P	complex amplitude of the unsteady pressure; the physical pressure = $\text{Re}(Pe^{i\omega t})$
PINF	free-stream static pressure, N/m^2
PL,PU	mean value of surface pressure, N/m^2
PTOT	total pressure, N/m^2
QINF	dynamic pressure, N/m^2

PRECEDING PAGE UNRECORDED

Re, RE	chord Reynolds number
T	period of the motion, sec
t	time, sec
U	free-stream velocity, m/sec
X, x	distance along airfoil, m
α	complex amplitude of unsteady angle of attack, deg
α_m	mean angle of attack, deg
$\alpha(t)$	instantaneous angle of attack, deg

Complex notation:

Im[]	imaginary part of []
Mag[]	magnitude of []
Ph[]	phase of [], deg
Re[]	real part of []

EXPERIMENTAL UNSTEADY AERODYNAMICS OF CONVENTIONAL
AND SUPERCRITICAL AIRFOILS

Sanford S. Davis and Gerald N. Malcolm

Ames Research Center

SUMMARY

Experimental data on the unsteady aerodynamics of oscillating airfoils in transonic flow are presented. Two 0.5-m-chord airfoil models — an NACA 64A010 and an NLR 7301 — were tested in the NASA-Ames 11- by 11-Foot Transonic Wind Tunnel at Mach numbers to 0.85, at chord Reynolds numbers to 12×10^6 , and at mean angles of attack to 4° . The airfoils were subjected to both pitching and plunging motions at reduced frequencies to 0.3 (physical frequencies to 53 Hz).

The new hardware and the extensive use of computer-experiment integration developed for this test are described. The geometrical configuration of the model and the test arrangement are described in detail. Mean and first harmonic data are presented in both tabular and graphical form to aid in comparisons with other data and with numerical computations.

1. INTRODUCTION

The unsteady aerodynamics of both fixed- and rotary-wing airfoil sections must be thoroughly understood in order to provide safe margins for flutter, buffett, and other undesirable aerodynamic phenomena. This need is most apparent in the critical transonic speed regime where these detrimental effects are most prevalent. Recent developments in numerical simulations of transonic unsteady aerodynamics have also highlighted the need for new experimental activity in this area. In response to these needs, an extensive test program was developed at Ames Research Center to measure the unsteady aerodynamics of both a conventional and a supercritical airfoil under a wide range of flow conditions. The objective of the test was to measure unsteady pressure distributions at higher Reynolds numbers over a more extensive range of test conditions than had heretofore been attempted. This report presents, in graphical and tabular form, the mean and fundamental frequency data from that test.

The data were obtained in the 11- by 11-Foot Transonic Wind Tunnel at Ames Research Center. Over 200 data sets, representing various combinations of airfoil geometry, Mach number, Reynolds number, mean angle of attack, motion mode, motion amplitude, and frequency are reported. For each data set both the mean and first harmonic loads are tabulated, and the pressure distributions are presented in both tabular and graphical form.

Section 2 describes the important features of the test apparatus in detail, including the wind tunnel, model installation, motion generators, model construction, and model geometry. (Some of the hardware was also described in ref. 1.) A discussion of the computerized data system, developed especially for this test, is provided in section 3. The software was written such that on-line comparisons could be made between the current data set and theoretical predictions. The measuring system is also described in references 1 and 2. Section 4 outlines the test program and section 5 presents the data. The method used to integrate the chordwise pressure distribution is described in appendix A, and the tabulated first harmonic pressure data, enclosed in microfiche form, is designated appendix B.

Some of the data have already been analyzed and can be found in references 3-6. A small subset of the data has been selected by AGARD for inclusion in its "Standards for Aeroelastic Application"; it is cited in section 4.

2. TEST HARDWARE

The arrangement of the apparatus and the special two-dimensional flow channel installed in the 11- by 11-Foot Transonic Wind Tunnel were based on the choice of an acceptable ratio of wind-tunnel height to wing chord (greater than 6). A chord of 0.5 m was chosen, resulting in the ratio (height)/(chord) = 6.8. Lowest hardware cost and minimum overall tunnel blockage could be obtained with a model spanning the tunnel, but construction of a full-span 0.5-m-chord model was impractical because first priority was assigned to obtaining high frequencies with minimal aeroelastic effects. An acceptable span-to-chord ratio of approximately 3 (1.35-m span) dictated the use of the splitter-plate arrangement shown in figure 1. Although previous investigators have successfully used splitter plates, a pilot test of the concept was nonetheless conducted in the Ames 2- by 2-Foot Transonic Wind Tunnel (ref. 7). This test demonstrated that good quality transonic flow could be obtained with the chosen splitter plate arrangement.

Figure 1 shows the general arrangement of the wing/splitter-plate/actuator system as installed in the wind-tunnel test section. The normal 3.35 m x 3.35 m test section was segmented with two steel splitter plates, 3.35 m high by 2.8 m long. To minimize blockage, the thickness was the minimum necessary to accommodate the push-pull drive rods. To prevent excessive deflections of the splitter plates, side struts were installed for lateral support. The splitters extended into the tunnel's plenum area at the top and bottom; there they were bolted to I-beam anchors. Access panels for instrumentation cables and clearance for the push-pull rods were included in the splitter plate design.

The wing model was instrumented near its midspan station and attached to independently controlled hydraulic actuators through the push-pull rods. Thus, the wing was free to pitch and plunge in response to the actuator's command signal. The wing was restrained in the fore-aft direction by a pair

of carbon-epoxy drag rods, and in the lateral, roll, and yaw directions by sliding cover plates, which moved with the wing on the inner surface of the splitter plates. The hydraulic actuators, located in the lower plenum area, were supported by flexures; they bore directly into a massive concrete foundation through the four support columns. With this design, the tunnel pressure shell does not have to support the oscillatory reaction loads induced by the actuator's motion.

The capabilities of the test apparatus include sinusoidal pitching oscillations over a frequency range of 0 to 60 Hz, with the maximum oscillation varying from $\pm 2^\circ$ at low frequencies to $\pm 0.8^\circ$ at 60 Hz about any chord-wise axis, and a vertical plunging motion up to ± 5 cm (2 in.).

The various components that make up the system will be described in more detail since the basic performance requirements dictated state-of-the-art designs in many cases. Many of the components are shown in the installation photograph in figure 2 and the pre-test setup in figure 3. In the following description it may be helpful to refer to these photographs to visualize the interrelationship among the various components.

11- by 11-Foot Transonic Wind Tunnel

The 11- by 11-Foot Transonic Wind Tunnel is a closed-return, variable density facility with a $3.35 \times 3.35 \times 6.7$ m ($11 \times 11 \times 22$ ft) test section enclosed in a 6-m (20-ft) diameter cylindrical pressure cell. The air is driven by a three-stage, axial-flow compressor powered by four induction motors with a maximum continuous combined output of 135 MW (180,000 hp). The Mach number can be varied continuously from 0.4 to 1.4 with the stagnation pressure variable from 50 kN/m^2 to 225 kN/m^2 (0.5 to 2.25 atm) resulting in Reynolds numbers from $6 \times 10^6/\text{m}$ to $31 \times 10^6/\text{m}$. Maximum Mach and Reynolds numbers for this test were 0.85 and $25 \times 10^6/\text{m}$, respectively.

The ventilated wall of the 11-Foot Transonic Wind Tunnel has a baffled slot arrangement (fig. 4). Six slots — 1.78 cm (0.7 in.) wide — between the splitter plates yield an effective open area ratio of approximately 8%. A resistive baffle fabricated from 0.16 cm (1/16 in.) sheet stock was inserted in each slot. The baffle is flush with the floor and ceiling, extends 5.72 cm (2.25 in.) into the slot, and has a "wavelength" of 3.43 cm (1.35 in.).

Splitter Plates

Vertical splitter plates with trailing-edge flaps and horizontal side struts form the support structure for the wing. They each have a sharp leading edge and a movable trailing-edge flap which is manually adjustable between $\pm 2^\circ$ from the plane of the splitter plate. All testing was done with the flaps set at 0° . Horizontal side struts attach to the outside of the splitter plates just below the horizontal plane of symmetry and protrude through the test section into the exterior structure. They provide stabilization and eliminate excessive lateral deflection from the aerodynamic loads. The

splitter plates were installed with a 0.1° divergence angle from tunnel centerline to account for boundary-layer growth. The thickness of the splitter plates varies in the streamwise direction in the following manner: following the sharp leading edge the next immediate section is 3.2 cm (1.25 in.) thick; it is followed by a 5-cm (2-in.) thick section in the center to accommodate the push-pull rods. The trailing-edge section is 4.4 cm (1.75 in.) thick and tapers to a sharp trailing edge. The inside surface of the splitter plate is straight with all thickness variations taking place on the outer surface.

Openings in the splitter plate (figs. 5, 6) permit the wing to be attached to the top of the push-pull rods, which are centered in four channels cut into the lower portion of the splitter plates. When the wing is oscillating, sliding covers (figs. 7, 8) attached to the wing seal the openings. The covers are made of graphite epoxy to reduce weight and are Teflon-lined for free sliding.

The splitter plates contain a total of 125 static-pressure orifices distributed over the inside and outside surfaces of both plates. The inside orifices were utilized to select the proper channel Mach number and, in conjunction with the outer taps, were used to monitor the loading on the splitter plates. While testing, accelerometers on the trailing-edge flaps were used to sense any large or potentially destructive flutter motions such as might be produced from the oscillating flow behind the wing or naturally induced from the channel air flow.

Wings and Push-Pull Rods

Model geometry- Two airfoil sections were chosen for this test program -- one a conventional airfoil (an NACA 64A010) and the other a supercritical airfoil (the NLR 7301). The two wing models -- span 1.35 m (53.2 in.), chord 0.5 m (19.685 in.) -- were designed to withstand accelerations of 2.3×10^3 m/sec² (230 g) and aerodynamic loads of 44,000 N (10,000 lb). Both airfoils were subsequently chosen for inclusion in the AGARD standard series of test cases for aeroelastic applications (refs. 8, 9). Photographs of the models installed in the wind tunnel are presented in figures 7 and 8. Due to expansion of the molds in fabricating the models, the actual airfoil sections were slightly thicker than their theoretical counterparts. To expedite numerical simulations, three sets of ordinates are presented -- the measured ordinates, smoothed versions of the measured ordinates from Olsen's computations (ref. 8), and the theoretical ordinates. Because the measured ordinates contain large variations in the higher derivatives that adversely affected some trial solutions, it is recommended that either the smoothed or theoretical ordinates be used for computing. Computations using the theoretical ordinates were satisfactory for the flow conditions attempted.

The measured and theoretical airfoil sections are shown in figure 9. In each case the measurements correspond to the thicker section. Data for the NACA 64A010 and NLR 7301 airfoils are presented in tables 1 and 2, respectively.

Model instrumentation- The wing is instrumented with static pressure taps and dynamic pressure transducers, all of which are located at approximately midspan. The dynamic pressure transducers communicate to the wing surface via a small orifice with a small volume cavity. Locations of the static and dynamic orifices in both wings are shown in tables 3 and 4. It should be noted that dynamic transducers were not installed in the lower surface of the NLR 7301 airfoil. The lower surface unsteady pressures were sacrificed on that airfoil for the sake of increased resolution on the upper surface. Static pressure tubes are routed from the end of the wing through a cavity in the splitter plate to the tunnel plenum chamber below, and out an access port to scanivalve-transducer units exterior to the tunnel shell. Dynamic transducers are mounted in the wing by inserting the transducer (2.36 mm diameter) in the end of a long plastic sleeve, which is, in turn, inserted into a cylindrical channel molded into the interior of the wing. The sleeve terminates at the center of the wing at the orifice communicating to the wing surface. The lead wires are then routed out the opposite end of the sleeve in the wing (fig. 6) through the splitter plates and out through the tunnel walls to the data acquisition equipment in the tunnel control room. A single reference pressure tube from each dynamic transducer is also inserted into the plastic sleeve and routed through the splitter plate to the scanivalve-transducer assembly outside the tunnel. The transducer reference pressure can be selected to be the static pressure of the adjacent static orifice on the wing or any other selected pressure (such as the tunnel static pressure). Six accelerometers were mounted inside the wing, one at each of the attachment points of the four push-pull rods near the corners of the wing and two at midspan near the leading and trailing edges. The actual motion of the wing can be determined from the accelerometer output and compared with the output of the motion transducers located in the actuator piston rods. These data showed that the wing motions were faithfully recorded by the motion transducers.

Model support system- The wing model, mounted between the splitter plates, is connected to the push-pull rods through special flexure bearings. The push-pull rods are, in turn, screwed directly into the actuator pistons. Both the wing and the push-pull rods are fabricated from a lightweight graphite-epoxy material. A short discussion of the fabrication of the rods and wings is given later in this section. The push-pull rods, 0.0412 m (1.625 in.) in diameter, are each capable of a 22,000 N (5,000 lb) tension load. The flexures located between the push-pull rods and the wing are also designed for a 22,000 N (5,000 lb) load. A pair of graphite-epoxy rods mounted to the wing with a flexure support and attached to the splitter plates forward of the wing provide a means of counteracting the drag loads (see fig. 5); each rod can withstand 6,700 N (1,500 lb).

Model fabrication- The fabrication of both the wing models and the push-pull rods required an extensive development effort by the Ames Model Development Branch. The requirements for maximum strength, stiffness, and light weight suggested the use of composite fiber materials. The problem of constructing the wing was compounded by the requirement for internal mounting of the pressure transducers. The following description will illustrate briefly the steps used to fabricate the wing models.

The outside contour of the wing was defined by using a steel female mold split into two halves and machined to the coordinates of the airfoil section. The mold was made of common steel with a coefficient of thermal expansion compatible with that of the carbon graphite composite fibers. Using this mold, a fiberglass mold was made to construct the four interior silicone mandrels about which the carbon graphite fibers were wrapped to form the internal structure. These mandrels were later removed from the wing after curing, leaving hollow sections between the webs (see fig. 6). The core mandrels were pregrooved for instrumentation tubes before wrapping with the appropriate number of layers of fiber strips. Tapered steel rods were inserted in the pre-cut grooves. The ribs between the four cores joining the upper and lower surfaces together were individually laminated and placed between the wrapped cores. A fixture was built to hold the four cores in place for wrapping of the entire model. Thirty-two plies of unidirectional graphite tape were wrapped around the pre-wrapped cores with plies at 0°, 45°, and 90° with respect to the chord. The model layup was then sandwiched between the two halves of the steel mold and caps were bolted on the ends. The entire assembly was heated in an autoclave to 250° F to expand the silicone core. This cycle forced the layup tightly against the interior walls of the mold. The model was subjected to a cure cycle of 350° F for 2 hr. After cooling, the model was removed from the mold and the cores removed. The tapered steel rods were also removed and a 0.5-mm hole drilled through the surface of the model to intersect the cavity left by the rods. The dynamic transducers were mounted in the end of a long plastic tube, which was inserted into the hollow cavity in the wing. The transducer body sealed against a shoulder in the tube forming a pneumatic seal. The volume between the transducer diaphragm and the orifice on the model surface was quite small, thus providing good high-frequency response.

The push-pull rods were constructed of carbon-graphite fibers, using similar procedures. A two-part mold was made from mild steel with outside dimensions of 10.16 cm (4 in.) square by 203 cm (80 in.) long and a 4.13-cm (1.625-in.) bore. A silicone core approximately 2.5 cm (1 in.) in diameter was made, and graphite fibers were carefully wrapped around it to a wall thickness of approximately 0.63 cm (0.25 in.). After curing and removing the core, the ends of the rods were attached to steel end caps which provided an attachment point for the actuator system and flexures.

Motion Generators

The servo-hydraulic actuator system was designed especially for this test. It is driven by two 11-kW (150-hp) hydraulic pump units rated at 4.1×10^{-3} m³/sec (65 gal/min) at 20.7×10^6 N/m² (3,000 lb/in.²). Each of the four actuators consists of two separate pistons on a single rod enclosed in a dual-chamber cylinder. The upper piston is used for generating dynamic forces, the lower piston for load biasing. The load bias system is necessary to support the mean aerodynamic lift load, thereby reducing the power required to drive the dynamic piston. As static bias requirements change, the servo-valve system responds to produce the required force output to maintain the set position. Velocity and position transducers are combined into a single

physical unit with coils and cores aligned axially for mounting in the center of the actuator.

Pretest Verification of System Components

Because every part of this system was new, there was no test information available for judging performance and reliability of the apparatus. Therefore, a special pretest facility was built to permit a detailed checkout program. Many of the components, including the wing, push-pull rods, drag restraints, and the hydraulic actuator motion generator system, were new designs and could not be risked in the wind tunnel without pretest experiments. A special test stand was built for system verification. Figure 3 is a photograph of the assembly in the test area. A support structure was constructed to which the various components were attached. The hydraulic actuators were mounted at the base with the push-pull rods attached to the top of the pistons. The wing was mounted on the push-pull rods with flexures and angle-of-attack blocks between the rod end and the wing end cap. The drag restraint was fastened on top of the rear flexures and the other end tied to the support frame. Lift loads were simulated by an inflatable bag between the lower surface of the wing and a support cradle fastened to the support stand. Drag loads were simulated by a pneumatically activated piston coupled to cables and straps looped over the wing. A nearly complete envelope of test conditions could be evaluated on the test stand. In the early stages of the test checkout a wing constructed of fiberglass (shown in fig. 3) was used before risking the graphite-epoxy test wing. This proved to be an extremely valuable and low-risk method of evaluating the performance of the entire system. The only real limitations were that the fiberglass wing was not stiff enough to prevent large deflections at midspan (particularly in plunging) at frequencies above 30 Hz, and was not strong enough to accept the maximum lift loads. A limited amount of testing was done with the carbon-epoxy wing before installation in the wind tunnel.

3. DATA ACQUISITION SYSTEM

In the past, multichannel unsteady aerodynamic data were acquired using analog tape recorders where raw data were recorded and stored for future analysis. On-line analysis was restricted to a few selected channels, using special instrumentation to extract usable data from the great mass of incoming data. These systems suffered from long time lags between acquisition and analysis and the probability of unknowingly recording spurious data. In the present test a new computational data acquisition and analysis system was developed for on-line display of steady and unsteady aerodynamic data. Figure 10 depicts the main elements of the new system. It can graphically display the first-harmonic pressure distribution (both magnitude and phase) due to arbitrary pitch-plunge motions of the airfoil along with the conventional static pressure distribution. At the user's option, an overlay of selected theoretical or experimental pressure distributions from computer-resident codes or from a dedicated data bank can be accessed.

The system comprises a Data General Eclipse Model S/200 minicomputer, a high-speed (500 kHz) multichannel analog-to-digital converter, a large capacity (92 Mbyte) storage device, and a graphics terminal. The software system consists of approximately 50 independent Fortran-coded programs. The independent programs are controlled by two executive programs: one for dynamic data, the other for static data.

Dynamic Data Acquisition

The raw data come from a variety of sensors, the two most important being the airfoil motion (the input) and the surface pressures on the model (the output). The same sinusoidal signal that drives the four-channel hydraulic actuator system, which in turn drives the four push-pull rods attached to the wing, is also used to trigger a pulse to initiate the unsteady data acquisition process. Once the actuator control system is adjusted to impart the desired motion to the wing, the motion of the four push-pull rods is continuously monitored and acquired along with the unsteady data.

The dynamic signals from up to 41 miniature pressure transducers are amplified and filtered before they enter the analog-to-digital converter. Because the signal is periodic, it is possible to obtain good waveform samples with minimum storage per data point by signal-averaging the data. Theoretically, a periodic signal is completely defined by just one cycle of data (e.g., a 40-msec record is all that is necessary to characterize a 25-Hz periodic oscillation). However, the experimental signal is usually so contaminated by random pressure fluctuations due to wind-tunnel and model-induced turbulence that one cycle of data is not very useful.

The signal-averaging technique is implemented as follows: the raw data are synchronized with a pulse train which is triggered at the same phase position for each cycle of the airfoil's motion. These timing relations are shown in figure 11. At time t_0 , the sample waveform is recorded for τ seconds. At time $t_0 + nT$ the waveform is recorded again for τ seconds. The process is repeated M times. These M samples, each being initiated by the phase-locked pulse, are then ensemble-averaged to obtain the averaged signal. In the current experiment τ is chosen to be slightly greater than one period, $n = 2$, and $M = 100$ is sufficient for a good average. At the user's option, the signal-averaged waveform and its M th realization for any selected channel can be displayed on the graphics terminal.

For on-line analysis, the first harmonic of the response is most useful. A simple Fourier analysis algorithm is implemented to extract the magnitude and phase information at the fundamental frequency. These data are displayed in tabular form on the graphics unit within 30 sec of the termination of data acquisition. These data are usually sufficient to determine if the unsteady data acquisition process was successful. If more on-line analysis is required, the first-harmonic data may be displayed graphically in pressure coefficient form. The magnitude and phase of the chordwise pressure distributions on the upper and lower surfaces of the airfoil are displayed along with certain theoretical curves, such as (1) linear, incompressible small-disturbance theory

(Theodorsen function) and (2) linear, compressible small-disturbance theory (Possio integral equation solver). For time-efficient on-line analysis it does not seem feasible to include unsteady transonic codes on the current generation of minicomputers.

Also available for comparison are the results of other investigations (theoretical or experimental) which have been stored in the data bank. For comparing with NACA 64A010 data, the theoretical investigations of Magnus (ref. 10) are available. For the NLR 7301 wing, experimental data obtained at NLR-Amsterdam (ref. 11) are available. It is possible to obtain a comparison between the current data and the selected theoretical-experimental overlay in approximately 45 sec after the termination of data acquisition.

Static Data Acquisition

The static pressures are sensed with a conventional system using pneumatic tubing connected to a pressure scanning valve. The electrical output of the pressure cell to which the unknown pressures are multiplexed are read with a digital voltmeter whose BCD (Binary Coded Decimal) output feeds directly into the minicomputer.

The splitter-plate arrangement used for the oscillatory airfoil test requires special attention with regard to the free-stream Mach number (M_∞). As discussed in previous reports (refs. 2, 7) the Mach number in the channel between the plates is not the same as that computed from a static pressure tap in the plenum chamber. To obtain the approach Mach number (M_∞), the splitter plates are equipped with 125 static pressure orifices distributed among 10 rows above and below the plane of the wing on the inner and outer walls of the splitter plates. These pressures are also sensed by the scanning system. The computed Mach numbers on the splitters are displayed on the graphics unit and the approach Mach number is selected interactively by fairing the graphics unit's horizontal cursor to the data. Using this procedure, the Mach number can be selected to an accuracy of ± 0.002 .

Once the Mach number has been chosen, the static-pressure distribution on the wing is displayed along with selected overlays. A static pressure distribution with overlays can be displayed in approximately 30 sec after the raw data have been acquired.

4. TEST PROGRAM

As mentioned in the introduction, the test program was designed to meet the following primary goals: (1) to expand the existing unsteady test envelope to higher Reynolds numbers, higher reduced frequencies, different modes, and more diverse mean flow conditions; (2) to overlap the existing data base wherever possible; and (3) to provide a data base for the computation of unsteady transonic flows. A wide range of static and dynamic parameters was investigated in meeting these goals. The selected parameters are listed in

table 5. All of the data presented here were measured without a boundary-layer trip. Of the thousands of possible combinations, a subset of approximately 200 comprises the current test matrix. Each selected combination is identified by a unique dynamic index (DI). A complete list of the test program in ascending numerical order is presented in table 6. The data in sets of "frequency sweeps" according to airfoil type and motion are given in table 7 for the NACA 64A010 airfoil and in table 8 for the NLR 7301 airfoil.

In reference 9 a series of airfoils was designated as AGARD standards for validating computational methods. The two airfoil sections used in this experiment are included in the standard series. Certain preferred flow conditions were chosen for comparative purposes. Ten cases for the NACA 64A010 are presented in table 8 of reference 9. The corresponding dynamic indices are listed below:

Test Case	1	2	3	4	5	6	7	8	9	10
DI	7	29	51	52	53	55	57	49	65	12

Table 12 of reference 9 gives 14 test cases for the NLR 7301. These test cases were selected from the data reported in reference 11 and do not correspond exactly with the current series. In particular, mean flow conditions at the supercritical design point were slightly different. In table 8 of this report, the NLR 7301 frequency sweeps designated by rows 1-8 are the experimentally determined shock-free design conditions for this airfoil in the Ames 11-Foot Wind Tunnel. They should be used for assessing computational methods.

5. DATA REDUCTION AND PRESENTATION

The primary output data are the pressure distributions on the airfoil along with quantities derivable from them. The data reduction and scaling applied to the raw data are described in this section. The data include static pressure coefficients, integrated static loads, complex amplitudes of the first harmonic pressure coefficients, and integrated first harmonic loads.

Static-Pressure Coefficients

The static pressure data were converted to coefficient form using the conventional scaling:

$$\left. \begin{aligned} CPU &= (PU - P_{INF})/Q_{INF} \\ CPU &= (PL - P_{INF})/Q_{INF} \end{aligned} \right\} \quad (1)$$

where PU and PL are the measured mean pressures (in newtons per square meter) on the airfoil, and both P_{INF} and Q_{INF} are flow parameters. (All symbols are defined in the nomenclature list.) The static-pressure data are presented in tabular and graphical form along with the dynamic data to be discussed subsequently.

Integrated Static Pressures

The chordwise static pressure data were integrated according to the following formulas:

$$IU(Q) = \int_0^1 [CPU(X/C)] [(X/C)^Q] d(X/C) \tag{2a}$$

$$IL(Q) = \int_0^1 [CPL(X/C)] [(X/C)^Q] d(X/C)$$

$$CL = IL(0) - IU(0) \tag{2b}$$

$$CM = -[IL(1) - IU(1)]$$

The I-integrals are the Qth moments of the static-pressure distributions. Note that the moment coefficient is defined at the leading edge, nose-up positive. Some difficulties were encountered with the usual trapezoidal-type numerical integration scheme. The integration method that was ultimately adopted is described in detail in appendix A.

Each static pressure run is associated with a unique identification — the static index (SI). Table 9 associates a static index with each dynamic index. Table 10 presents the integrated upper surface, lower surface, and total load on the airfoil for each static index.

Dynamic Pressure Complex Amplitudes

The dynamic pressure data needed some preliminary processing. The first step was to Fourier-analyze the time-history data up to its fundamental frequency component. The fundamental frequency component is interpreted as a complex number that indicates its magnitude and phase shift with respect to the input motion. Figure 12 shows the steps used in decomposing the time-history into its real and imaginary components. The complex amplitudes CPU,A(CPL,A) are the quantities presented in this report. The physically realizable first harmonic unsteady pressure time-history is given by

$$\left. \begin{aligned} CPUD &= [Mag(A)] [Re(CPU,A) \cos \omega t - Im(CPU,A) \sin \omega t] \\ CPLD &= [Mag(A)] [Re(CPL,A) \cos \omega t - Im(CPL,A) \sin \omega t] \end{aligned} \right\} \tag{3}$$

where the complex amplitudes of the pressure coefficients CPU,A(CPL,A) have been normalized by the amplitude of the input motion Mag(A). The time-history of the input motion is (fig. 12)

$$A = [Mag(A)] \cos \omega t$$

where A is interpreted as an angular quantity for pitching motion or a translational quantity for plunging motion.

The 209 sets of first harmonic data, arranged by dynamic index (DI), are presented graphically (real and imaginary parts) in figure 13. The corresponding static pressure distribution is also shown for reference. The tabulated static and dynamic data are presented in the enclosed microfiche (appendix B). Note that only upper surface dynamic data were measured on the supercritical airfoil (DI \geq 115).

Integrated Dynamic Pressures

The first harmonic data were integrated in the same manner as the static data (eq. (1)).

$$IU,A(Q) = \int_0^1 [CPU,A(X/C)] [(X/C)^Q] d(X/C) \quad (4a)$$

$$IL,A(Q) = \int_0^1 [CPL,A(X/C)] [(X/C)^Q] d(X/C)$$

$$CL,A = IL,A(0) - IU,A(0) \quad (4b)$$

$$CM,A = -[IL,A(1) - IU,A(1)]$$

These complex numbers are converted to time histories in exactly the same manner as in equation (3). The sign convention, interpretation of the lift and leading-edge moment, as well as the integration scheme, are the same as used in the preceding subsection on integrated static pressures.

The six quantities in equation (4b) are given in table 11 for the NACA 64A010 airfoil and in table 12 for the NLR 7301 supercritical airfoil.

6. SUMMARY OF RESULTS

Unsteady pressure data from an oscillating airfoil experiment in the Ames 11- by 11-Foot Transonic Wind Tunnel were presented. The data covered a wide range of parameters including airfoil geometry, mean flow conditions, motion mode, and frequency. These experimental results should be useful both for validating new computational methods and as an aid in aeroelastic analysis.

To aid in the interpretation of the data, detailed discussions were included on the tunnel installation, tunnel geometry, and airfoil contour. The novel model fabrication and the new experimental techniques that were developed especially for this test program were also discussed.

The data, presented in tabular and graphical form, include measurements of the mean pressure coefficients and real and imaginary parts of the fundamental (first harmonic) frequency unsteady pressure coefficients. The

pressure coefficient data are also presented in integrated form to facilitate interpretation of parametric trends.

The data show that the unsteady aerodynamic response can be sensitive to all of the parameters considered in this experiment. For subcritical flows, the two most important parameters are Mach number and frequency. In the range of mild transonic flows, airfoil geometry is an additional important factor. Finally, in the flow regime where strong shock-wave/boundary-layer interactions are important, Reynolds number becomes another important parameter. This progression into increasingly complicated flows is consistent with the theoretical methods that are used to predict these flows. Linearized subsonic theory includes the effect of the flow parameters M and k , and transonic theory correctly accounts for airfoil geometry. In the most complex flow regime, Navier-Stokes modeling will be necessary to correctly predict the unsteady viscous interactions.

APPENDIX A

METHODS FOR INTEGRATING EXPERIMENTAL PRESSURE DISTRIBUTIONS

The integration of a function that is defined at a discrete number of points is not a simple problem. If a smooth curve can be fit through one or more of the discrete points, the integration becomes simple. The difficult part is to choose the appropriate family of smooth curves.

A simple example will best illustrate the problem. Consider a pressure distribution having the functional form

$$CP(\bar{X}) = \sqrt{1 - \bar{X}} / \sqrt{\bar{X}} \quad 0 \leq \bar{X} \leq 1 \quad (A1)$$

This is the distribution that would be computed from thin-airfoil theory. The area under the curve, defined as the integral of equation (A1) between the limits 0 to 1 is 6.283 (to four significant figures).

Now consider a routine application of the trapezoidal rule. (The family of curves is simply the straight line connecting successive data points.) It is most convenient to consider the trapezoidal rule with equally spaced increments. A typical case is shown in figure 14, where the function is divided into 20 strips. The value at the leading edge was approximated by extrapolating the slope at the first chord position backwards to the leading edge. The computed loads for a 20-strip integration was 5.546. Compared with the exact area, this represents an error of 11.7%.

In actual practice, the leading-edge singularity is ameliorated by leading-edge bluntness and the errors computed above are probable upper bounds. However, in oscillating airfoil experiments, these leading-edge suction peaks can be quite high. This problem was pointed out some time ago by Runyan et al. (ref. 12).

If the problem were only one of square-root-type singularities, an elegant solution is available. Gaussian quadrature techniques have been developed (ref. 13) to approximate definite integrals by the finite sum

$$\int_0^1 W(\bar{X}) f(\bar{X}) d\bar{X} = \sum_{i=1}^N W_i f_i \quad (A2)$$

They have not been widely used because the value of the function must be computed at sample points \bar{X}_i that are usually irrational numbers. Standard tables are available giving the sample points and weights W_i for a given weight function $W(\bar{X})$. One such method — the Gauss-Jacobi quadrature — has a weight function $W(\bar{X}) = \sqrt{1 - \bar{X}} / \sqrt{\bar{X}}$. Figure 15 shows the sample points needed for a 20-strip Gauss-Jacobi quadrature. The computed area is 6.283, essentially the exact value. Gauss-Jacobi quadratures have been used extensively

in a recent theoretical report on oscillating airfoils in wind tunnels (ref. 14). A serious defect in the quadrature method for transonic flows is clear from figure 15. Sample points are sparsely located in the central region of the airfoil. Transonic flows with discontinuous pressure distributions (shock waves) are not well approximated by a scheme with such large increments in the region of discontinuity. Numerical experiments with discontinuous pressure distributions have confirmed that unacceptably large errors can result.

The numerical integration scheme that was finally adopted was the one described by Woodward (ref. 15). This method rectifies the leading-edge singularity by a simple transformation of variables:

$$\left. \begin{aligned} X' &= \sqrt{X} \\ CP' &= 2\sqrt{X} CP \end{aligned} \right\} \quad (A3)$$

The pressure distribution presented in figure 14 is shown in the primed coordinate system in figure 16. The curve is finite everywhere and a simple trapezoidal rule with 20 intervals has approximately six elementary trapezoids in the first 10% of chord. (Compare with fig. 14 where only two intervals constitute the first 10% of the chord.) Higher resolution is not compromised by a coarse mesh width in the area of discontinuities. Extensive numerical experiments have confirmed the validity of this procedure. For example, computations with a 20-strip integration resulted in an area of 6.288. The accuracy of the integrated quantities has been augmented by performing both a 20- and 40-strip integration and by using a Richardson's extrapolation (ref. 16) to increase the accuracy.

Once the integration scheme is selected, the remaining computational problem is to choose an acceptable interpolation-extrapolation scheme to transform the physical pressure tap locations to the desired mesh points. The method adopted was a polynomial fitting method for interpolating between data points and a linear extrapolation method for predicting values very near the leading and trailing edges.

APPENDIX B

TABULATED FUNDAMENTAL FREQUENCY DATA

Refer to the enclosed microfiche (inside back cover) for the 209 sets of tabulated steady and unsteady pressure data.

REFERENCES

1. Malcolm, G.; and Davis, S.: New NASA-Ames Wind Tunnel Techniques for Studying Airplane Spin and Two-Dimensional Unsteady Aerodynamics. Dynamic Stability Parameters, AGARD CP-235, Nov. 1978, pp. 3-1 to 3-12.
2. Davis, S.: Computer/Experiment Integration for Unsteady Aerodynamic Research. International Congress on Instrumentation in Aerospace Simulation Facilities, ICIASE 79 Record, Sept. 1979, pp. 237-250.
3. Davis, S.; and Malcolm, G.: Experiments in Unsteady Transonic Flow. AIAA Paper 79-769, St. Louis, MO, Apr. 1979.
4. Chyu, W.; and Davis, S.: Calculation of Unsteady Transonic Flow over an Arbitrary Airfoil. AIAA Paper 79-1554, Williamsburg, VA, July 1979.
5. Davis, S.; and Malcolm, G.: Unsteady Aerodynamics of Conventional and Supercritical Airfoils. AIAA Paper 80-734, Seattle, WA, May 1980.
6. Davis, S.: Experimental Studies of Scale Effects on Oscillating Airfoils at Transonic Speeds. Paper presented at AGARD Specialists Meeting, Aix-en-Provence, France, Sept. 1980.
7. Davis, S.; and Satyanarayana, B.: Two-Dimensional Transonic Testing with Splitter Plates. NASA TP-1153, 1978.
8. Olsen, J. J.: AGARD Standard Configurations for Aeroelastic Applications of Transonic Unsteady Aerodynamics. AFFDL-TM-76-6-FBR, 1978.
9. Bland, S. R.: AGARD Two-Dimensional Aeroelastic Configurations. AGARD AR-156, Aug. 1979.
10. Magnus, R. J.: Calculations of Some Unsteady Transonic Flows about the NACA 64A006 and 64A010 Airfoils. AFFDL TR-77-46, July 1977.
11. Tijdeman, H.: Investigations of the Transonic Flow Around Oscillating Airfoils. NLR TR 77090U, Oct. 1977.
12. Rungan, H. L.; Woolston, D. S.; and Rainey, A. G.: Theoretical and Experimental Investigation of the Effect of Tunnel Walls on the Forces on an Oscillating Airfoil in Two-Dimensional Subsonic Compressible Flow. NACA TR-1262, 1956.
13. Abramowitz, M.; and Stegun, I.: Handbook of Mathematical Functions. Department of Commerce, National Bureau of Standards, Applied Mathematics Series, No. 55, 1964, pp. 887-890.
14. Fromme, Joseph; Golberg, Michael; and Werth, John: Two Dimensional Aerodynamic Interference Effects on Oscillating Airfoils with Flaps in Ventilated Subsonic Wind Tunnels. NASA CR-3210, 1979.

15. Woodward, D. S.: On the Integration of Functions Specified Only at Discrete Data Points, with Special Reference to the Processing of Wind Tunnel Pressure Measurements. TR 67151, British Royal Aircraft Establishment, 1967.
16. Salvadori, G.; and Baron, M. L.: Numerical Methods in Engineering. Second ed. Prentice-Hall, Inc., 1964, pp. 96-101.

TABLE 1.- GEOMETRY OF THE NACA 64A010 AIRFOIL SECTION

		Upper surface geometry				Lower surface geometry			
I	Wing station, X/C	Ordinates, Y/C		I	Wing station, X/C	Ordinates, Y/C			
		Measured	Smoothered			Theoretical	Measured	Smoothered	Theoretical
1	0.0000	0.0000	0.0000	1	0.0000	0.0000	0.0000		
2	.0010	.0043	.0038	2	.0010	-.0033	-.0038		
3	.0020	.0056	.0052	3	.0020	-.0050	-.0052		
4	.0030	.0070	.0066	4	.0030	-.0065	-.0066		
5	.0040	.0081	.0076	5	.0040	-.0077	-.0076		
6	.0050	.0089	.0084	6	.0050	-.0086	-.0082		
7	.0050	.0097	.0092	7	.0060	-.0095	-.0089		
8	.0070	.0104	.0099	8	.0070	-.0102	-.0096		
9	.0080	.0110	.0106	9	.0080	-.0109	-.0102		
10	.0090	.0116	.0112	10	.0090	-.0115	-.0108		
11	.0100	.0121	.0118	11	.0100	-.0121	-.0113		
12	.0140	.0141	.0139	12	.0140	-.0142	-.0133		
13	.0180	.0157	.0156	13	.0180	-.0158	-.0146		
14	.0220	.0172	.0172	14	.0220	-.0173	-.0161		
15	.0260	.0185	.0186	15	.0260	-.0187	-.0173		
16	.0300	.0198	.0199	16	.0300	-.0199	-.0185		
17	.0340	.0208	.0210	17	.0340	-.0210	-.0196		
18	.0380	.0219	.0221	18	.0380	-.0220	-.0206		
19	.0420	.0229	.0232	19	.0420	-.0230	-.0216		
20	.0460	.0238	.0242	20	.0460	-.0239	-.0225		
21	.0500	.0246	.0251	21	.0500	-.0248	-.0234		
22	.0600	.0267	.0272	22	.0600	-.0268	-.0255		
23	.0700	.0286	.0291	23	.0700	-.0288	-.0274		
24	.0800	.0304	.0308	24	.0800	-.0305	-.0291		
25	.0900	.0321	.0324	25	.0900	-.0322	-.0307		
26	.1000	.0337	.0338	26	.1000	-.0337	-.0322		
27	.1100	.0351	.0352	27	.1100	-.0352	-.0336		
28	.1200	.0365	.0364	28	.1200	-.0365	-.0349		
29	.1300	.0379	.0376	29	.1300	-.0378	-.0362		

TABLE 1.- Concluded.

Upper surface geometry				Lower surface geometry			
I	Wing station, X/C	Ordinates, Y/C		I	Wing station, X/C	Ordinates, Y/C	
		Measured	Smoothed			Theoretical	Measured
30	0.1400	0.0391	0.0387	30	0.1400	-0.0390	-0.0386
31	.1500	.0403	.0398	31	.1500	-.0402	-.0396
32	.2000	.0453	.0443	32	.2000	-.0450	-.0440
33	.2500	.0489	.0478	33	.2500	-.0488	-.0475
34	.3000	.0515	.0505	34	.3000	-.0514	-.0502
35	.3500	.0530	.0523	35	.3500	-.0529	-.0521
36	.4051	.0531	.0529	36	.4051	-.0532	-.0529
37	.4500	.0523	.0521	37	.4500	-.0524	-.0522
38	.5000	.0500	.0500	38	.5000	-.0502	-.0503
39	.5500	.0468	.0469	39	.5500	-.0470	-.0472
40	.6000	.0429	.0430	40	.6000	-.0432	-.0433
41	.6500	.0383	.0385	41	.6500	-.0386	-.0387
42	.7000	.0333	.0334	42	.7000	-.0337	-.0337
43	.7500	.0280	.0281	43	.7500	-.0284	-.0283
44	.8000	.0227	.0226	44	.8000	-.0229	-.0228
45	.8500	.0173	.0169	45	.8500	-.0174	-.0171
46	.9000	.0118	.0112	46	.9000	-.0117	-.0113
47	.9500	.0064	.0055	47	.9500	-.0061	-.0055
48	1.000	.0000	-.0003	48	1.0000	.0000	.0003

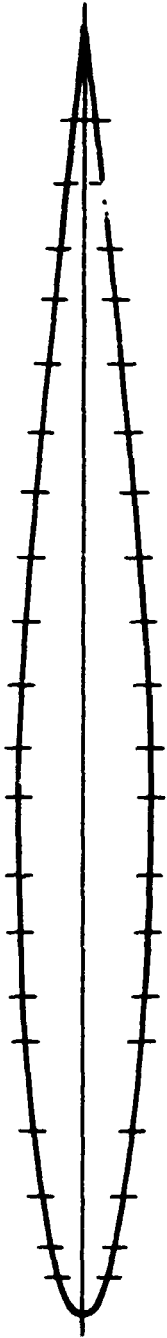
TABLE 2.- GEOMETRY OF NLR 7301 AIRFOIL SECTION

Upper surface geometry				Lower surface geometry			
I	Wing station, X/C	Ordinates, Y/C		I	Wing station, X/C	Ordinates, Y/C	
		Measured	Smoothed			Theoretical	Measured
1	0.0000	0.0000	-0.0000	1	0.0000	0.0000	-0.0000
2	.0006	.0088	.0101	2	.0005	-.0059	-.0072
3	.0012	.0131	.0141	3	.0009	-.0089	-.0098
4	.0018	.0158	.0170	4	.0014	-.0103	-.0117
5	.0023	.0180	.0190	5	.0021	-.0128	-.0141
6	.0029	.0198	.0211	6	.0046	-.0183	-.0194
7	.0057	.0275	.0283	7	.0073	-.0226	-.0237
8	.0083	.0326	.0331	8	.0107	-.0266	-.0276
9	.0121	.0385	.0385	9	.0154	-.0307	-.0318
10	.0166	.0438	.0433	10	.0197	-.0336	-.0348
11	.0204	.0473	.0467	11	.0244	-.0365	-.0376
12	.0242	.0502	.0495	12	.0295	-.0392	-.0402
13	.0267	.0518	.0511	13	.0358	-.0421	-.0430
14	.0277	.0525	.0518	14	.0451	-.0458	-.0464
15	.0293	.0533	.0527	15	.0619	-.0510	-.0515
16	.0312	.0544	.0538	16	.0810	-.0556	-.0560
17	.0380	.0575	.0571	17	.0965	-.0586	-.0590
18	.0474	.0609	.0608	18	.1114	-.0611	-.0615
19	.0616	.0649	.0652	19	.1338	-.0644	-.0648
20	.0810	.0691	.0696	20	.1667	-.0683	-.0688
21	.0969	.0719	.0724	21	.1997	-.0715	-.0719
22	.1227	.0756	.0761	22	.2361	-.0744	-.0745
23	.1534	.0792	.0796	23	.2764	-.0767	-.0764
24	.1832	.0820	.0823	24	.3153	-.0778	-.0774
25	.2066	.0839	.0842	25	.3560	-.0778	-.0776
26	.2296	.0856	.0858	26	.3966	-.0769	-.0768
27	.2549	.0873	.0873	27	.4372	-.0752	-.0750
28	.2830	.0887	.0886	28	.4744	-.0728	-.0721
29	.3138	.0898	.0896	29	.5200	-.0679	-.0668

TABLE 2.- Concluded.

Upper surface geometry				Lower surface geometry			
I	Wing station, X/C	Ordinates, Y/C		I	Wing station, X/C	Ordinates, Y/C	
		Measured	Smootherd			Theoretical	Measured
30	0.3476	0.0905	0.0903	30	0.5634	-0.0614	-0.0614
31	.3837	.0904	.0905	31	.6196	-.0505	-.0505
32	.4207	.0899	.0901	32	.6636	-.0408	-.0408
33	.4731	.0892	.0886	33	.7223	-.0281	-.0281
34	.5160	.0876	.0963	34	.7506	-.0220	-.0220
35	.5616	.0844	.0827	35	.7752	-.0169	-.0169
36	.5995	.0806	.0789	36	.8040	-.0113	-.0113
37	.6331	.0762	.0749	37	.8396	-.0055	-.0055
38	.6744	.0701	.0692	38	.8763	-.0008	-.0008
39	.7096	.0644	.0636	39	.9129	.0018	.0018
40	.7392	.0590	.0584	40	.9579	.0022	.0022
41	.7705	.0526	.0525	41	.9885	.0005	.0005
42	.8040	.0454	.0458	42	.9972	-.0002	-.0002
43	.8407	.0370	.0379				
44	.8806	.0277	.0290				
45	.9240	.0176	.0188				
46	.9637	.0085	.0093				
47	.9831	.0042	.0047				
48	.9977	.0009	.0012				

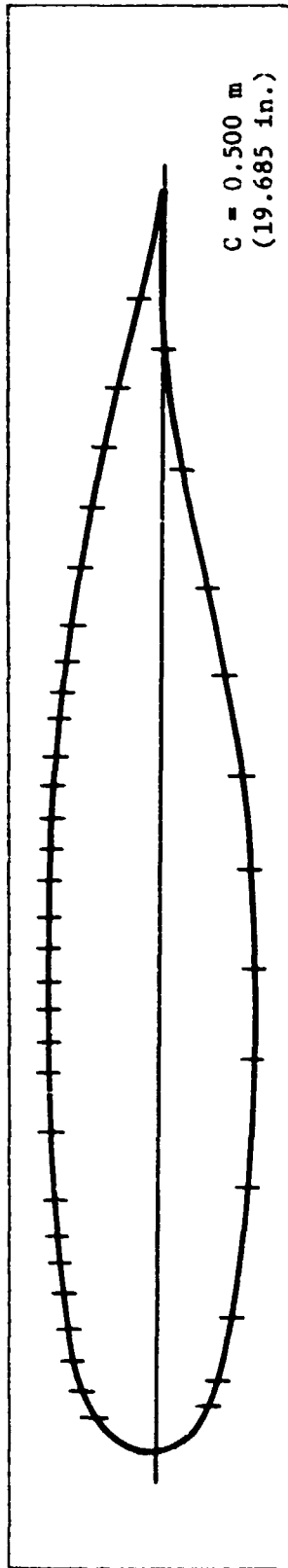
TABLE 3.- NACA 64A010 AIRFOIL SECTION: ORIFICE LOCATIONS



C = 0.500 m
(19.685 in.)

Dynamic orifices											
Static orifices						Dynamic orifices					
Upper surface			Lower surface			Upper surface			Lower surface		
X, cm	X, in.	X/C	X, cm	X, in.	X/C	X, cm	X, in.	X/C	X, cm	X, in.	X/C
0	0	0	0	0	0	0	0	0	0	0	0
1.486	.585	.030	1.605	0.632	0.032	1.659	.653	.033	1.699	0.669	0.034
2.598	1.023	.052	2.662	1.048	.053	2.616	1.030	.057	2.956	1.064	.054
4.557	1.794	.091	4.633	1.824	.093	4.526	1.782	.091	4.709	1.854	.094
7.122	2.804	.142	7.102	2.796	.142	7.015	2.762	.140	7.054	2.777	.141
10.533	4.147	.211	9.952	3.918	.199	10.427	4.105	.208	10.013	3.942	.200
12.131	4.776	.243	12.212	4.808	.244	12.172	4.792	.243	12.128	4.775	.243
14.605	5.750	.292	14.674	5.777	.293	14.676	5.778	.294	14.625	5.758	.293
17.046	6.711	.341	17.026	6.703	.341	16.947	6.672	.339	17.059	6.716	.341
19.962	7.859	.399	19.639	7.732	.393	20.091	7.910	.402	19.698	7.755	.394
22.019	8.669	.440	22.012	8.666	.440	21.796	8.652	.440	22.029	8.673	.441
24.364	9.592	.487	24.508	9.649	.490	24.389	9.602	.488	24.478	9.637	.490
26.838	10.566	.537	26.858	10.574	.537	26.881	10.583	.538	26.858	10.574	.537
29.238	11.511	.585	29.174	11.486	.583	29.205	11.498	.584	29.108	11.460	.582
31.725	12.490	.634	31.232	12.296	.625	31.633	12.454	.633	31.549	12.421	.631
34.097	13.424	.682	33.960	13.370	.679	34.077	13.416	.682	33.896	13.345	.678
36.670	14.437	.733	36.700	14.449	.734	36.672	14.438	.733	36.665	14.435	.733
39.134	15.407	.783	39.434	15.525	.789	39.052	15.375	.781	39.040	15.370	.781
41.374	16.289	.827	41.605	16.380	.832	41.463	16.324	.829	41.539	16.354	.831
43.701	17.205	.874	44.277	17.432	.886	43.612	17.170	.872	44.422	17.489	.888
46.190	18.185	.924	47.046	18.522	.941	47.041	18.520	.941	46.136	18.114	.923

TABLE 4.- NLR 7301 AIRFOIL SECTION: ORIFICE LOCATIONS



C = 0.500 m
(19.685 in.)

		Static orifices				Dynamic orifices			
Upper surface		Lower surface		Upper surface		Upper surface			
X, cm	X, in.	X, cm	X, in.	X, cm	X, in.	X, cm	X, in.	X, cm	X/C
1.161	0.457	1.671	0.658	0.787	0.033	0.310	0.016		
2.268	.893	2.649	1.043	2.146	.053	.845	.043		
3.482	1.371	5.291	2.083	3.338	.106	1.314	.067		
4.709	1.854	10.485	4.128	4.585	.209	1.805	.092		
6.121	2.410	15.461	6.087	5.842	.309	2.300	.117		
7.361	2.898	19.052	7.501	7.122	.381	2.804	.142		
8.390	3.303	23.030	9.067	8.227	.460	3.239	.164		
9.729	3.850	26.642	10.489	9.578	.532	3.771	.191		
12.446	4.900	30.777	12.095	12.245	.614	4.821	.245		
14.877	5.857	34.257	13.485	14.691	.684	5.784	.294		
16.088	6.334	39.014	15.360	15.949	.779	6.279	.319		
17.407	6.853	43.752	17.225	17.183	.874	6.765	.343		
18.461	7.268			18.333		7.218	.366		
19.822	7.804			19.672		7.745	.393		
21.031	8.280			21.239		8.362	.424		
22.514	8.864			22.413		8.824	.448		
23.698	9.330			23.515		9.258	.470		
24.978	9.834			24.854		9.785	.496		
26.213	10.320			26.070		10.264	.521		
27.541	10.843			27.396		10.786	.547		

TABLE 4.- Concluded.

Static orifices							Dynamic orifices		
Upper surface			Lower surface			Upper surface			
X, cm	X, in.	X/C	X, cm	X, in.	X/C	X, cm	X, in.	X/C	
28.931	11.390	0.578				28.478	11.212	0.569	
30.020	11.819	.600				29.764	11.718	.595	
31.242	12.300	.624				30.937	12.180	.618	
32.657	12.857	.652				32.385	12.750	.647	
35.037	13.794	.700				34.897	13.739	.697	
37.473	14.753	.749				37.338	14.700	.746	
39.883	15.702	.797				39.827	15.650	.796	
42.156	16.597	.842				42.080	16.567	.841	
45.750	18.012	.914				45.857	18.054	.916	

TABLE 5.- RANGE OF PARAMETERS USED IN TEST PROGRAM

Parameter	Symbol	Range of values
Static quantities		
Airfoil geometry		NACA 64A010, NLR 7301
Free-stream Mach number	M_∞	0.45, 0.50, 0.65, 0.70, 0.75, 0.80, 0.85
Mean angle of attack, deg	α_m	0, 0.37, 0.57, 2.5, 4
Reynolds number	Re	2.5×10^6 to 12.6×10^6 , depending on M_∞
Dynamic quantities		
Motion mode		Pitching, plunging
Pitching axis location		0.25C, 0.40C, 0.50C
Pitching amplitude, deg	α	± 0.25 , ± 0.50 , ± 1 , ± 2
Plunging amplitude, cm	h	± 1
Reduced frequency	k	0.025, 0.05, 0.10, 0.15, 0.20, 0.25, 0.30

TABLE 6.- TEST PROGRAM ARRANGED IN ASCENDING ORDER

DI	Airfoil	M_∞	α , deg	$Re \times 10^{-6}$	Motion	f, Hz	k
1	NACA 64A010 ↓	0.489	0.03	2.51	Plunging 0.35 cm (0.137 in.)	5.0	0.048
2		.489	.01	2.50	Pitching 0.94 deg about X/C = 0.236	20.8	.200
3		.488	-.00	2.50	Pitching .95 deg about X/C = .512	20.8	.200
4		.489	.01	2.31	Plunging 1.01 cm (.396 in.)	20.8	.200
5		.490	-.01	2.52	Pitching .96 deg about X/C = .507	26.0	.249
6		.490	-.01	2.52	Pitching .96 deg about X/C = .238	15.7	.151
7		.490	-.01	2.52	Pitching .96 deg about X/C = .233	10.4	.100
8		.490	-.01	2.52	Pitching .97 deg about X/C = .230	5.2	.050
9		.490	-.01	2.52	Pitching 1.01 deg about X/C = .224	2.6	.025
10		.489	-.00	2.51	Pitching 1.98 deg about X/C = .249	5.2	.050
11		.802	-.00	3.38	Pitching 1.45 deg about X/C = .250	20.8	.200
12		.802	-.00	3.38	Pitching .94 deg about X/C = .237	33.2	.200
13		.802	-.00	3.38	Pitching 1.27 deg about X/C = .431	33.2	.200
14		.797	-.06	3.39	Plunging .89 cm (.349 in.)	33.1	.201
15		.797	-.06	3.39	Pitching .95 deg about X/C = .234	41.3	.250
16		.703	.01	6.67	Pitching .96 deg about X/C = .252	33.3	.201
17		.795	.01	6.67	Pitching .98 deg about X/C = .501	33.3	.201
18		.795	.01	6.67	Plunging .38 cm (.346 in.)	33.3	.201
19		.795	.01	6.67	Pitching 1.10 deg about X/C = .505	41.6	.251
20		.497	.04	5.03	Pitching .01 deg about X/C = .946	5.0	.047
21		.497	.04	5.03	Pitching .99 deg about X/C = .257	21.3	.201
22		.497	.04	5.03	Pitching 1.07 deg about X/C = .504	21.3	.201
23		.497	.04	5.03	Plunging 1.02 cm (.400 in.)	21.3	.201
24		1.074	-.00	6.58	Plunging .44 cm (.173 in.)	5.0	.024
25		.497	1.98	5.00	Plunging .00 cm (.000 in.)	5.0	.047
26		.502	-.22	9.98	Pitching .00 deg about X/C = .150	5.0	.046
27		.502	-.22	9.98	Pitching .24 deg about X/C = .234	10.8	.100
28		.502	-.22	9.98	Pitching .51 deg about X/C = .269	10.8	.100
29		.502	-.22	9.98	Pitching 1.02 deg about X/C = .169	10.8	.100
30		.499	-.21	9.90	Pitching .26 deg about X/C = .177	21.5	.201
31		.499	-.13	9.89	Pitching .50 deg about X/C = .271	21.5	.200
32		.499	-.13	9.89	Pitching 1.00 deg about X/C = .269	21.5	.200
33		.499	-.13	9.89	Pitching 2.01 deg about X/C = .267	21.5	.200

TABLE 6.- Continued.

DI	Airfoil	M_∞	α_m , deg	$Re \times 10^{-6}$	Motion	f, Hz	k
34	NACA 64A010 ↓	0.499	-0.13	9.89	Pitching 2.13 deg about X/C = 0.503	21.5	0.200
35		.499	-.13	9.89	Pitching 1.06 deg about X/C = .506	21.5	.200
36		.499	-.13	9.89	Plunging 1.01 cm (.399 in.)	21.5	.200
37		.499	-.13	9.89	Pitching 1.00 deg about X/C = .252	26.9	.251
38		.499	-.13	9.89	Pitching 1.07 deg about X/C = .506	26.9	.251
39		.499	-.13	9.89	Pitching 1.00 deg about X/C = .250	16.2	.151
40		.499	-.13	9.89	Plunging 1.01 cm (.396 in.)	16.2	.151
41		.499	-.13	9.89	Plunging 1.02 cm (.401 in.)	10.8	.101
42		.499	-.13	9.89	Plunging 1.03 cm (.405 in.)	5.4	.050
43		.499	-.13	9.89	Pitching 1.02 deg about X/C = .248	5.4	.050
44		.499	-.13	9.89	Pitching 2.04 deg about X/C = .245	10.8	.101
45		.648	-.22	11.63	Pitching .97 deg about X/C = .249	27.8	.201
46		.744	-.22	12.31	Fitching 1.01 deg about X/C = .248	32.0	.201
47		.796	-.21	12.56	Pitching .30 deg about X/C = .202	17.1	.101
48		.796	-.21	12.56	Pitching .25 deg about X/C = .234	34.2	.201
49		.796	-.21	12.56	Pitching .51 deg about X/C = .247	17.1	.101
50		.796	-.21	12.56	Pitching .50 deg about X/C = .248	34.2	.201
51		.796	-.21	12.56	Pitching 1.03 deg about X/C = .249	4.2	.025
52		.796	-.21	12.56	Pitching 1.02 deg about X/C = .246	8.6	.051
53		.796	-.21	12.56	Pitching 1.02 deg about X/C = .248	17.2	.101
54		.796	-.21	12.56	Pitching 1.01 deg about X/C = .254	25.7	.151
55		.796	-.21	12.56	Pitching 1.01 deg about X/C = .248	34.4	.202
56		.796	-.21	12.56	Pitching 1.02 deg about X/C = .248	42.0	.247
57		.796	-.21	12.56	Pitching deg about X/C = .252	51.5	.303
58		.796	-.21	12.56	Pitching 1.08 deg about X/C = .502	42.9	.252
59		.796	-.21	12.56	Pitching 1.09 deg about X/C = .500	34.4	.202
60	.796	-.21	12.56	Pitching 1.08 deg about X/C = .502	17.2	.101	
61	.796	-.21	12.56	Pitching 1.09 deg about X/C = .501	8.6	.051	
62	.796	-.21	12.56	Pitching 1.12 deg about X/C = .499	4.3	.025	
63	.797	-.08	12.40	Pitching 1.95 deg about X/C = .471	34.3	.201	
64	.797	-.08	12.40	Pitching 1.94 deg about X/C = .231	34.3	.201	
65	.797	-.08	12.40	Pitching 2.00 deg about X/C = .239	17.2	.101	
66	.797	-.08	12.40	Plunging 1.01 cm (.396 in.)	34.3	.201	

TABLE 6.- Continued.

DI	Airfoil	M_∞	α_m , deg.	$Re \times 10^{-6}$	Motion	f, Hz	k
67	NACA 64A010 ↓	0.797	-0.38	12.40	Plunging 1.02 cm (0.401 in.)	25.8	0.151
68		.797	-0.08	12.40	Plunging 1.02 cm (.400 in.)	17.4	.102
69		.797	-0.08	12.40	Plunging 1.02 cm (.400 in.)	8.6	.050
70		.797	-0.08	12.40	Plunging 1.04 cm (.409 in.)	4.3	.025
71		.842	-0.00	12.45	Pitching 1.01 deg about X/C = .248	36.4	.202
72		.842	-0.22	12.43	Pitching 1.01 deg about X/C = .247	36.5	.202
73		.805	-0.00	3.34	Pitching 1.01 deg about X/C = .247	25.1	.149
74		.805	-0.00	3.34	Plunging .44 cm (.173 in.)	5.0	.030
75		.805	-0.00	3.34	Pitching 1.02 deg about X/C = .248	8.3	.049
76		.805	-0.00	3.34	Pitching 2.03 deg about X/C = .248	8.3	.049
77		.805	-0.00	3.34	Pitching 2.00 deg about X/C = .248	33.3	.198
78		.794	.08	12.40	Pitching .64 deg about X/C = .328	10.0	.059
79		.782	4.00	12.01	Pitching .25 deg about X/C = .232	17.3	.102
80		.782	4.00	12.01	Pitching .25 deg about X/C = .229	34.7	.205
81		.782	4.00	12.01	Pitching .51 deg about X/C = .244	17.4	.103
82		.792	3.93	6.15	Pitching 1.01 deg about X/C = .247	34.3	.203
83		.793	4.01	6.18	Pitching 1.02 deg about X/C = .248	34.2	.202
84		.789	4.00	11.88	Pitching .51 deg about X/C = .234	34.9	.203
85		.789	4.00	11.88	Pitching 1.04 deg about X/C = .246	4.4	.026
86		.789	4.00	11.88	Pitching 1.03 deg about X/C = .246	8.8	.051
87	.789	4.00	11.88	Pitching 1.02 deg about X/C = .248	17.5	.102	
88	.789	4.00	11.88	Pitching 1.01 deg about X/C = .247	26.3	.153	
89	.789	4.00	11.88	Pitching 1.01 deg about X/C = .249	35.1	.204	
90	.789	4.00	11.88	Pitching 1.01 deg about X/C = .248	43.9	.255	
91	.789	4.00	11.88	Pitching 1.00 deg about X/C = .248	52.7	.306	
92	.789	4.00	11.88	Pitching 1.08 deg about X/C = .499	35.2	.205	
93	.789	4.00	11.88	Plunging .84 cm (.330 in.)	35.2	.205	
94	.789	4.00	11.88	Pitching 1.08 deg about X/C = .501	44.0	.256	
95	.789	4.00	11.88	Pitching 2.00 deg about X/C = .245	17.6	.102	
96	.741	4.03	11.22	Pitching 1.02 deg about X/C = .246	35.2	.215	
97	.642	3.99	10.60	Pitching 1.01 deg about X/C = .247	28.8	.203	
98	.504	4.00	10.20	Pitching 1.02 deg about X/C = .249	22.2	.199	
99	.506	3.99	9.45	Pitching 1.09 deg about X/C = .499	22.0	.198	

TABLE 6.- Continued.

DI	Airfoil	M_∞	α_m , deg	$Re \times 10^{-6}$	Motion	f, Hz	k
100	NACA 64A010	0.506	3.99	9.45	Plunging 1.01 cm (0.397 in.)	22.0	0.198
101		.506	3.99	9.45	Pitching 1.09 deg about X/C = .302	27.5	.247
102		.506	3.99	9.45	Pitching 2.14 deg about X/C = .502	27.5	.247
103		.790	4.00	11.72	Pitching 2.01 deg about X/C = .243	35.0	.203
104		.503	4.00	4.94	Pitching 1.01 deg about X/C = .245	21.6	.199
105		.503	4.00	4.94	Pitching 1.09 deg about X/C = .499	21.6	.199
106		.503	4.00	4.94	Plunging 1.02 cm (.401 in.)	21.6	.199
107		.503	4.00	4.94	Pitching 1.06 deg about X/C = .502	26.9	.248
108		.642	3.78	5.92	Pitching 1.02 deg about X/C = .250	27.6	.203
109		.747	3.89	6.36	Pitching 1.02 deg about X/C = .247	31.0	.197
110		.797	4.01	6.30	Pitching 1.09 deg about X/C = .500	33.5	.201
111		.797	4.01	6.50	Plunging 1.01 cm (.398 in.)	33.5	.201
112		.797	4.01	6.50	Pitching 1.08 deg about X/C = .502	42.0	.252
113		.848	3.89	6.59	Pitching 1.01 deg about X/C = .248	35.5	.201
114	.840	3.79	12.39	Pitching 1.01 deg about X/C = .248	36.3	.202	
115	NLR 7301	.453	.57	4.47	Pitching .52 deg about X/C = .394	2.7	.028
116		.453	.57	4.47	Pitching .50 deg about X/C = .404	5.4	.055
117		.453	.57	4.47	Pitching .48 deg about X/C = .400	10.7	.110
118		.453	.57	4.47	Pitching .49 deg about X/C = .391	21.5	.221
119		.453	.57	4.47	Pitching .49 deg about X/C = .394	32.2	.331
120		.453	.57	4.47	Pitching 1.04 deg about X/C = .384	5.4	.055
121		.453	.57	4.47	Pitching 1. deg about X/C = .389	21.5	.221
122		.453	.57	4.47	Pitching 2. deg about X/C = .393	5.4	.055
123		.453	.57	4.47	Pitching 2.00 deg about X/C = .403	21.5	.221
124		.708	.58	6.15	Pitching .52 deg about X/C = .394	3.7	.025
125		.708	.58	6.15	Pitching .50 deg about X/C = .401	7.5	.050
126		.708	.58	6.15	Pitching .49 deg about X/C = .402	29.9	.200
127		.708	.58	6.15	Pitching 1.01 deg about X/C = .397	7.5	.050
128		.708	.58	6.15	Pitching 1.00 deg about X/C = .398	29.9	.200
129		.708	.58	6.15	Pitching 2.02 deg about X/C = .401	7.5	.050
130		.708	.58	6.15	Pitching 2.00 deg about X/C = .399	29.9	.200
131		.752	.37	6.21	Pitching .51 deg about X/C = .401	4.0	.025
132		.752	.37	6.21	Pitching .50 deg about X/C = .401	8.0	.050

TABLE 6. - Continued.

DI	Airfoil	M_∞	α_m , deg	$Re \times 10^{-6}$	Motion	f, Hz	k
133	NLR 7301	0.752	C .37	6.21	Pitching 0.50 deg about X/C = 0.402	16.0	0.100
134		.752	.37	6.21	Pitching .49 deg about X/C = .403	32.0	.200
135		.752	.37	6.21	Pitching .50 deg about X/C = .403	48.0	.300
136		.752	.37	6.21	Pitching 1.01 deg about X/C = .398	8.0	.050
137		.752	.37	6.21	Pitching 1.00 deg about X/C = .397	32.0	.200
138		.752	.37	6.21	Pitching 2.02 deg about X/C = .400	8.0	.050
139		.752	.37	6.21	Pitching 2.01 deg about X/C = .399	32.0	.200
140		.808	.36	6.26	Pitching .50 deg about X/C = .402	8.5	.050
141		.808	.36	6.26	Pitching .50 deg about X/C = .407	34.0	.199
142		.807	.36	11.78	Pitching .49 deg about X/C = .404	8.7	.050
143		.807	.36	11.78	Pitching .49 deg about X/C = .398	35.0	.200
144		.751	.37	11.48	Pitching .50 deg about X/C = .403	8.2	.050
145		.751	.37	11.48	Pitching .51 deg about X/C = .399	4.1	.025
146		.751	.37	11.48	Pitching .49 deg about X/C = .400	16.5	.100
147		.751	.37	11.48	Pitching .49 deg about X/C = .401	24.7	.150
148		.751	.37	11.48	Pitching .50 deg about X/C = .403	33.0	.201
149		.751	.37	11.48	Pitching .50 deg about X/C = .400	49.5	.301
150		.751	.37	11.48	Pitching 1.00 deg about X/C = .398	8.2	.050
151		.751	.37	11.48	Pitching 1.00 deg about X/C = .400	32.8	.200
152		.751	.37	11.48	Pitching 2.02 deg about X/C = .399	8.2	.050
153		.751	.37	11.48	Pitching 2.00 deg about X/C = .402	32.8	.200
154		.751	.37	11.48	Plunging 1.00 cm (.395 in.)	8.2	.050
155		.751	.37	11.48	Plunging .98 cm (.386 in.)	32.8	.200
156	.706	.59	11.22	Pitching .51 deg about X/C = .400	3.9	.025	
157	.706	.59	11.22	Pitching .50 deg about X/C = .402	7.7	.050	
158	.706	.59	11.22	Pitching .50 deg about X/C = .399	15.4	.099	
159	.706	.59	11.22	Pitching .49 deg about X/C = .401	30.8	.199	
160	.706	.59	11.22	Pitching .49 deg about X/C = .404	46.2	.298	
161	.706	.59	11.22	Pitching 1.01 deg about X/C = .398	7.7	.050	
162	.706	.59	11.22	Pitching 1.00 deg about X/C = .398	30.8	.159	
163	.706	.59	11.22	Pitching 2.01 deg about X/C = .401	7.7	.050	
164	.706	.59	11.22	Pitching 2.00 deg about X/C = .402	30.8	.199	
165	.706	.59	11.22	Plunging 1.00 cm (.393 in.)	7.7	.050	

TABLE 6.- Continued.

DI	Airfoil	M_∞	α_m , deg	$Re \times 10^{-6}$	Motion	f, Hz	k
166	NLR 7301 ↓	0.706	0.59	11.22	Plunging 1.00 cm (0.392 in.)	30.8	0.199
167		.505	.58	9.34	Pitching .53 deg about X/C = .396	2.8	.025
168		.505	.58	9.34	Pitching .51 deg about X/C = .401	5.5	.049
169		.505	.58	9.34	Pitching .50 deg about X/C = .403	11.0	.099
170		.505	.58	9.34	Pitching .50 deg about X/C = .404	22.0	.198
171		.505	.58	9.34	Pitching .50 deg about X/C = .404	33.0	.297
172		.505	.58	9.34	Pitching 1.02 deg about X/C = .399	5.5	.049
173		.505	.58	9.34	Pitching 1.01 deg about X/C = .399	22.0	.198
174		.505	.58	9.34	Pitching 2.04 deg about X/C = .400	5.5	.049
175		.505	.58	9.34	Pitching 2.01 deg about X/C = .402	22.0	.198
176		.505	.58	9.34	Plunging 1.01 cm (.396 in.)	5.5	.049
177		.505	.58	9.34	Plunging .99 cm (.389 in.)	22.0	.198
178		.712	.58	3.09	Pitching .50 deg about X/C = .403	7.4	.049
179		.712	.58	3.09	Pitching .49 deg about X/C = .403	29.7	.197
180		.712	.58	3.09	Pitching 2.02 deg about X/C = .402	7.4	.049
181		.712	.58	3.09	Pitching 2.00 deg about X/C = .402	29.7	.197
182		.712	.58	3.09	Plunging 1.00 cm (.394 in.)	7.4	.049
183		.712	.58	3.09	Plunging .98 cm (.388 in.)	29.7	.197
184		.508	.58	2.54	Pitching .50 deg about X/C = .402	5.4	.050
185		.508	.58	2.54	Pitching .50 deg about X/C = .405	21.4	.197
186		.508	.58	2.54	Pitching 2.03 deg about X/C = .400	5.4	.050
187		.508	.58	2.54	Pitching 2.00 deg about X/C = .401	21.4	.197
188		.508	.58	2.54	Plunging 1.01 cm (.396 in.)	5.4	.050
189		.508	.58	2.54	Plunging .99 cm (.389 in.)	21.4	.197
190		.752	.37	3.25	Pitching .50 deg about X/C = .403	7.8	.050
191		.752	.37	3.25	Pitching .50 deg about X/C = .401	31.4	.200
192		.752	.37	3.25	Pitching 2.02 deg about X/C = .401	7.8	.050
193		.752	.37	3.25	Pitching 2.00 deg about X/C = .401	31.4	.200
194	.752	.37	3.25	Plunging 1.00 cm (.394 in.)	7.8	.050	
195	.812	.35	3.29	Pitching .50 deg about X/C = .403	8.4	.050	
196	.812	.35	3.29	Pitching .50 deg about X/C = .404	33.4	.198	
197	.700	2.53	11.80	Pitching .49 deg about X/C = .406	7.5	.050	
198	.700	2.53	11.80	Pitching .49 deg about X/C = .405	30.2	.201	

TABLE 6.- Concluded.

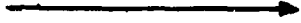
DI	Airfoil	M_∞	α_m , deg	$Re \times 10^{-6}$	Motion	f, Hz	k
199	NLR 7301 	0.700	2.53	11.80	Pitching 1.01 deg about X/C = 0.398	7.5	0.050
200		.700	2.53	11.80	Pitching 1.00 deg about X/C = .399	30.2	.201
201		.700	2.53	11.80	Pitching 1.31 deg about X/C = .403	7.5	.050
202		.700	2.54	11.69	Plunging 1.00 cm (.395 in.)	7.5	.050
203		.700	2.54	11.69	Plunging .86 cm (.339 in.)	30.2	.201
204		.710	2.53	3.15	Pitching .50 deg about X/C = .403	7.4	.050
205		.710	2.53	3.15	Pitching .50 deg about X/C = .403	29.5	.199
206		.710	2.53	3.15	Pitching 1.01 deg about X/C = .400	7.4	.050
207		.710	2.53	3.15	Pitching 1.00 deg about X/C = .399	29.5	.199
208		.710	2.53	3.15	Plunging 1.01 cm (.398 in.)	7.4	.050
209		.710	2.53	3.15	Plunging .87 cm (.341 in.)	29.5	.199

TABLE 7.- TEST PROGRAM ARRANGED ACCORDING TO FREQUENCY SWEEPS: NACA 64A010

M_∞	α_m , deg	$Re \times 10^{-6}$	$\pm \alpha$, deg	k = 0.025	k = 0.05	k = 0.10	k = 0.15	k = 0.20	k = 0.25	k = 0.30
Mode: Pitching at 0.25C										
1	0.50	10	± 0.25	9	8	27	6	30		
2	.50	10	$\pm .50$			28		31		
3	.50	2.5	± 1			7		2		
4	.50	5	± 1					21		
5	.50	10	± 1		43	29	39	32	37	
6	.50	2.5	± 2		10			11		
7	.50	10	$\pm .$			44		33		
8	.65	11.6	± 1					45		
9	.75	12.3	± 1					46		
10	.80	3.3	± 1		75		73	12	15	
11	.80	12.5	$\pm .25$					48		
12	.80	12.5	$\pm .50$		78	49		50		
13	.80	6.7	± 1					16		
14	.80	12.6	± 1	51	52	53	54	55	56	57
15	.80	12.4	± 2			65		64		
16	.85	12.4	± 1					72		
17	.50	4.9	± 1					104		
18	.50	4.0	± 1					98		
19	.65	4.0	± 1					108		
20	.65	10.6	± 1					97		
21	.75	6.4	± 1					109		
22	.75	11.2	± 1					96		
23	.80	12	$\pm .25$			79		80		
24	.80	12	$\pm .50$			81		84		
25	.80	6.2	± 1					82		
26	.80	11.9	± 1	85	86	87	88	89	90	91
27	.80	11.9	± 2			95		103		
28	.85	6.6	± 1					113		

TABLE 7.- Concluded.

M_∞	α_m , deg	$Re \times 10^{-6}$	$\pm \alpha$, deg	k = 0.025	k = 0.05	k = 0.10	k = 0.15	k = 0.20	k = 0.25	k = 0.30
Mode: Pitching at 0.5C										
29	0.50	0	± 1					3	5	
30	.50	0	± 1					22		
31	.50	0	± 1					35	38	
32	.50	0	± 2					34		
33	.80	0	± 1					13		
34	.80	0	± 1					17	19	
35	.80	0	± 1	62	61	60		59	58	
36	.80	0	± 2					63		
37	.50	4	± 1					105	107	
38	.50	4	± 1					99	101	
39	.50	4	± 2						102	
40	.80	4	± 1					110	112	
41	.80	4	± 1					92	94	
Mode: Plunging ± 1 cm										
42	.50	0	--							4
43	.50	0	--							23
44	.50	0	--		42	41	40			36
45	.80	0	--							14
46	.80	0	--							18
47	.80	0	--							66
48	.50	4	--							106
49	.50	4	--							100
50	.80	4	--							111
51	.80	4	--							93

TABLE 8.- TEST PROGRAM ARRANGED ACCORDING TO FREQUENCY SWEEPS: NLR 7301

1	M _∞	α _m , deg	Re × 10 ⁻⁶	±α, deg	Mode: Pitching at 0.4C							
					k = 0.025	k = 0.05	k = 0.10	k = 0.15	k = 0.20	k = 0.25	k = 0.30	
1	0.75	0.37	3.3	±0.50	131	190	133	147	191			135
2	.75	.37	6.2	±.50	145	132	146		134			149
3	.75	.37	11.5	±.50		144			148			
4	.75	.37	6.2	±1		136			137			
5	.75	.37	11.5	±1		150			151			
6	.75	.37	3.3	±2		192			193			
7	.75	.37	6.2	±2		138			139			
8	.75	.37	11.5	±2		152			153			
9	.80	.37	3.3	±.50		195			196			
10	.80	.37	6.3	±.50		140			141			
11	.80	.37	11.7	±.50		142			143			
12	.50	.57	2.5	±.50		184			185			
13	.45	.57	4.5	±.50	115	116	117		118			119
14	.50	.57	9.3	±.50	167	168	169		170			171
15	.45	.57	4.5	±1		120			121			
16	.50	.57	9.5	±1		172			173			
17	.50	.57	2.5	±2		186			187			
18	.45	.57	4.5	±2		122			123			
19	.50	.57	9.3	±2		174			175			
20	.71	.57	3.1	±.50		178			179			
21	.70	.57	6.2	±.50	124	125			126			
22	.70	.57	11.2	±.50	156	157	158		159			160
23	.70	.57	6.2	±1		127			128			
24	.70	.57	11.2	±1		161			162			
25	.71	.57	3.1	±2		180			181			
26	.70	.57	6.2	±2		129			130			
27	.70	.57	11.2	±2		163			164			
28	.70	2.5	3.2	±.5		204			205			
29	.70	2.5	11.8	±.5		197			198			
30	.70	2.5	3.2	±1		206			207			
31	.70	2.5	11.8	±1		199			200			

TABLE 8.- Concluded.

M_∞	α_m , deg	$Re \times 10^{-6}$	$\pm \alpha$, deg	k = 0.025	k = 0.05	k = 0.10	k = 0.15	k = 0.20	k = 0.25	k = 0.30
Mode: Plunging ± 1 cm										
32	0.75	0.37	3.3		194			155		
33	.75	.37	11.5		154			189		
34	.50	.57	2.5		188			177		
35	.50	.57	9.3		176			183		
36	.71	.57	3.1		182			166		
37	.70	.57	11.2		165			209		
38	.70	2.5	3.2		208			203		
39	.70	2.5	11.7		202					

TABLE 9.- IDENTIFICATION OF STATIC DATA CORRESPONDING TO EACH DATA SET

DI	SI	DI	SI	DI	SI	DI	SI	DI	SI
1	1	43	26	85	44	127	72	169	78
2	2	44	26	86	44	128	72	170	78
3	3	45	28	87	44	129	72	171	78
4	4	46	29	88	44	130	72	172	78
5	5	47	30	89	44	131	73	173	78
6	5	48	30	90	44	132	73	174	78
7	5	49	30	91	44	133	73	175	78
8	5	50	30	92	44	134	73	176	78
9	5	51	30	93	44	135	73	177	78
10	5	52	30	94	44	136	73	178	79
11	6	53	30	95	44	137	73	179	79
12	13	54	30	96	45	138	73	180	79
13	13	55	30	97	46	139	73	181	79
14	14	56	30	98	47	140	74	182	79
15	14	57	30	99	49	141	74	183	79
16	16	58	30	100	49	142	75	184	80
17	16	59	30	101	49	143	75	185	80
18	16	60	30	102	49	144	76	186	80
19	16	61	30	103	51	145	76	187	80
20	20	62	30	104	53	146	76	188	80
21	20	63	31	105	53	147	76	189	80
22	20	64	31	106	53	148	76	190	81
23	20	65	31	107	53	149	76	191	81
24	21	66	31	108	59	150	76	192	81
25	22	67	31	109	62	151	76	193	81
26	24	68	31	110	63	152	76	194	81
27	24	69	31	111	63	153	76	195	82
28	24	70	31	112	63	154	76	196	82
29	24	71	33	113	67	155	76	197	83
30	25	72	34	114	70	156	77	198	83
31	26	73	37	115	71	157	77	199	83
32	26	74	37	116	71	158	77	200	83
33	26	75	37	117	71	159	77	201	83
34	26	76	37	118	71	160	77	202	84
35	26	77	37	119	71	161	77	203	84
36	26	78	39	120	71	162	77	204	85
37	26	79	40	121	71	163	77	205	85
38	26	80	40	122	71	164	77	206	85
39	26	81	40	123	71	165	77	207	85
40	26	82	42	124	72	166	77	208	85
41	26	83	43	125	72	167	78	209	85
42	26	84	44	126	72	168	78		

TABLE 10.- STATIC PRESSURES: INTEGRATED VALUES

S.I.	1-(f)	IL(f)	(A)	10(1)	IL(1)	Cm	S.I.	1-(0)	IL(0)	CL	10(1)	IL(1)	Cm
1	-1.10	-1.75	.117	-.052	-.044	-.109	48	-.597	-.066	.531	-.192	-.540	-.132
2	-1.15	-.75	.011	-.050	-.044	-.066	45	-.599	.035	.633	-.143	-.012	-.131
3	-1.14	-1.57	.007	-.050	-.045	-.005	46	-.529	.066	.596	-.109	.006	-.115
4	-1.147	-1.54	.014	-.050	-.046	-.007	47	-.435	-.044	.510	-.101	.011	-.112
5	-1.145	-1.54	.006	-.050	-.046	-.004	44	-.153	-.149	.004	-.046	-.042	-.004
6	-1.149	-1.54	.005	-.050	-.046	-.004	49	-.829	.074	.505	-.099	.012	-.111
7	-1.143	-.47	.256	-.077	-.014	-.059	50	-.575	.153	.726	-.121	-.024	-.149
8	-1.145	-1.74	.004	-.054	-.050	-.005	51	-.542	-.064	.526	-.194	-.065	-.131
9	-1.149	-.207	.912	-.064	-.062	-.006	52	-.684	-.077	.571	-.230	-.094	-.132
10	-1.144	-.255	.113	-.077	-.072	-.005	53	-.424	.072	.486	-.100	.009	-.109
11	-.247	-.252	-.004	-.074	-.074	-.001	54	-.157	-.150	.007	-.047	-.048	-.003
12	-.245	-.572	.111	-.166	-.166	-.004	54	-.145	-.164	-.019	-.088	-.047	-.002
13	-.255	-.244	.009	-.080	-.074	-.004	54	-.164	-.164	-.020	-.052	-.054	-.002
14	-.242	-.256	.026	-.074	-.080	-.005	57	-.168	-.172	.007	-.038	-.050	-.004
15	-.234	-.221	.016	-.075	-.075	-.006	54	-.180	-.172	.607	-.050	-.050	-.004
16	-.240	-.177	.067	-.077	-.062	-.015	54	-.515	.050	.565	-.111	-.002	-.114
17	-.247	-.042	.394	-.152	-.034	-.113	60	-.194	-.224	-.024	-.063	-.067	-.006
18	-.218	-1.140	.044	-.045	-.054	-.004	61	-.214	-.184	-.026	-.067	-.064	-.003
19	-.244	-.315	.032	-.141	-.132	-.009	62	-.624	.025	.653	-.194	-.039	-.149
20	-.154	-.124	.035	-.047	-.034	-.004	63	-.604	-.075	.533	-.210	-.064	-.144
21	-.240	-.167	.007	-.075	-.040	-.000	64	-.750	-.059	.691	-.264	-.079	-.144
22	-.242	-.031	.261	-.075	-.016	-.054	65	-.346	-.342	.039	-.190	-.162	-.114
23	-.140	-.134	.046	-.052	-.041	-.011	64	-.374	.042	.036	-.174	-.159	-.114
24	-.144	-.130	.116	-.045	-.042	-.005	67	-.550	-.249	.240	-.224	-.197	-.027
25	-.144	-.142	.014	-.044	-.042	-.002	64	-.354	-.334	.022	-.162	-.155	-.007
26	-.144	-.143	.012	-.044	-.044	-.001	64	-.354	-.345	.009	-.164	-.160	-.004
27	-.240	-.007	.247	-.075	-.012	-.061	70	-.512	-.244	.225	-.194	-.203	-.005
28	-.145	-.144	.009	-.050	-.050	-.000	71	-.405	-.377	.424	-.295	-.093	-.202
29	-.192	-.224	-.051	-.060	-.063	-.003	72	-.539	-.190	.349	-.177	-.002	-.175
30	-.236	-.244	-.024	-.075	-.074	-.004	73	-.624	-.049	.534	-.217	-.009	-.204
31	-.239	-.257	.014	-.074	-.061	-.003	74	-.576	-.374	.194	-.249	-.217	-.032
32	-.434	-.240	.173	-.149	-.141	-.024	75	-.556	-.509	.047	-.224	-.224	-.004
33	-.236	-.331	.005	-.142	-.141	-.001	76	-.591	-.233	.354	-.194	-.014	-.140
34	-.242	-.545	-.024	-.136	-.144	-.004	77	-.551	-.192	.560	-.179	-.002	-.177
35	-.254	-.253	.005	-.084	-.082	-.002	74	-.443	-.104	.377	-.149	-.007	-.144
36	-.240	-.154	-.007	-.059	-.060	-.001	79	-.525	-.203	.522	-.171	-.007	-.144
37	-.254	-.243	.005	-.044	-.042	-.002	80	-.517	-.119	.394	-.161	-.015	-.154
38	-.274	-.195	.543	-.151	-.062	-.104	81	-.634	-.244	.586	-.222	-.014	-.205
39	-.237	-.250	-.013	-.074	-.074	-.003	82	-.613	-.565	.044	-.272	-.224	-.044
40	-.245	-.042	.644	-.194	-.044	-.144	83	-.612	-.772	.715	-.231	-.024	-.259
41	-.240	-.261	-.021	-.074	-.083	-.005	84	-.745	-.095	.647	-.237	-.024	-.244
42	-.241	-.044	.572	-.214	-.044	-.144	85	-.441	-.051	.740	-.264	-.037	-.264
43	-.224	-.055	.564	-.220	-.052	-.144							

TABLE 11.- NACA 64A010 AIRFOIL: DYNAMIC PRESSURE DATA, INTEGRATED VALUES

P.O.I.	U ₁ A(0)		U ₁ A(1)		U ₁ A(2)		U ₁ A(3)		C ₁ A		C ₂ A	
	REAL	IMAG	REAL	IMAG	REAL	IMAG	REAL	IMAG	REAL	IMAG	REAL	IMAG
1	-2.421	-1.042	1.169	2.327	-.110	-.430	.112	.465	.112	.465	-.222	-.495
2	-2.747	.403	-.250	-.653	-.562	-.111	.593	.092	.593	.092	-1.155	-.202
3	-2.740	.748	-.600	-1.248	-.577	-.036	.600	.017	.600	.017	-1.177	-.054
4	-.204	.632	-.241	-.273	.004	.140	.002	-.076	.002	-.076	.007	-.216
5	-2.419	.622	-.341	-1.064	-.552	-.161	.507	.059	.507	.059	-1.039	-.219
6	-2.915	.567	-.406	-.973	-.607	-.003	.623	.022	.623	.022	-1.229	-.025
7	-3.202	.674	-.477	-1.144	-.676	.084	.695	-.040	.695	-.040	-1.370	.124
8	-3.562	.444	-.594	-.943	-.778	.077	.773	-.076	.773	-.076	-1.551	.153
9	-3.662	.255	-.626	-.841	-.777	.052	.822	-.048	.822	-.048	-1.620	.100
10	-3.514	.404	-.643	-.644	-.777	.054	.752	-.042	.752	-.042	-1.529	.094
11	-2.708	.340	-.540	-.540	-.558	.126	.517	-.077	.517	-.077	-1.074	-.202
12	-2.508	1.349	-.740	-.271	-.832	.047	.879	-.015	.879	-.015	-1.711	.072
13	-2.502	1.426	-.740	-3.012	-.799	.244	.814	-.142	.814	-.142	-1.613	.584
14	-.418	.723	-.434	-.266	-.618	.215	-.009	.200	-.009	.200	.027	.414
15	-2.020	.977	-.540	-1.704	-.540	-.127	.533	.173	.533	.173	-1.115	-.301
16	-2.236	1.444	-.775	-2.600	-.605	.043	.743	-.043	.743	-.043	-1.347	-.009
17	-2.006	1.834	-.845	-5.244	-.618	.160	.728	-.101	.728	-.101	-1.346	.262
18	-.502	.548	-.631	-1.174	-.607	.194	-.068	-.242	-.068	-.242	.075	.435
19	-1.554	1.134	-.949	-2.047	-.441	.013	.624	-.076	.624	-.076	-1.064	-.043
20												
21	-2.442	.214	-.455	-.574	-.529	-.158	.540	.095	.540	.095	-1.069	-.252
22	-2.401	.501	-.630	-1.130	-.524	-.040	.532	.040	.532	.040	-1.056	-.120
23	-.040	.414	-.378	-.746	-.009	.102	-.009	-.090	-.009	-.090	-.000	.191
24												
25												
26												
27	-2.575	.422	-.516	-.934	-.675	.012	.662	-.054	.662	-.054	-1.334	.065
28	-3.175	.574	-.471	-1.047	-.705	.046	.654	-.024	.654	-.024	-1.459	.071
29	-3.147	.515	-.521	-1.034	-.704	.027	.671	-.031	.671	-.031	-1.374	.054
30	-2.491	.431	-.195	-.627	-.593	-.105	.543	.104	.543	.104	-1.155	-.208
31	-2.405	.414	-.269	-.644	-.599	-.105	.546	.115	.546	.115	-1.155	-.220
32	-2.723	.337	-.340	-.714	-.599	.113	.570	.103	.570	.103	-1.164	-.214
33	-2.422	.475	-.193	-.546	-.627	-.103	.591	.104	.591	.104	-1.219	-.207
34	-2.612	.621	-.708	-.546	-.588	.052	.574	.047	.574	.047	-1.162	.094
35	-2.654	.594	-.647	-1.329	-.599	-.054	.571	.044	.571	.044	-1.149	.112
36	-.182	.672	-.152	-1.241	-.540	.154	-.007	-.110	-.007	-.110	-.264	.264
37	-2.577	.044	-.141	-.227	-.532	-.216	.535	.206	.535	.206	-1.047	-.422
38	-2.440	.433	-.442	-.915	-.524	-.131	.540	.134	.540	.134	-1.043	-.265

TABLE 11.- Continued.

D.I.	IU,A(0)		IL,A(0)		CL,A		IU,A(1)		IL,A(1)		CL,A	
	REAL	IMAG	REAL	IMAG	REAL	IMAG	REAL	IMAG	REAL	IMAG	REAL	IMAG
39	-2.869	.465	2.562	-.430	5.731	-.895	-.646	-.027	-.058	-1.267	-.081	
40	.099	-.454	-2.516	-.372	-2.215	-.824	.003	.107	-.073	.018	.179	
41	.012	.336	-.028	-.331	-.039	-.865	-.007	.080	-.067	-.004	.147	
42	-.016	-.216	.014	-.224	.034	-.880	-.006	.088	-.049	-.011	.098	
43	-3.410	.332	3.414	-.364	6.624	-.696	-.782	.031	-.032	-1.529	.063	
44	-3.155	.894	3.185	-.509	6.340	-1.003	-.710	.018	-.018	-1.410	.037	
45	-2.554	.568	2.648	-.703	5.242	-1.291	-.541	-.112	.091	-1.124	-.203	
46	-2.413	.903	2.423	-.901	4.836	-1.804	-.597	-.055	.142	-1.133	-.197	
47	-3.709	1.621	3.604	-1.716	7.116	-3.536	-.974	.335	-.218	-1.867	.553	
48	-2.647	1.156	2.586	-1.453	5.232	-2.611	-.794	.042	-.054	-1.576	.095	
49	-3.414	1.716	3.377	-1.687	6.795	-3.403	-1.050	.315	-.222	-1.894	.537	
50	-2.452	1.214	2.477	-1.333	4.924	-2.751	-.701	.047	-.031	-1.468	.078	
51	-4.577	.615	4.739	-.765	9.316	-1.378	-1.154	.108	-.138	-2.330	.242	
52	-4.255	1.224	4.347	-1.251	8.622	-2.479	-1.056	.149	-.203	-2.160	.367	
53	-3.365	1.717	3.405	-1.670	6.790	-3.347	-.860	.247	-.213	-1.758	.459	
54	-2.526	1.423	2.478	-1.422	5.403	-2.845	-.637	.124	-.082	-1.460	.213	
55	-2.343	1.233	2.504	-1.248	4.847	-2.521	-.652	.017	-.039	-1.411	-.022	
56	-2.102	.847	2.273	-1.010	4.375	-1.497	-.556	-.241	.066	-1.297	-.309	
57	-3.031	.105	1.604	-.800	4.635	-.495	-.860	-.515	.262	-1.533	-.797	
58	-1.413	.992	1.915	-1.373	3.728	-2.365	-.526	-.054	-.082	-1.207	.027	
59	-2.145	1.529	2.249	-1.526	4.392	-3.057	-.640	.130	-.067	-1.343	.197	
60	-3.255	1.262	3.299	-1.524	6.555	-3.721	-.447	.298	-.256	-1.736	.554	
61	-4.144	1.360	4.357	-1.349	8.595	-2.704	-1.057	.222	-.227	-2.164	.449	
62	-4.520	.675	4.727	-.775	9.247	-1.450	-1.126	.130	-.139	-2.320	.264	
63	-1.971	1.735	2.273	-1.405	4.245	-3.140	-.691	.215	-.034	-1.419	.249	
64	-2.142	1.143	2.349	-1.039	4.541	-2.222	-.664	.019	.077	-1.396	-.054	
65	-3.114	1.650	3.025	-1.463	6.141	-3.113	-.494	.294	-.163	-1.774	.474	
66	.392	.522	-.293	-.316	-.644	-.838	.016	.165	-.007	-1.174	.300	
67	.145	.351	-.230	-.361	-.425	-.712	-.001	.103	-.123	.022	.226	
68	.050	.179	-.060	-.180	-.110	-.354	-.006	.052	-.043	-.004	.095	
69	.014	.213	-.009	-.242	-.025	-.455	-.007	.053	-.054	-.015	.104	
70	-.047	.051	.047	-.057	.095	-.104	-.016	.012	-.014	-.030	.024	
71	-1.497	.909	2.097	-.993	3.995	-1.902	-.745	.402	-.348	-1.653	.766	
72	-1.749	.719	2.104	-1.043	3.889	-1.802	-.742	.251	-.420	-1.644	.671	
73	-2.779	1.573	3.120	-1.443	5.449	-3.056	-.746	.162	-.147	-1.653	.329	
74												
75	-4.676	1.364	4.537	-1.264	9.213	-2.628	-1.208	.259	-.228	-2.431	.466	
76	-4.540	1.271	4.506	-1.254	9.046	-2.530	-1.267	.256	-.250	-2.521	.508	

TABLE 11.- Concluded.

N.I.	IU,A(0)		IL,A(0)		CL,A		IU,A(1)		IL,A(1)		CM,A	
	REAL	IMAG	REAL	IMAG	REAL	IMAG	REAL	IMAG	REAL	IMAG	REAL	IMAG
77	-2.641	1.304	2.638	-1.209	5.279	-2.517	-0.800	.054	.888	-0.024	-1.688	.062
78												
79	-2.407	-1.794	.546	1.894	2.953	3.688	-1.610	-.975	-.693	1.233	-.957	-2.204
80	-7.749	.627	5.042	2.436	12.411	1.609	-3.954	2.005	2.337	2.405	-6.291	.400
81	-1.936	-1.934	.549	1.969	2.484	3.903	-1.522	-.962	-.683	1.287	-.839	-2.249
82	-4.108	1.800	2.992	1.022	7.099	-7.776	-1.929	1.595	1.030	1.018	-2.954	.577
83	-4.156	1.754	3.110	.995	7.246	-7.763	-1.946	1.581	1.072	1.036	-3.014	.506
84	-6.609	1.257	4.458	1.360	11.067	.103	-3.368	1.906	2.112	1.778	-5.480	.124
85	-1.301	-.357	.360	.595	1.681	.751	-.825	-.214	-.534	.263	-.291	-.677
86	-1.479	-.764	.367	.703	1.684	1.471	-.991	-.440	-.581	.450	-.410	-.690
87	-2.562	-1.521	.904	1.800	3.266	3.321	-1.545	-.728	-.400	1.199	-1.186	-1.927
88	-4.067	-1.007	2.659	2.000	6.726	3.007	-2.477	-.049	.705	1.704	-3.142	-1.757
89	-5.331	1.637	4.017	1.232	9.349	-.406	-2.553	1.702	1.852	1.402	-4.405	.300
90	-3.003	2.112	3.421	.153	6.424	-1.959	-.860	1.751	1.593	.499	-2.453	1.252
91	-3.293	3.001	3.759	.245	7.052	-.755	-1.041	1.004	1.631	.691	-2.712	.313
92	-5.022	2.495	3.879	.302	8.901	-2.193	-2.237	2.104	1.891	.863	-4.127	1.241
93	.267	3.151	.705	-2.009	.437	-5.159	.602	1.603	.797	-.979	-.195	2.532
94	-2.592	2.441	3.140	-.587	5.772	-3.464	-.476	1.915	1.573	.060	-2.049	1.856
95	-2.693	-1.053	1.470	1.349	4.163	2.442	-1.556	-.516	.124	.975	-1.640	-1.493
96	-4.664	2.983	2.413	.493	7.041	-2.490	-1.706	1.383	.911	.567	-2.617	.617
97	-4.423	1.451	1.823	-.196	6.286	-1.687	-.339	-.424	.470	.119	-.809	-.543
98	-2.979	.604	2.014	-.164	4.993	-.768	-.510	-.102	.542	.107	-1.052	-.209
99	-2.876	.930	1.955	-.360	4.831	-1.290	-.513	-.032	.550	.073	-1.063	-.105
100	.164	.605	.114	-.386	-.279	-.991	-.011	.110	-.031	-.100	.019	.210
101	-2.654	.762	1.954	-.275	4.615	-1.037	-.438	-.140	.537	.116	-.975	-.257
102	-2.630	.577	2.001	-.254	4.631	-.835	-.470	-.191	.555	.124	-1.024	-.319
103	-3.965	1.345	3.243	.753	7.208	-.642	-1.785	1.122	1.559	1.034	-3.184	.088
104	-3.220	.561	2.222	.026	5.443	-1.535	-.549	-.124	.543	.121	-1.132	-.245
105	-3.076	.903	2.059	-.353	5.135	-1.254	-.538	-.060	.558	.046	-1.096	-.104
106	.153	.522	-.075	-.334	-.228	-.856	-.006	-.097	-.008	-.002	-.002	.184
107	-2.951	.742	2.019	-.247	4.970	-1.029	-.488	-.148	.551	.123	-1.039	-.271
108	-9.021	4.839	2.047	-.204	11.104	-5.042	-.708	-.045	.574	.136	-1.244	-.221
109	-4.442	2.303	2.234	.359	6.675	-1.948	-1.649	1.000	.737	.478	-2.361	.522
110	-4.262	1.924	3.432	1.023	7.694	-.905	-2.116	1.476	1.204	1.137	-3.320	.339
111	.144	1.306	.363	-.750	.219	-2.056	.236	.794	.439	-.279	-.203	1.073
112	-1.921	2.373	3.379	.013	5.300	-2.360	-.596	1.543	1.380	.470	-1.774	1.074
113	-1.514	.947	3.116	-.856	4.430	-1.883	-.291	.486	1.461	-.869	-1.751	1.175
114	-1.256	1.256	2.261	-1.304	3.497	-2.540	-.428	.670	1.067	-.736	-1.695	1.407

TABLE 12.- NLR 7301 AIRFOIL: DYNAMIC PRESSURE DATA, INTEGRATED VALUES

O.I.	IU,A(U)		IU,A(I)		O.I.	IU,A(O)		IU,A(I)	
	REAL	IMAG	REAL	IMAG		REAL	IMAG	REAL	IMAG
115	-5.194	.459	-1.009	.060	162	-2.899	1.607	-2.537	-.100
116	-4.949	.437	-.992	.107	163	-4.743	1.271	-4.806	.171
117	-4.542	1.160	-.881	.049	164	-2.784	1.891	-2.587	.098
118	-3.606	1.123	-.691	.074	165	-.060	.316	-.095	.050
119	-3.284	.809	-.586	-.107	166	.217	.599	-.069	.109
120	-4.963	.754	-.926	.120	167	-3.342	.311	-.769	.074
121	-3.606	1.094	-.622	.024	168	-3.342	.490	-4.462	.073
122	-1.486	.200	-.232	.021	169	-3.067	.745	-.577	.087
123	-3.519	1.128	-.523	.032	170	-2.484	.743	-.427	.007
124	-6.161	1.304	-1.132	.313	171	-2.296	.491	-.414	-.172
125	-5.233	2.135	-.902	.450	172	-3.407	.465	-.538	.035
126	9.497	4.047	4.776	1.196	173	-2.489	.747	-4.471	-.000
127	-5.313	1.851	-.930	.307	174	-3.386	.493	-.476	.089
128	-2.720	1.943	-.467	.041	175	-.504	.774	-.445	.029
129	-5.296	1.701	-.949	.243	176	6.033	.270	-.054	.117
130	-2.873	2.089	-.588	.140	177	.110	.437	-.042	.057
131	-6.403	1.439	-1.952	.374	178	-4.514	1.345	-.408	.179
132	-5.717	2.377	-1.430	.637	179	-2.439	1.642	-.469	-.044
133	-3.433	2.697	-1.235	.756	180	-4.902	1.690	-.483	.304
134	-2.343	2.821	-.889	.991	181	-2.717	2.022	-.428	.044
135	-.924	1.746	-.007	.664	182	.001	.231	-.045	.045
136	-5.346	1.941	-1.850	.491	183	.244	.481	-.026	.099
137	-2.280	2.504	-.470	.723	184	-4.949	.645	-.760	.069
138	-4.664	1.220	-1.603	.299	185	-3.391	1.034	-.562	-.002
139	-2.460	2.495	-.929	.766	186	-4.256	.590	-.682	.061
140	-.412	.151	.556	-.007	187	-3.261	1.003	-.524	.014
141	-.562	-.393	.146	-.410	188	-.052	.228	-.080	.049
142	-1.056	.254	.101	.014	189	.007	.601	-.040	.075
143	.115	.841	.723	.259	190	-5.626	3.177	-1.922	1.122
144	-5.229	2.070	-1.205	.305	191	-1.450	2.341	-.610	.797
145	-5.930	1.144	-1.362	.149	192	-4.693	1.434	-1.654	.505
146	-3.685	2.403	-1.012	.434	193	-1.984	2.351	-.623	.709
147	-2.504	2.662	-.817	.374	194	.072	.299	.006	.117
148	-2.205	2.209	-.430	.391	195	-2.341	.482	-.728	.125
149	-1.171	1.544	-.379	.375	196	-1.357	.687	-.348	.279
150	-4.960	1.431	-1.248	.164	197	-3.818	.642	-.635	.017
151	-2.271	2.443	-.435	.440	198	-2.714	1.531	-.769	-.081
152	-4.147	.893	-1.084	.034	199	-3.566	.695	-.485	-.016
153	-2.471	2.214	-1.065	.386	200	-2.516	1.462	-.702	-.143
154	.080	.294	.005	.053	201	-3.134	-.144	-.666	-.214
155	.340	.456	-.018	.165	202	-.052	-.045	-.012	-.014
156	-4.444	.601	-.576	.060	203	.087	.274	-.003	.093
157	-4.242	1.022	-.524	.067	204	-5.310	.541	-2.071	-.003
158	-1.584	1.474	-.430	.031	205	-3.728	2.718	-1.524	.905
159	-2.456	1.540	-.476	-.127	206	-4.889	.957	-1.482	.203
160	-2.113	1.722	-.463	-.146	207	-3.407	2.955	-1.296	1.077
161	-4.442	1.242	-.724	.133	208	.022	.226	-.003	.045
					209	.306	.502	-.107	-.200

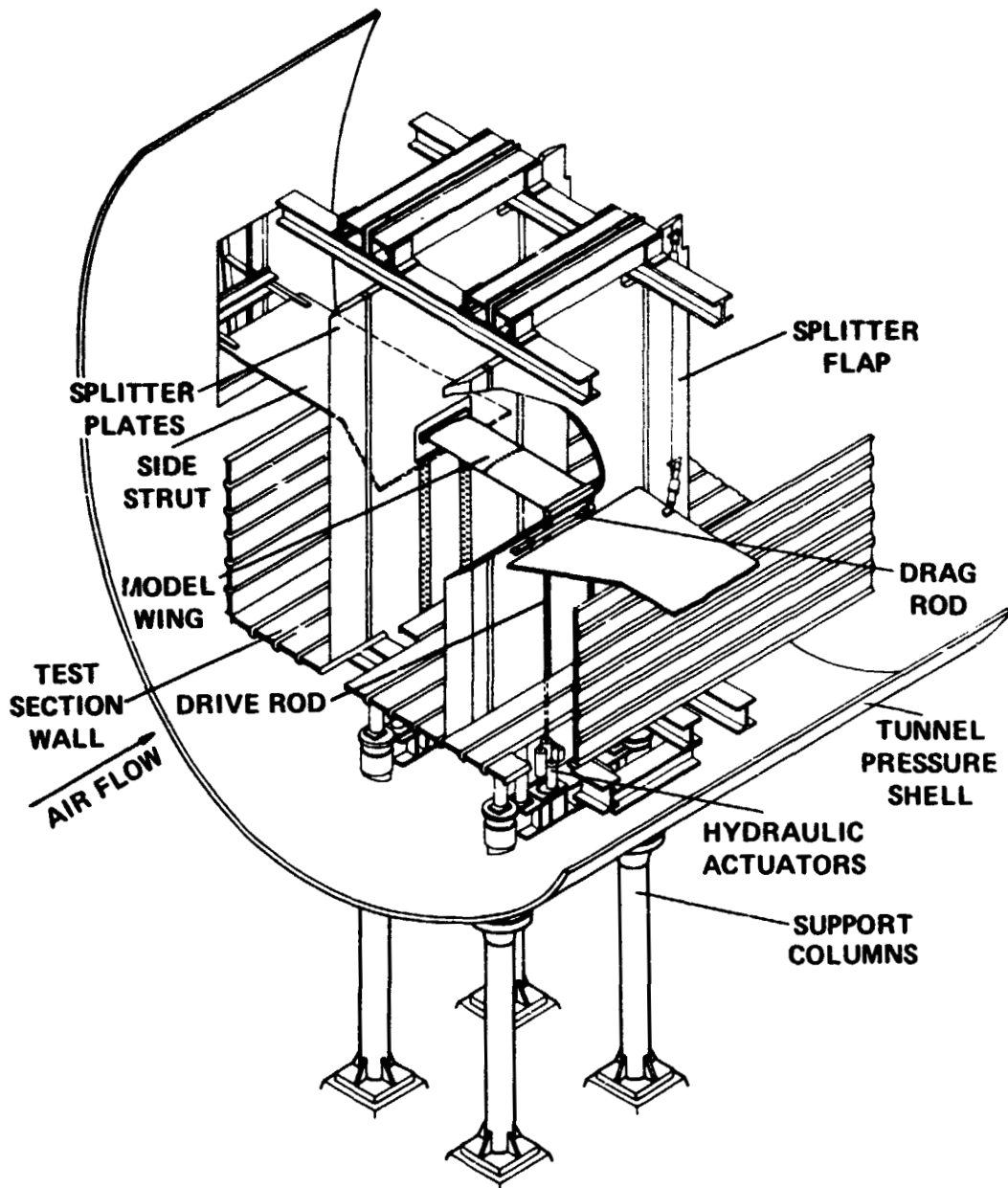


Figure 1.- General arrangement of oscillating airfoil test apparatus in NASA-Ames 11- by 11-Foot Transonic Wind Tunnel.

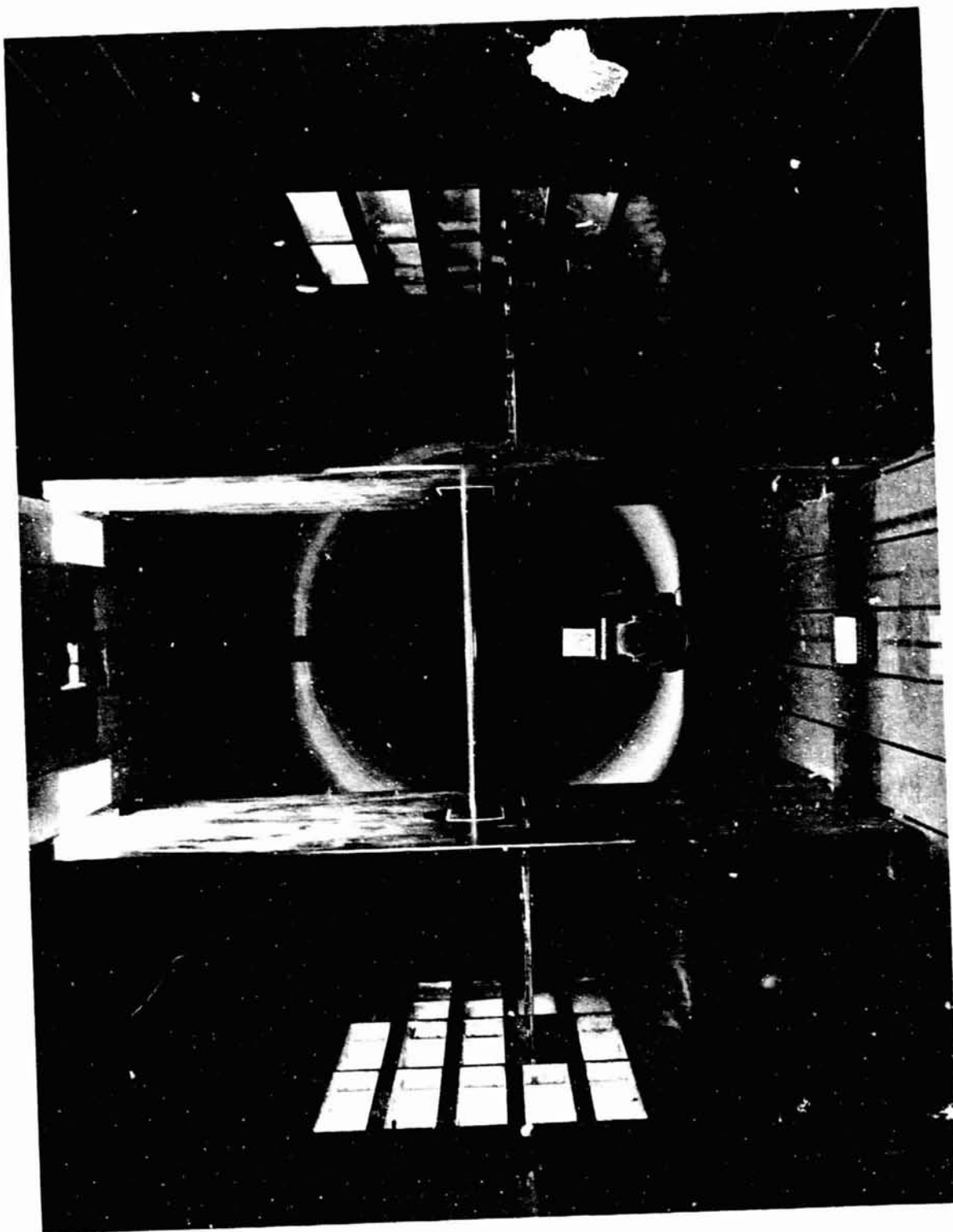


Figure 2.- Wing model and splitter plates in wind tunnel test section.

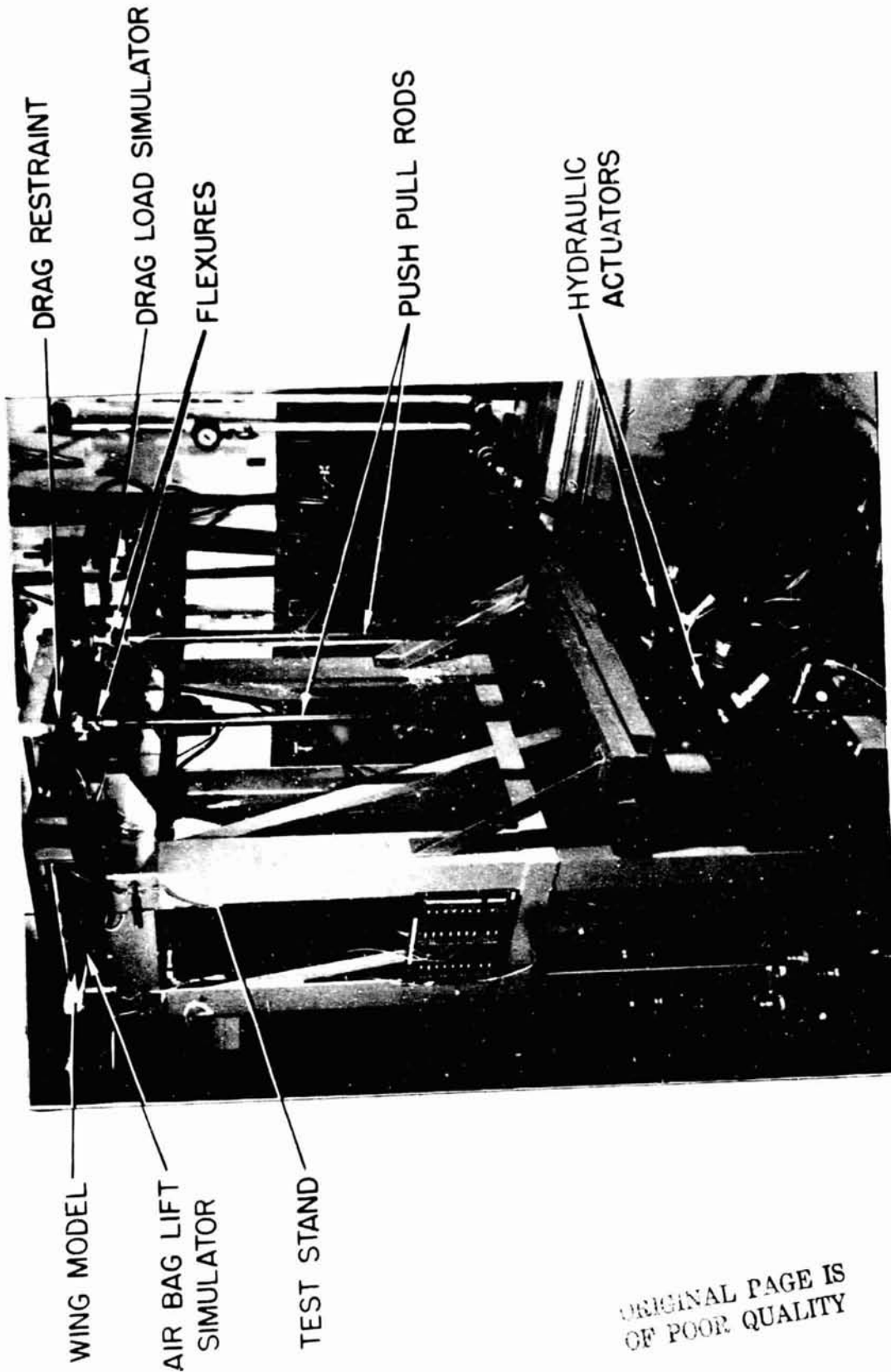


Figure 3.- Wing model and push-pull mechanism on test stand.

ORIGINAL PAGE IS
OF POOR QUALITY

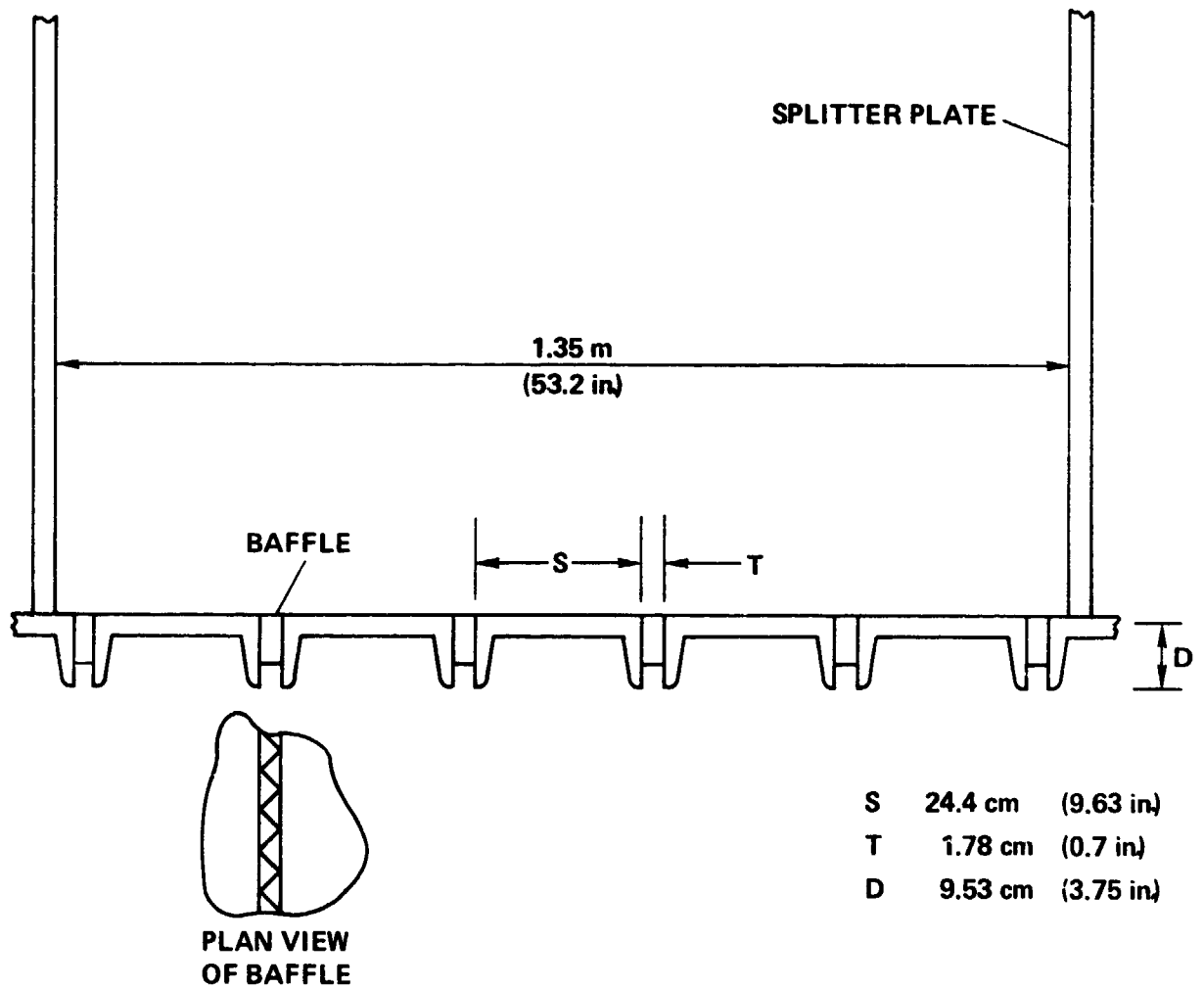


Figure 4.- Ventilated wall geometry of NASA-Ames 11- by 11-Foot Transonic Wind Tunnel.

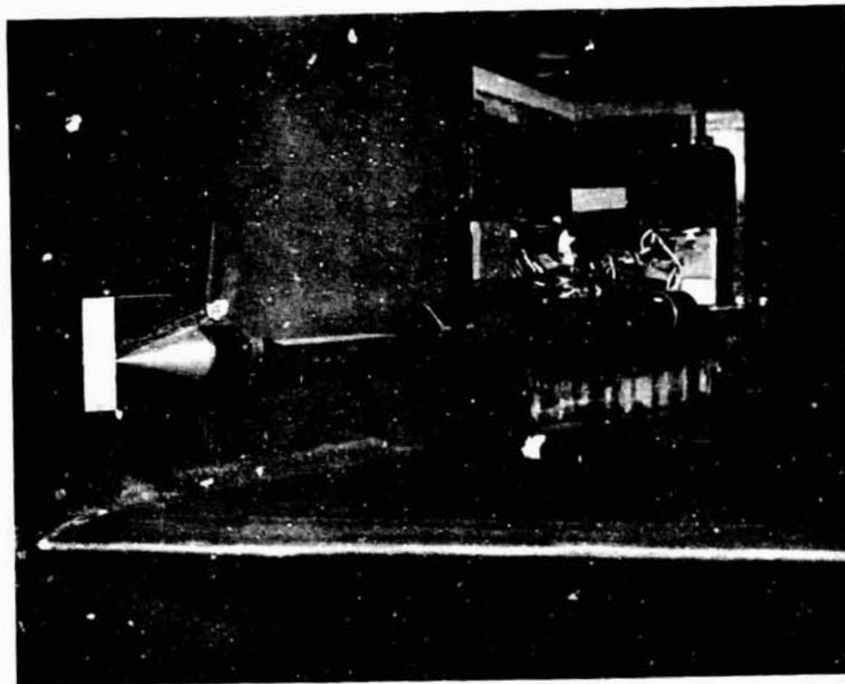


Figure 5.- Detail of drag restraint and side strut support.

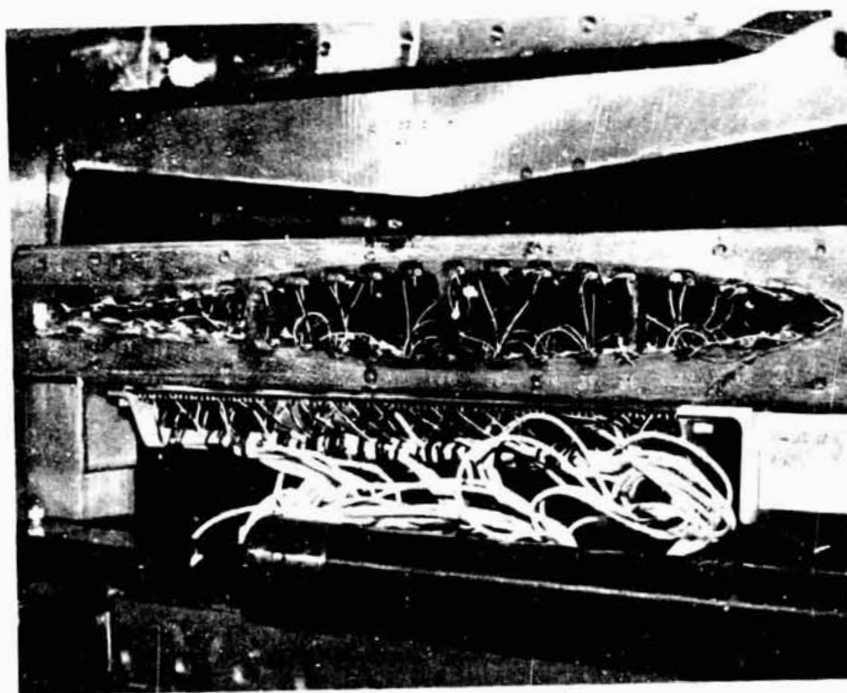


Figure 6.- Wing end section with dynamic instrumentation leads.

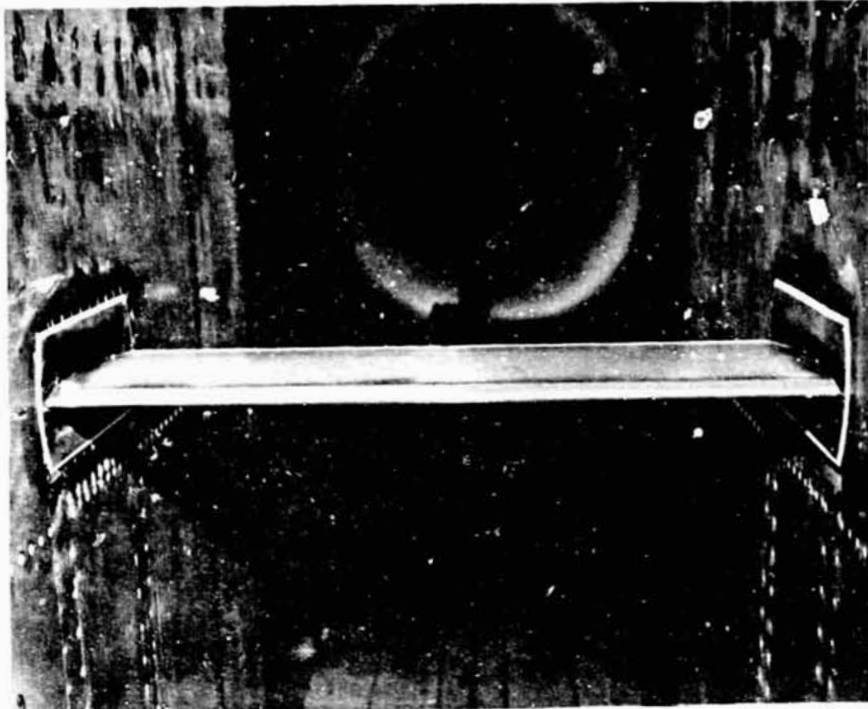


Figure 7.- NACA 64A010 model installati

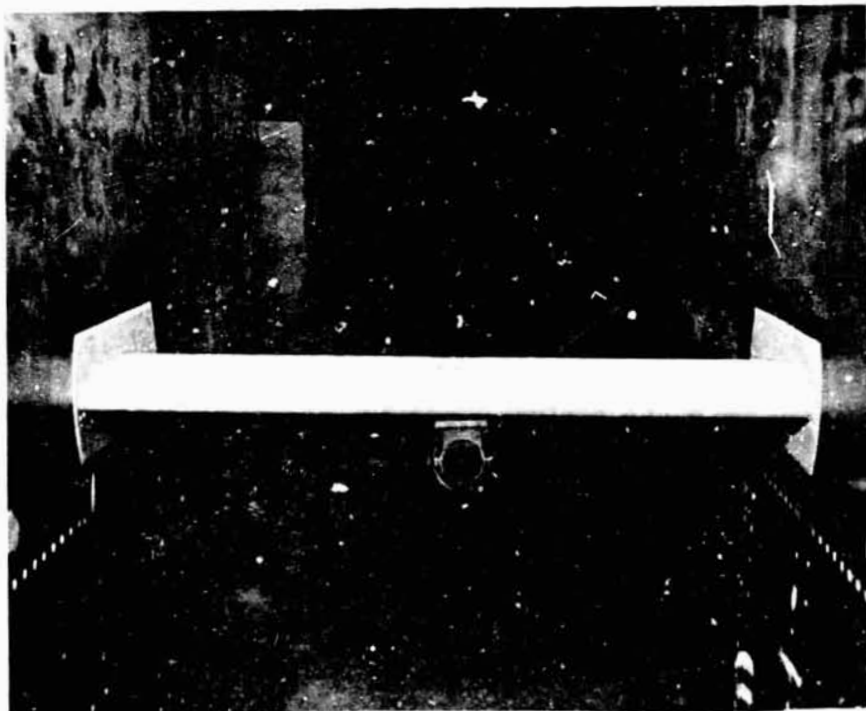
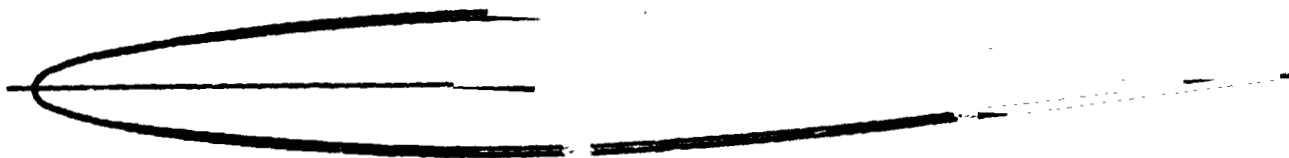


Figure 8.- NLR 7301 model installation.

ORIGINAL PAGE IS
OF POOR QUALITY

NACA 64A010



NLR 7301

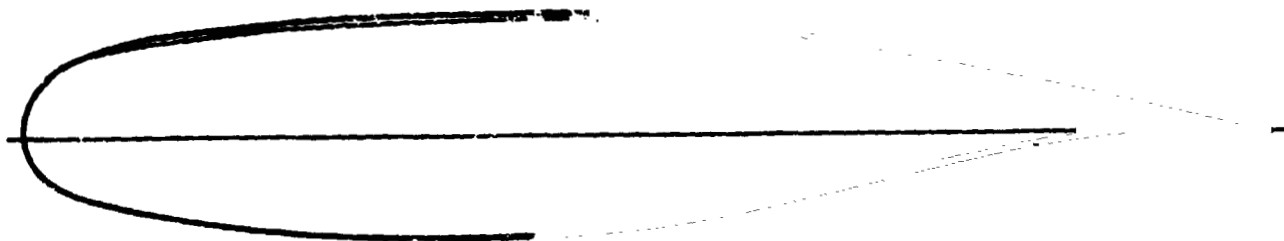


Figure 9.- Sketch of airfoil profiles used in test program.

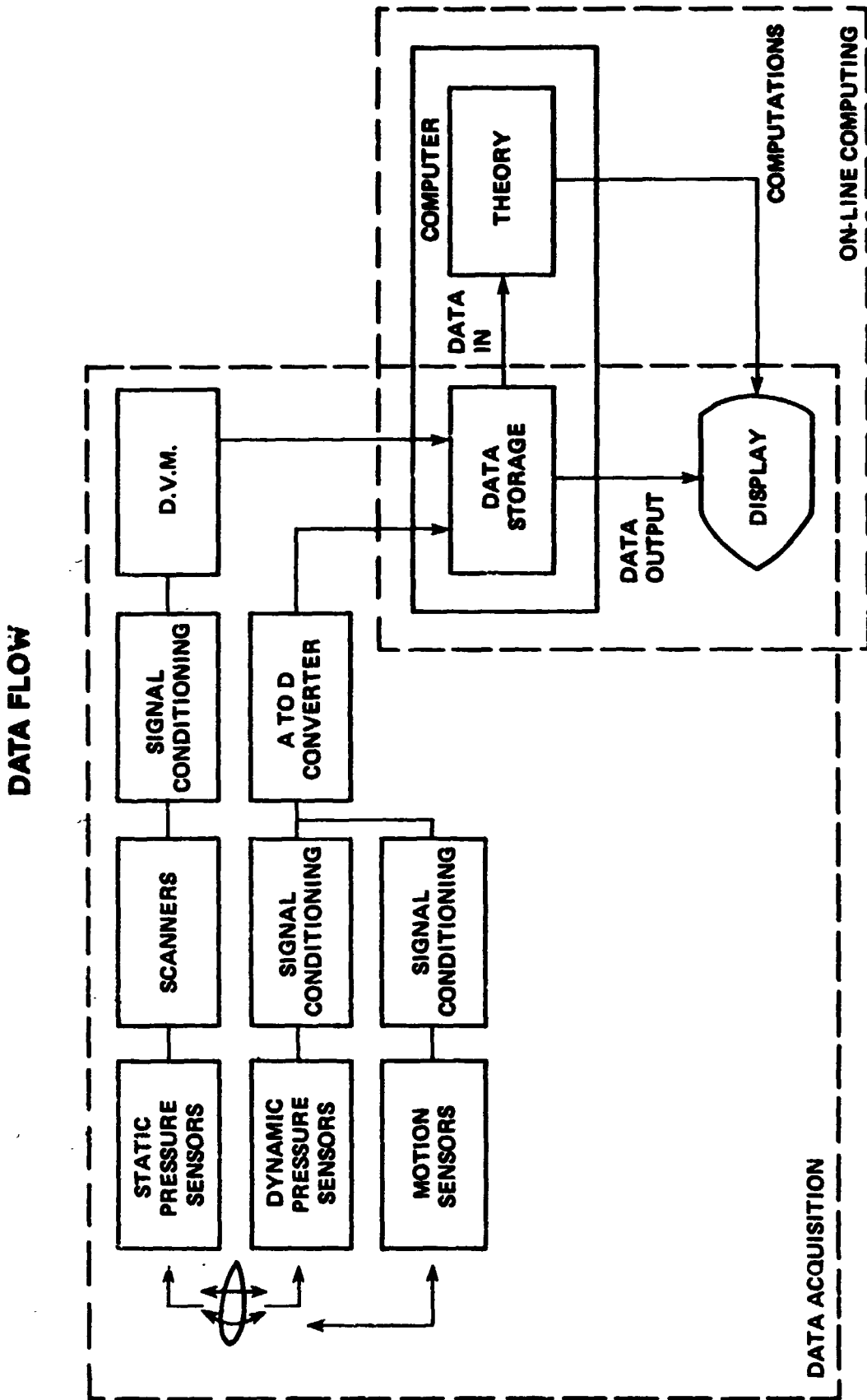


Figure 10.- Block diagram of the data acquisition scheme for the oscillating airfoil experiment.

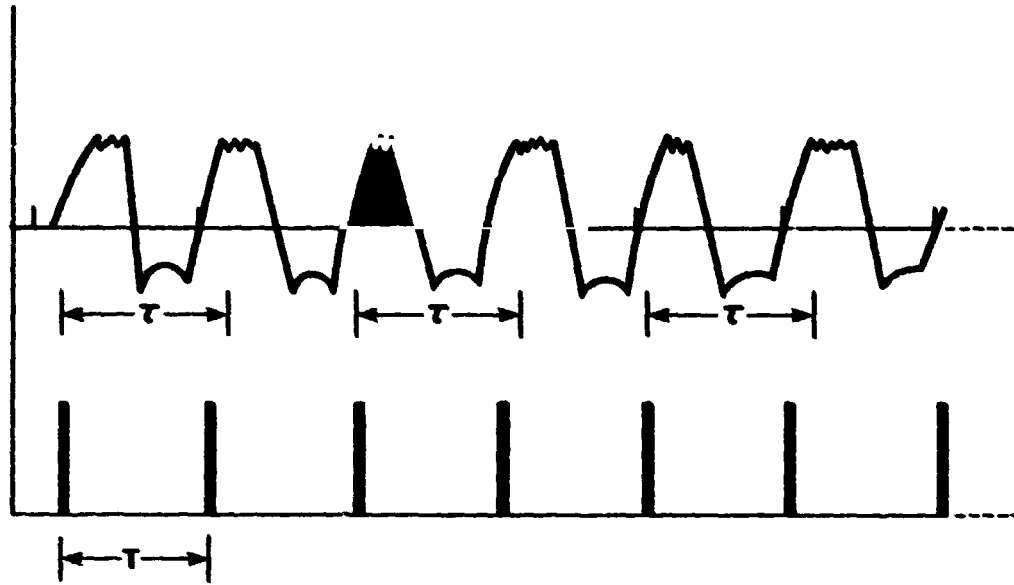


Figure 11.- Timing diagram for dynamic data acquisition. Upper trace: dynamic data signal, τ , is slight'y greater than one period. Lower trace: trigger for analog-to-digital conversion, $T = \text{period}$, $n = 2$.

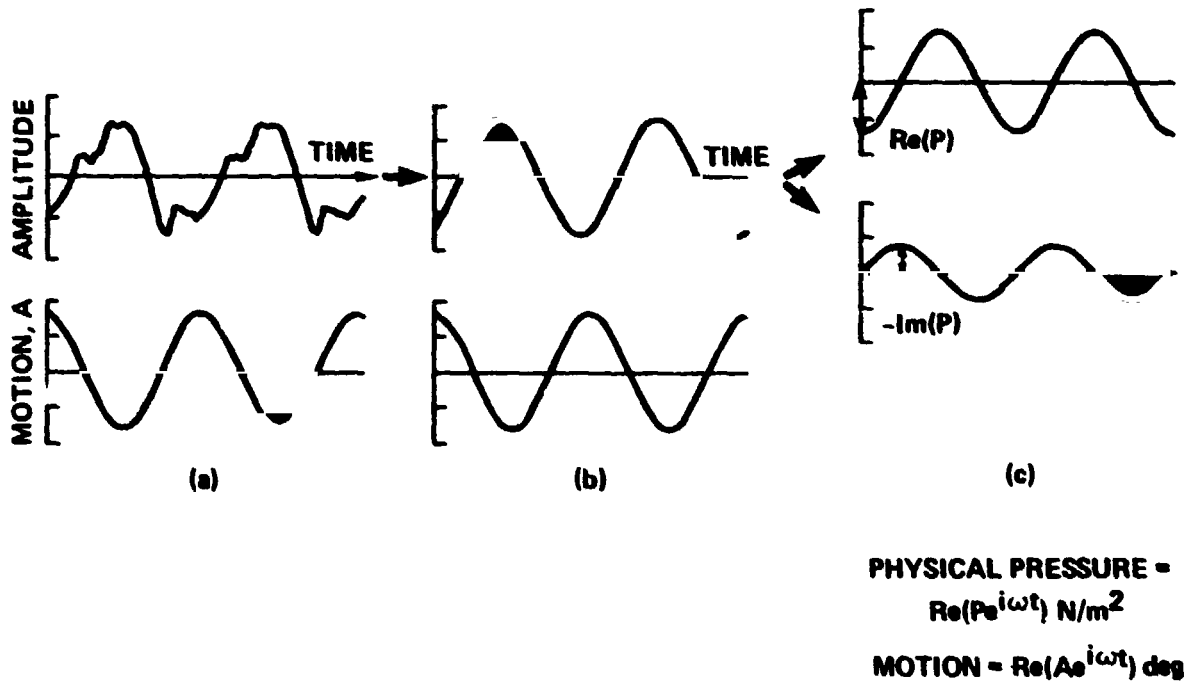
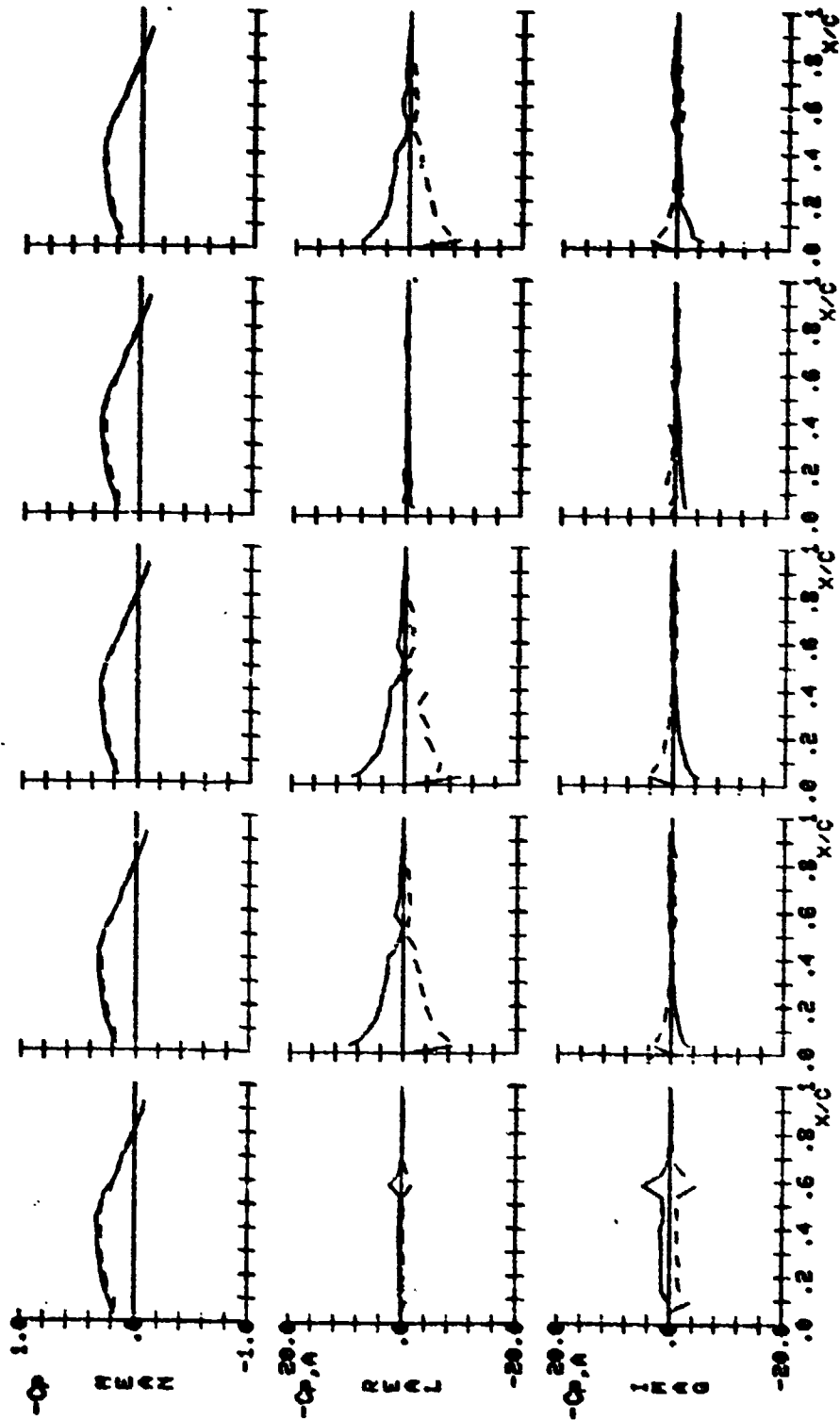
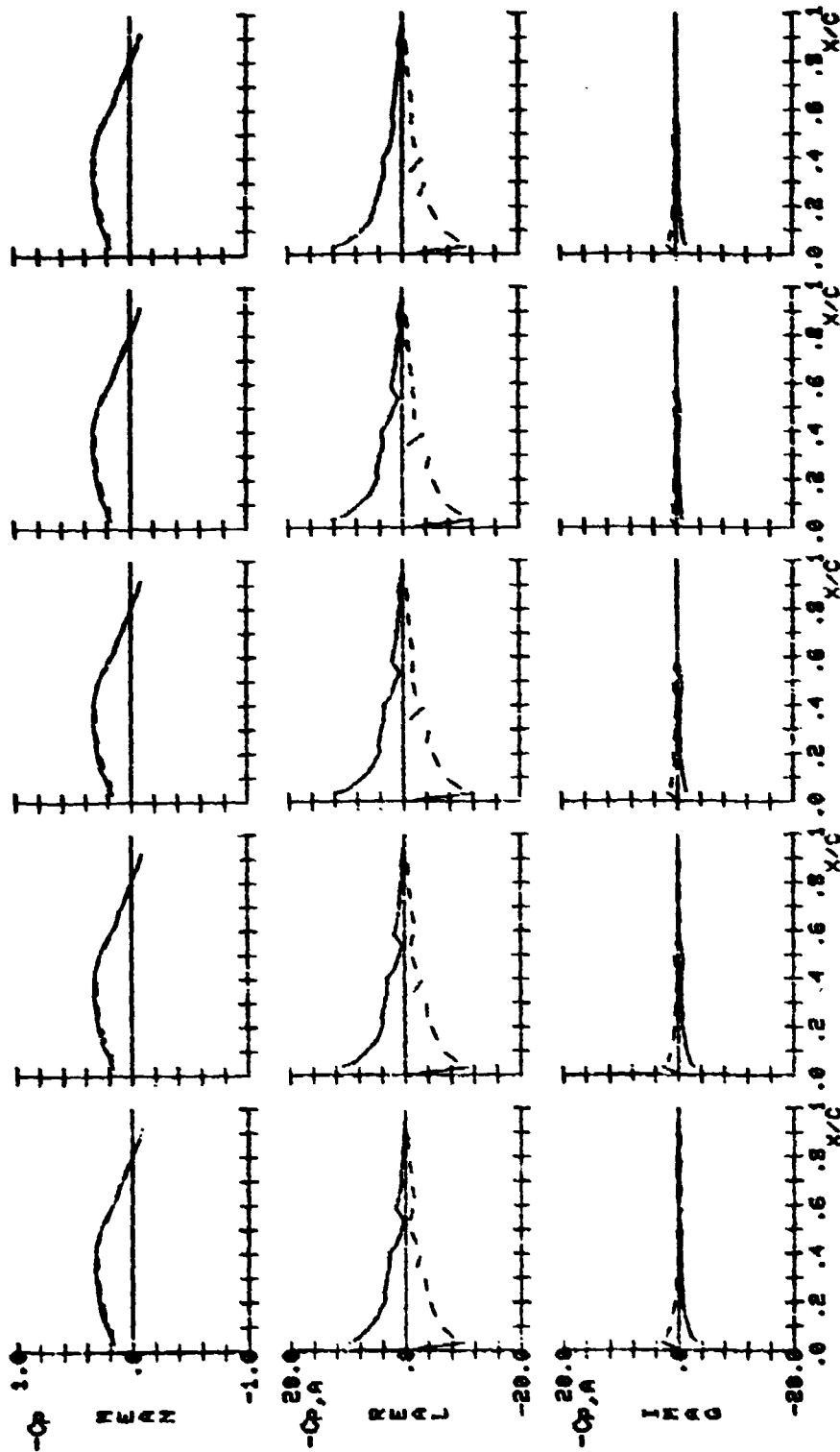


Figure 12.- Decomposition of pressure time histories into first harmonic complex amplitudes. (a) actual motion, (b) fundamental frequency component, (c) real and imaginary parts (amplitudes proportional to cosine and sine waves, respectively).



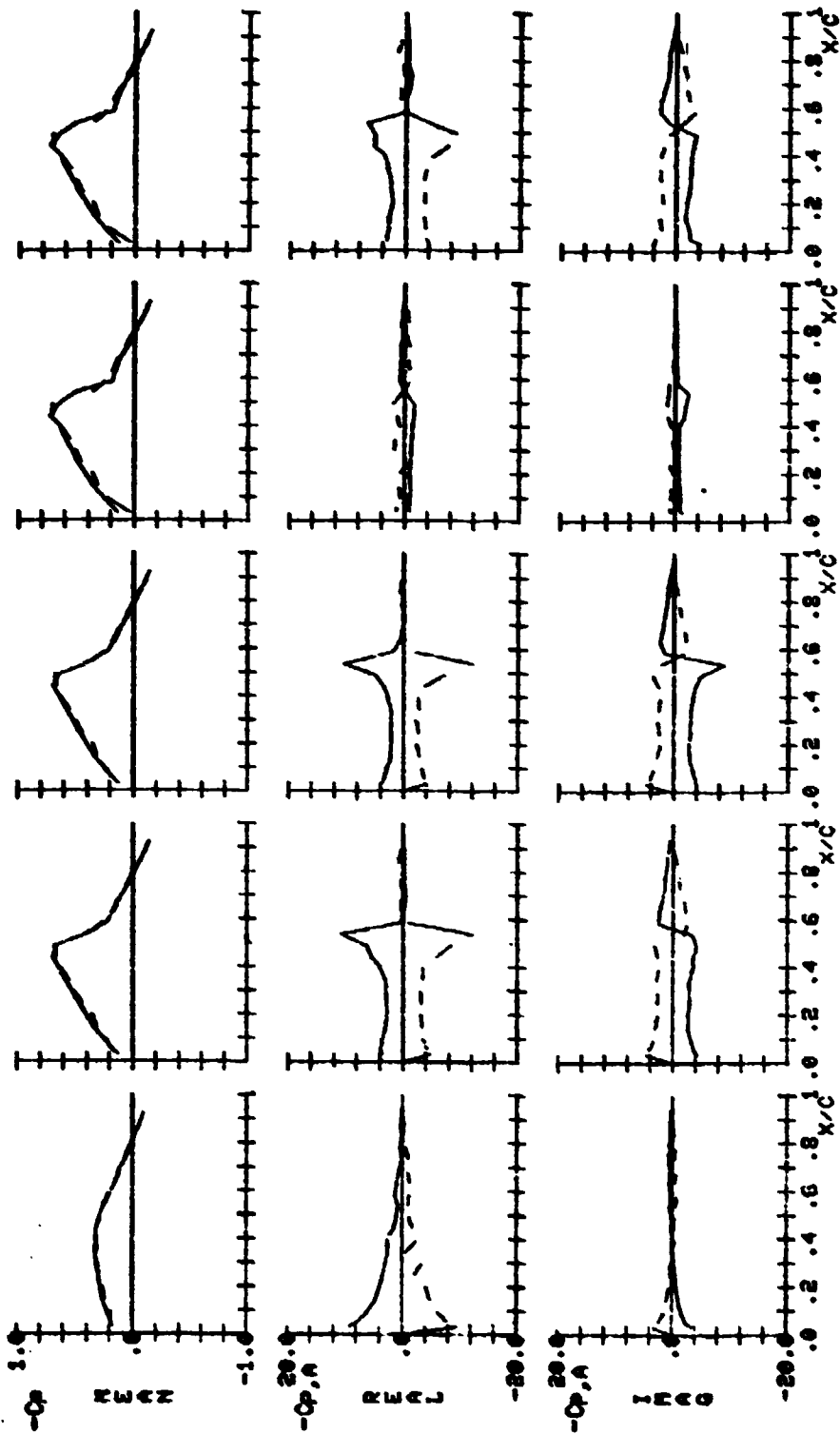
D.I. = 1 D.I. = 2 D.I. = 3 D.I. = 4 D.I. = 5

Figure 13.- Pressure coefficient data: static and first harmonic complex amplitudes (note: dashed lines refer to lower surface).



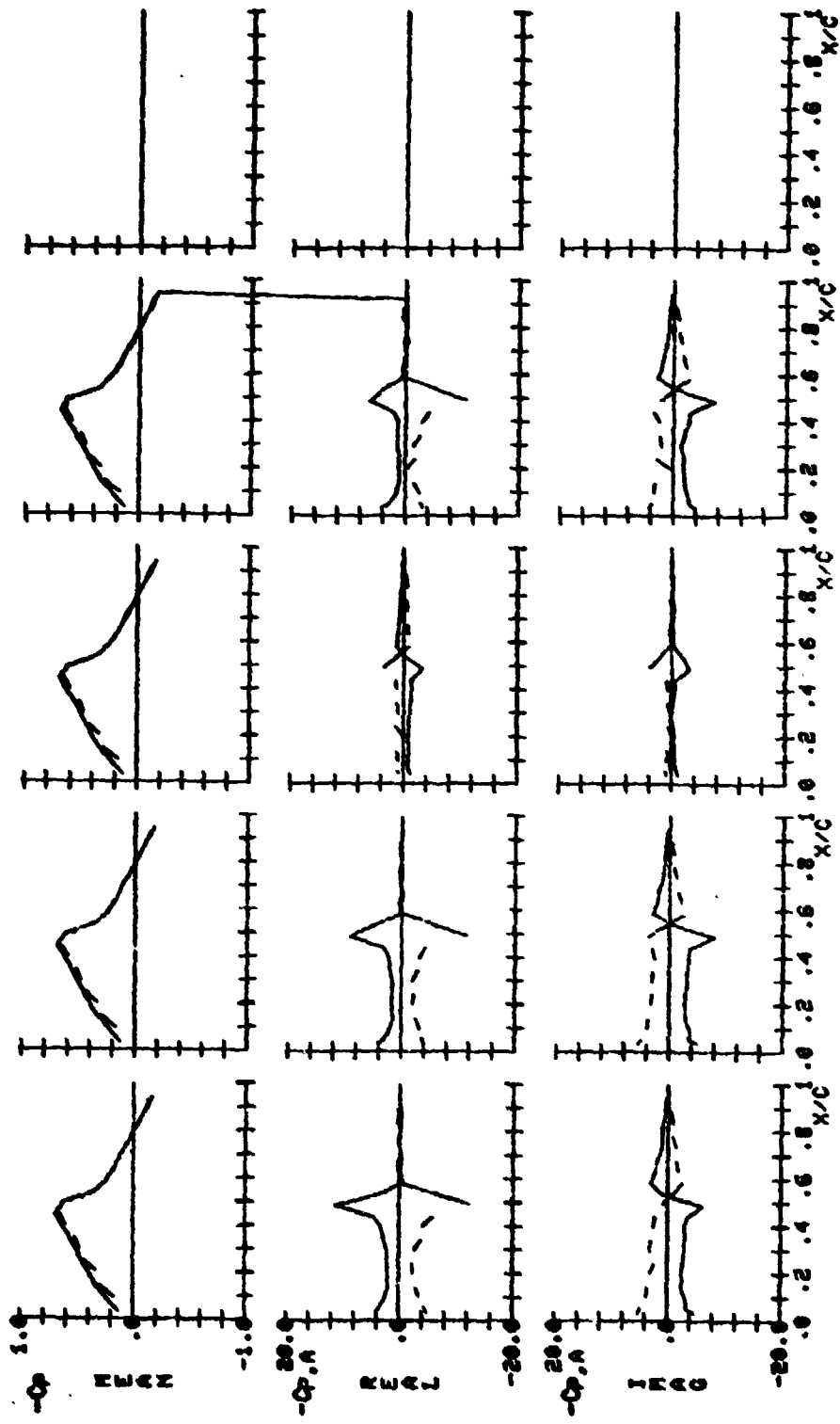
D.I. = 6 D.I. = 7 D.I. = 8 D.I. = 9 D.I. = 10

Figure 13.- Continued.



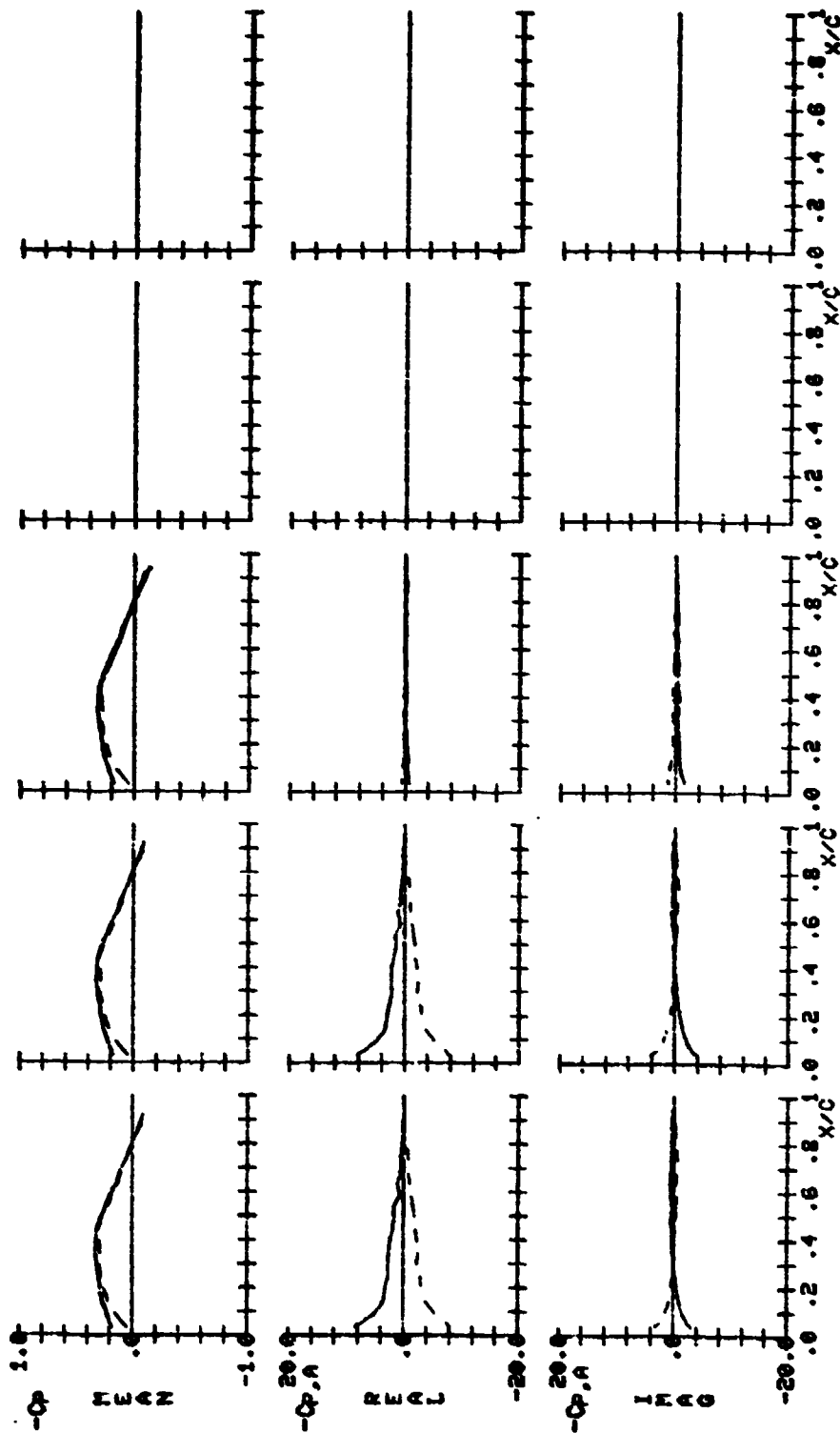
D.I. = 11 D.I. = 12 D.I. = 13 D.I. = 14 D.I. = 15

Figure 13.- Continued.



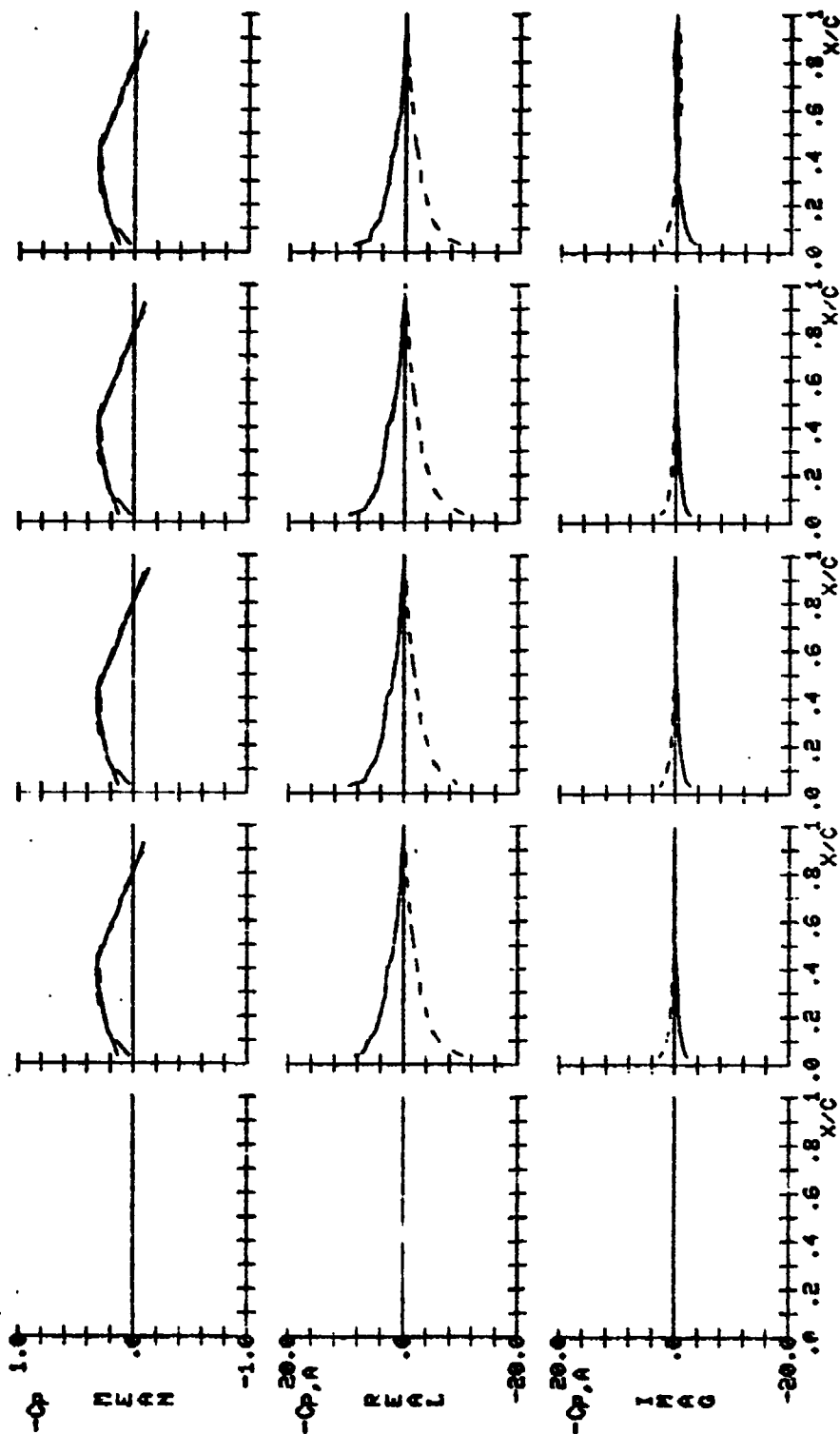
D.I. = 16 D.I. = 17 D.I. = 18 D.I. = 19 D.I. = 20

Figure 13.- Continued.



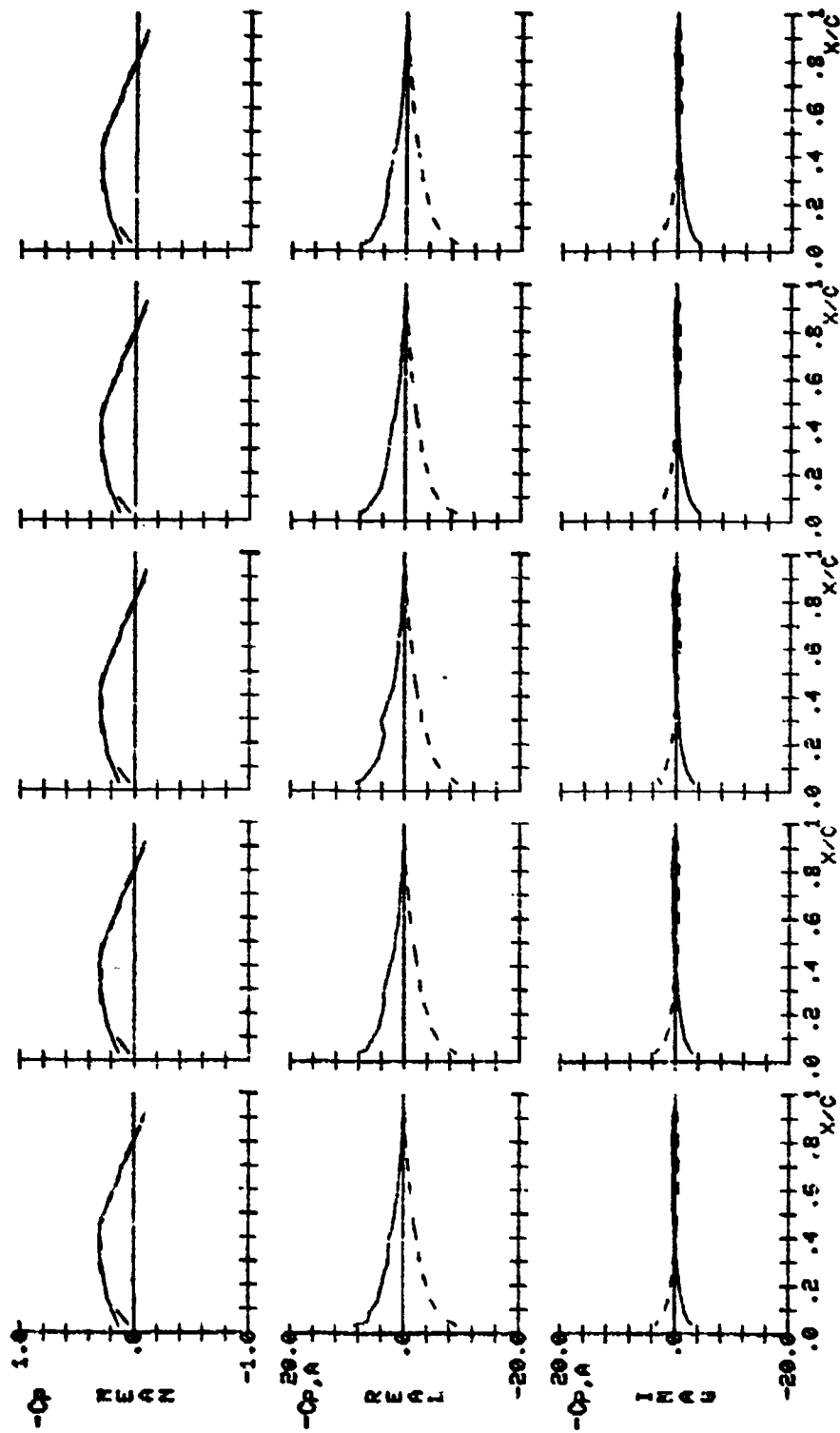
D.I. = 21 D.I. = 22 D.I. = 23 D.I. = 24 D.I. = 25

Figure 13.- Continued.



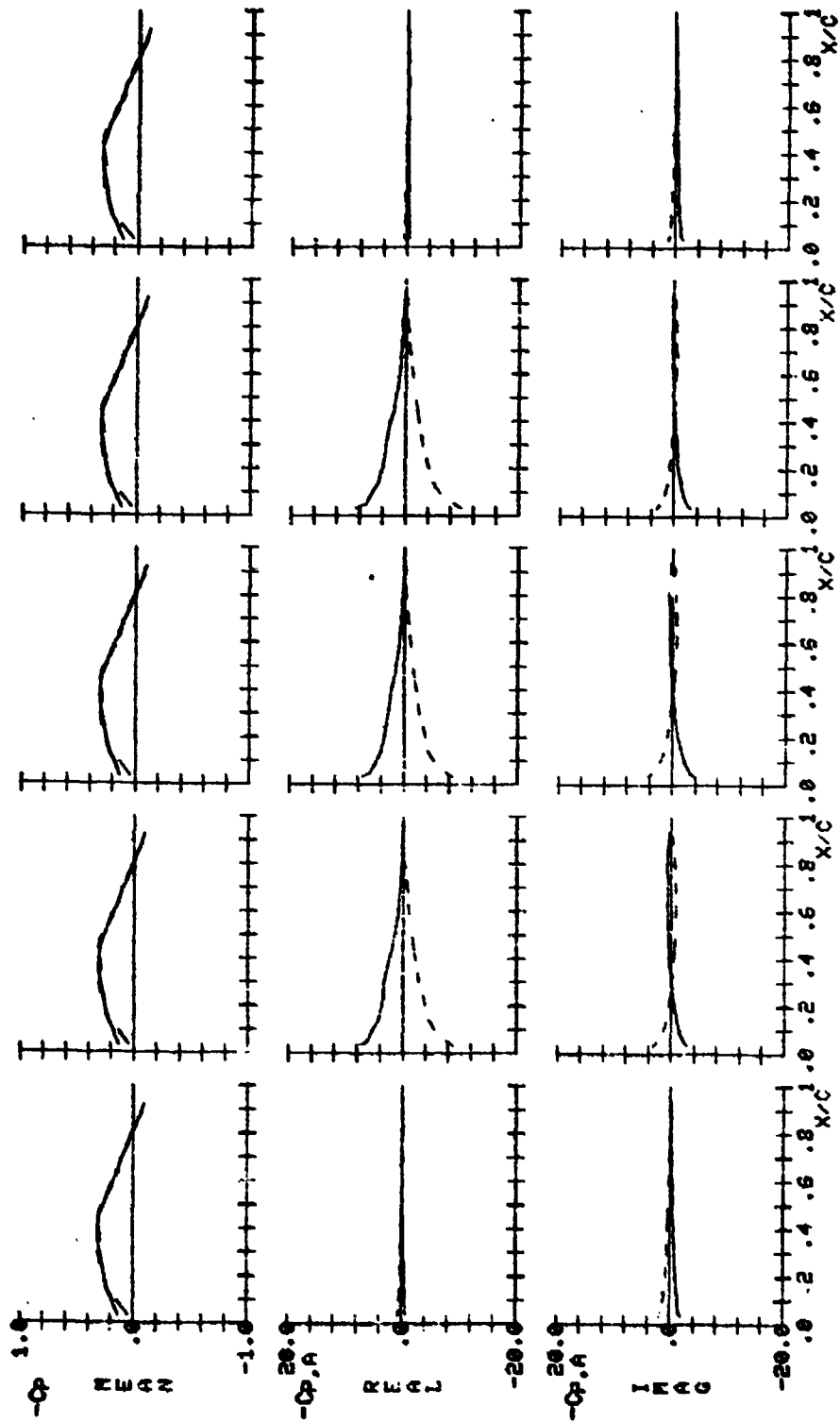
D.I. = 26 D.I. = 27 D.I. = 28 D.I. = 29 D.I. = 30

Figure 13.- Continued.



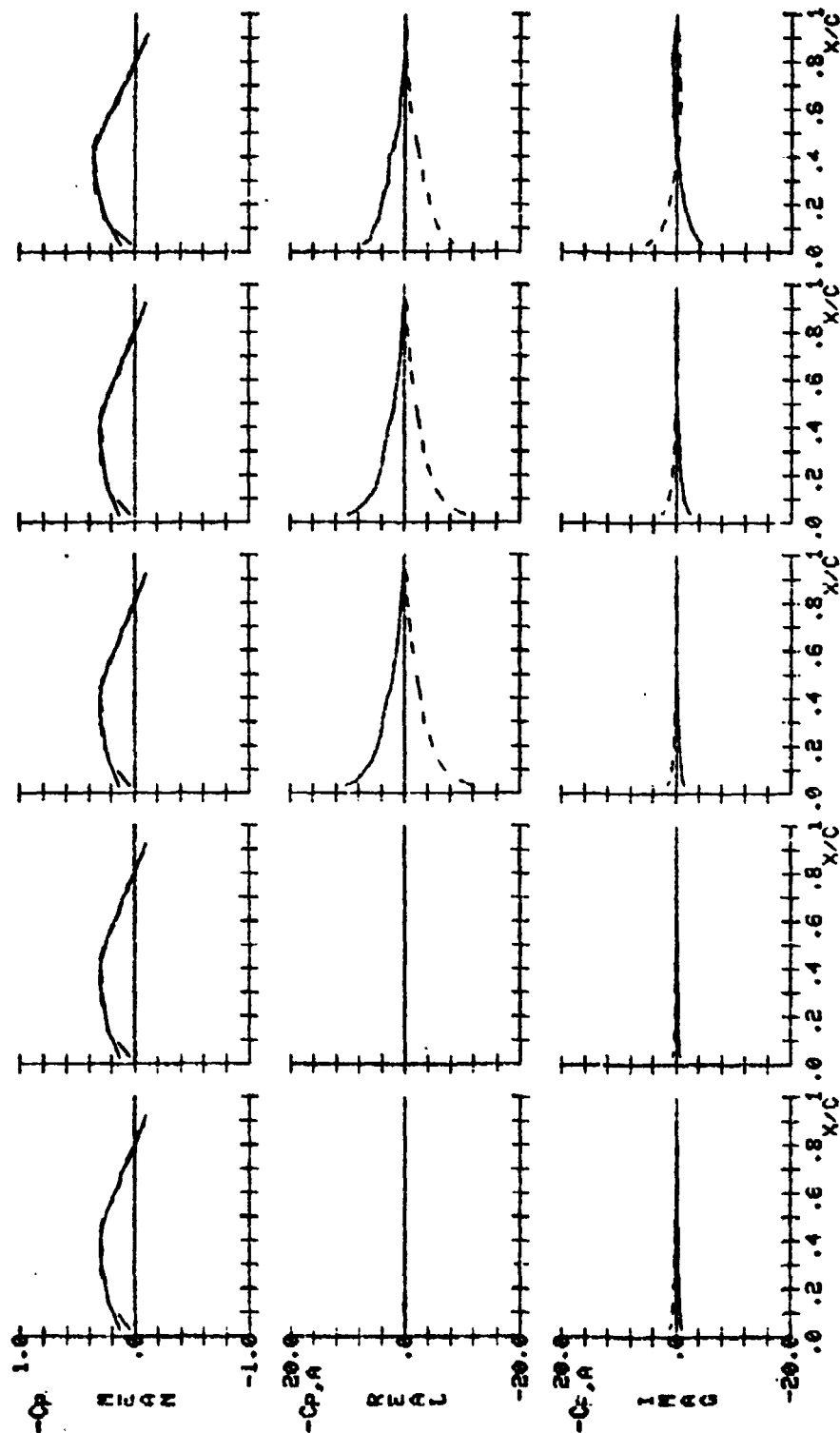
D.I. = 31 D.I. = 32 D.I. = 33 D.I. = 34 D.I. = 35

Figure 13.- Continued.



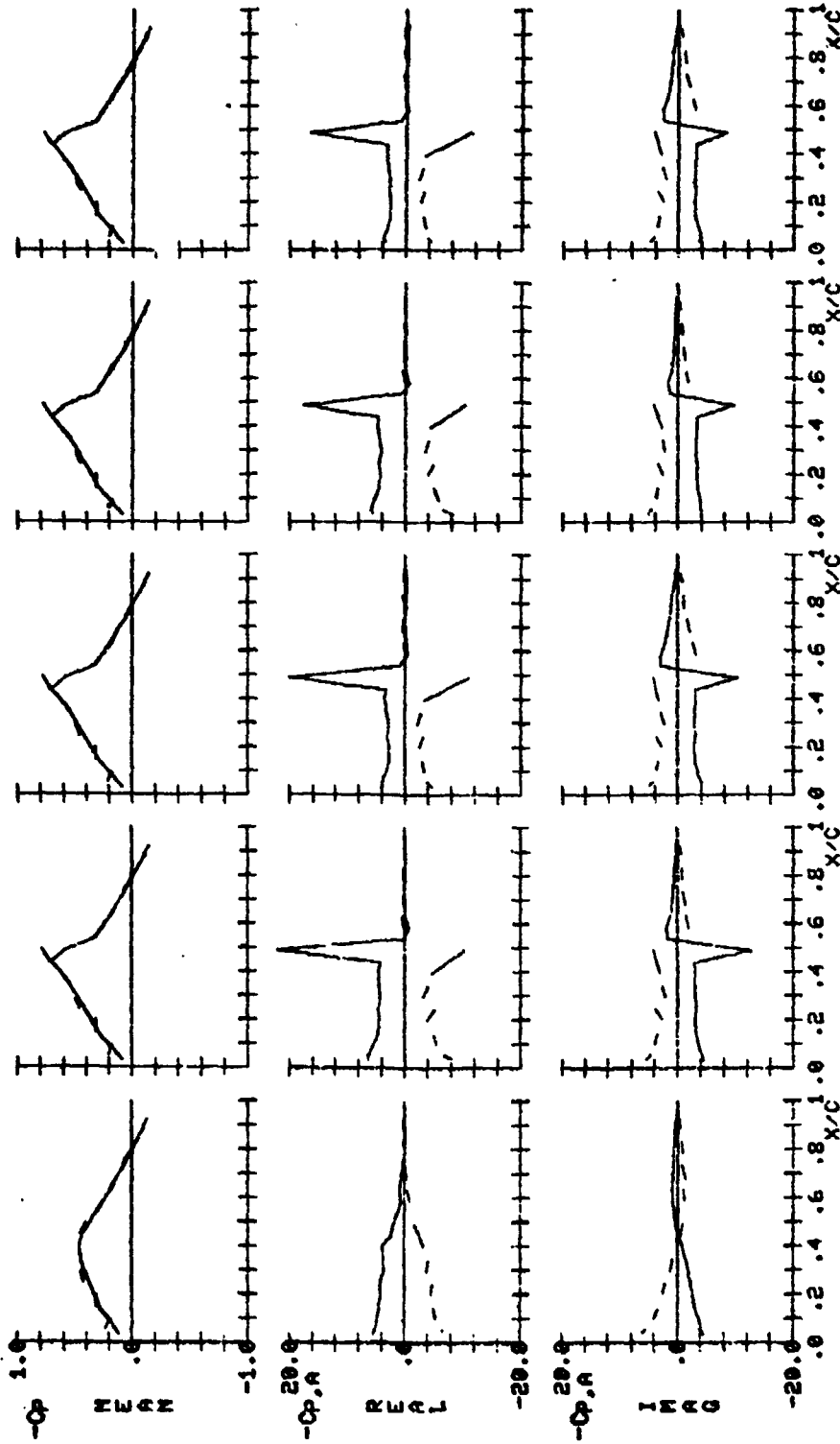
D.I. = 36 D.I. = 37 D.I. = 38 D.I. = 39 D.I. = 40

Figure 13.- Continued.



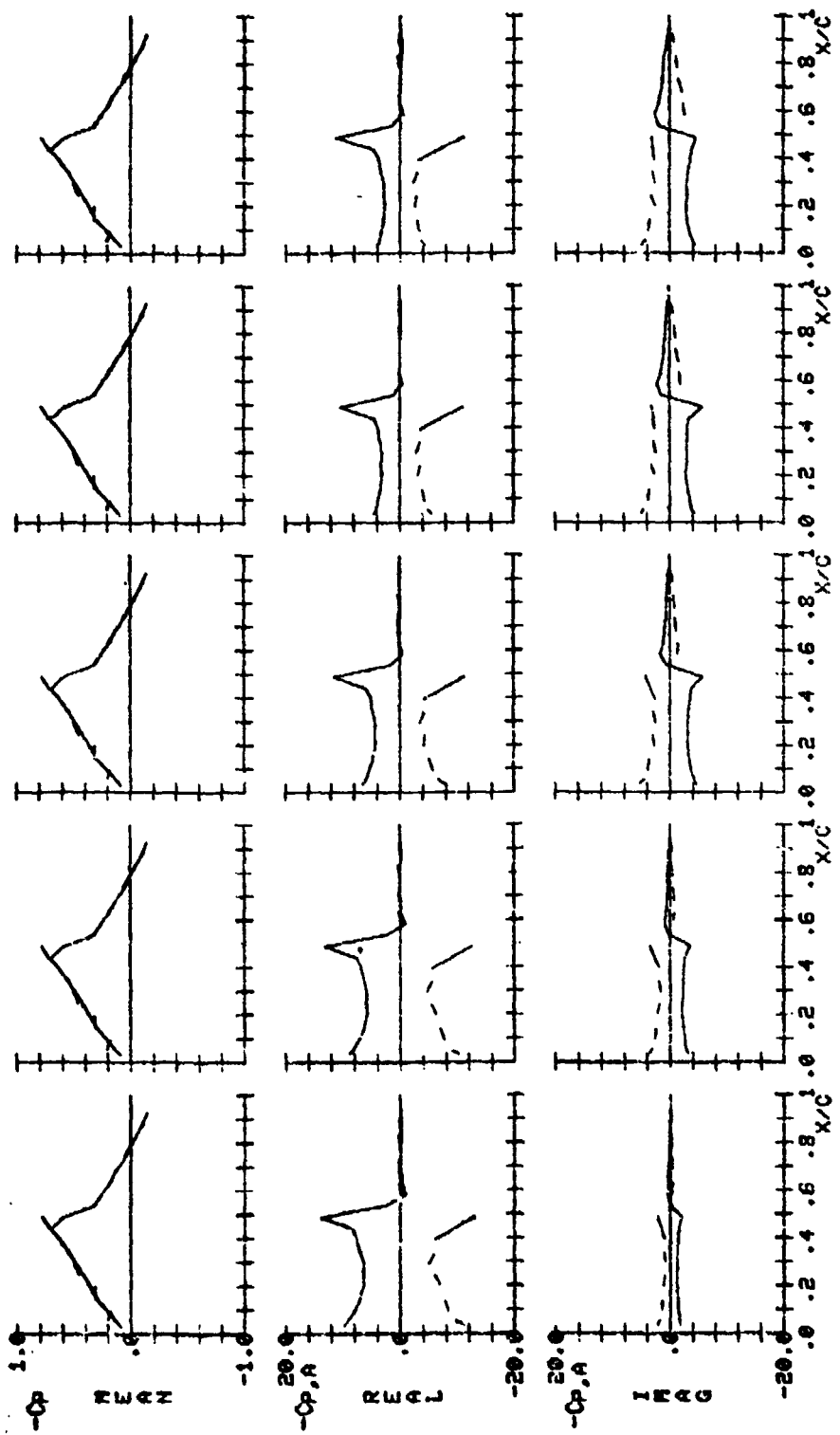
D.I. = 41 D.I. = 42 D.I. = 43 D.I. = 44 D.I. = 45

Figure 13.- Continued.



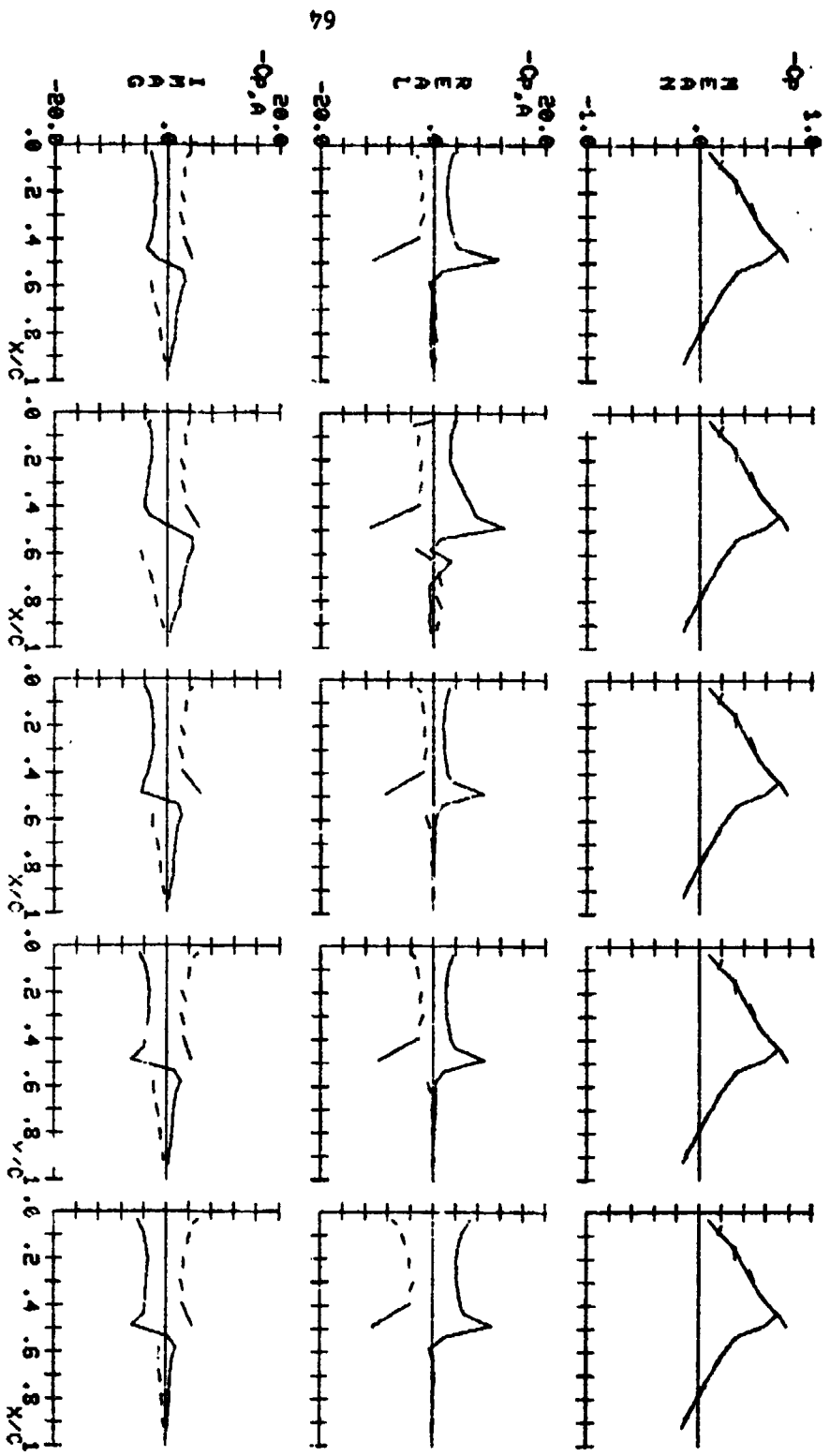
D.I. = 46 D.I. = 47 D.I. = 48 D.I. = 49 D.I. = 50

Figure 13.- Continued.



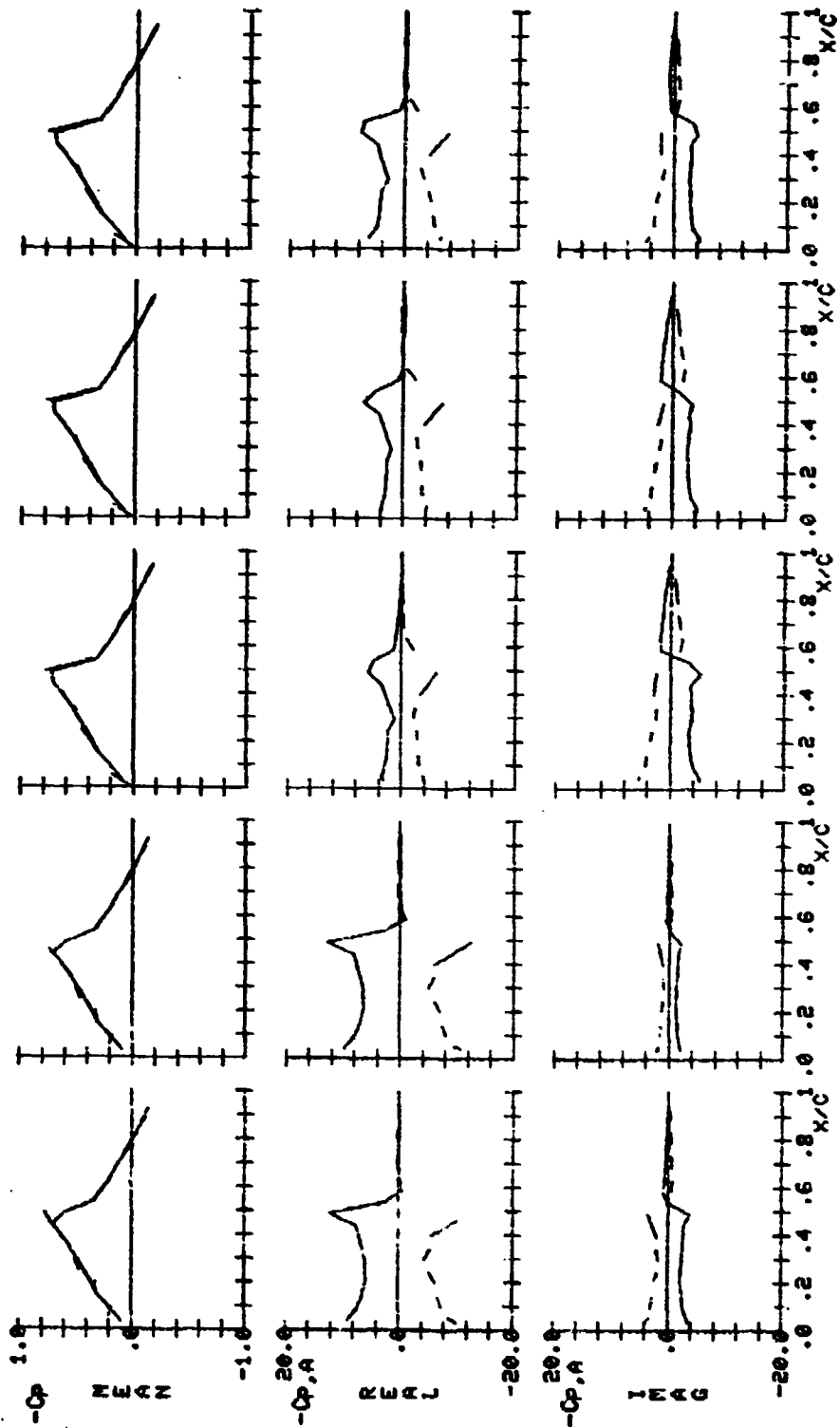
D.I. = 51 D.I. = 52 D.I. = 53 D.I. = 54 D.I. = 55

Figure 13.- Continued.



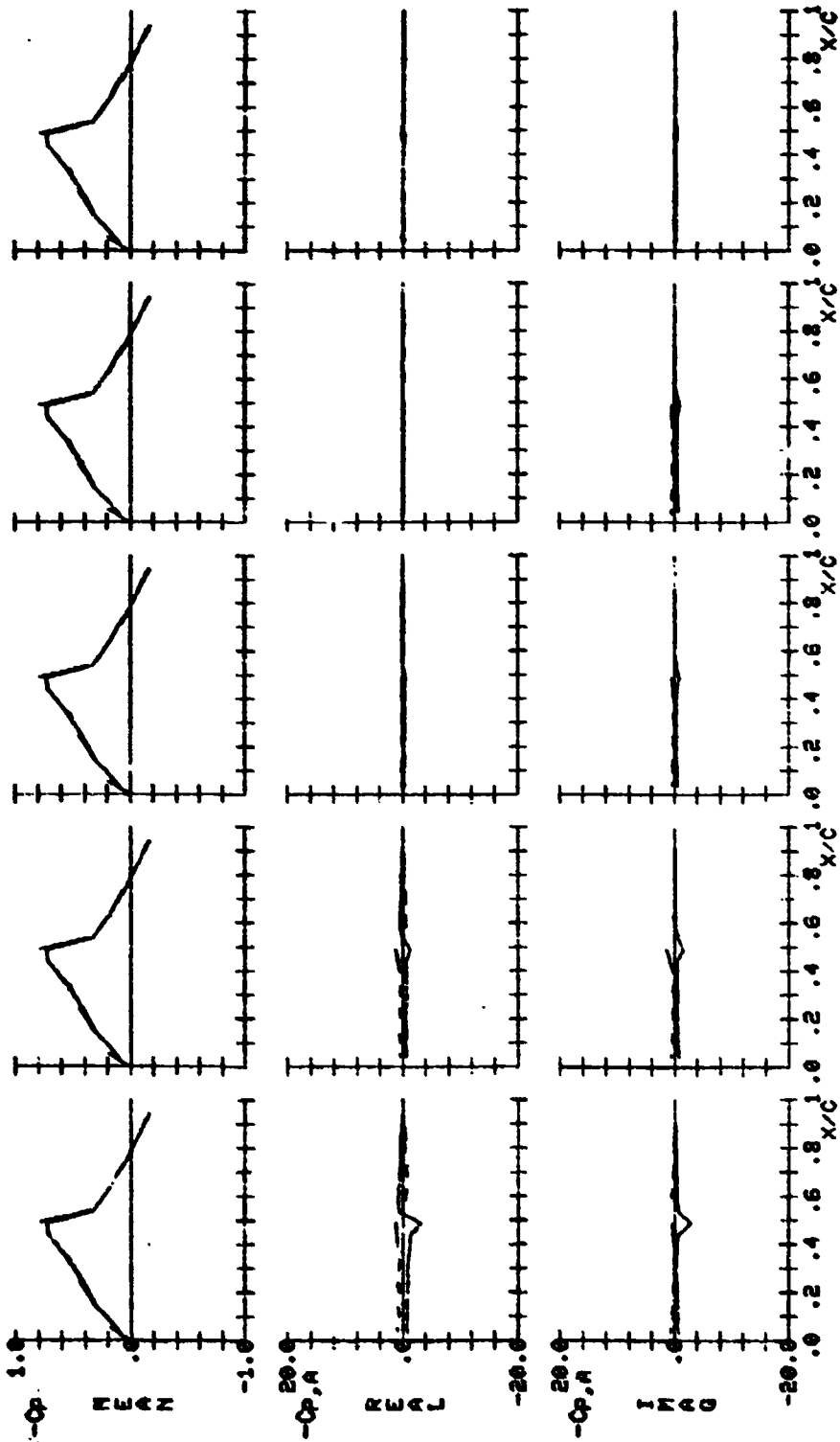
D.I. = 56 D.I. = 57 D.I. = 58 D.I. = 59 D.I. = 60

Figure 13.- Continued.



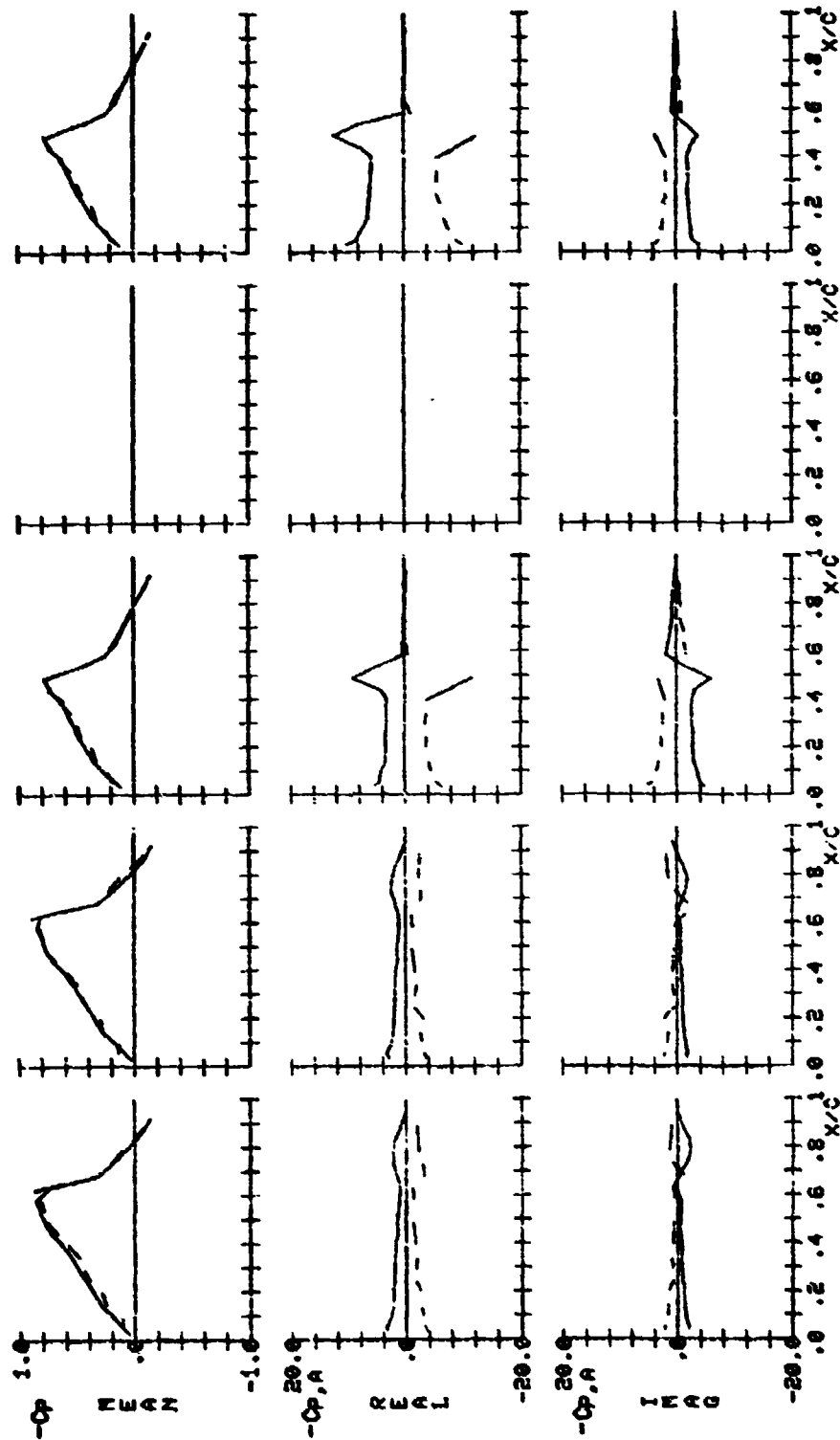
D.I. = 61 D.I. = 62 D.I. = 63 D.I. = 64 D.I. = 65

Figure 13.- Continued.



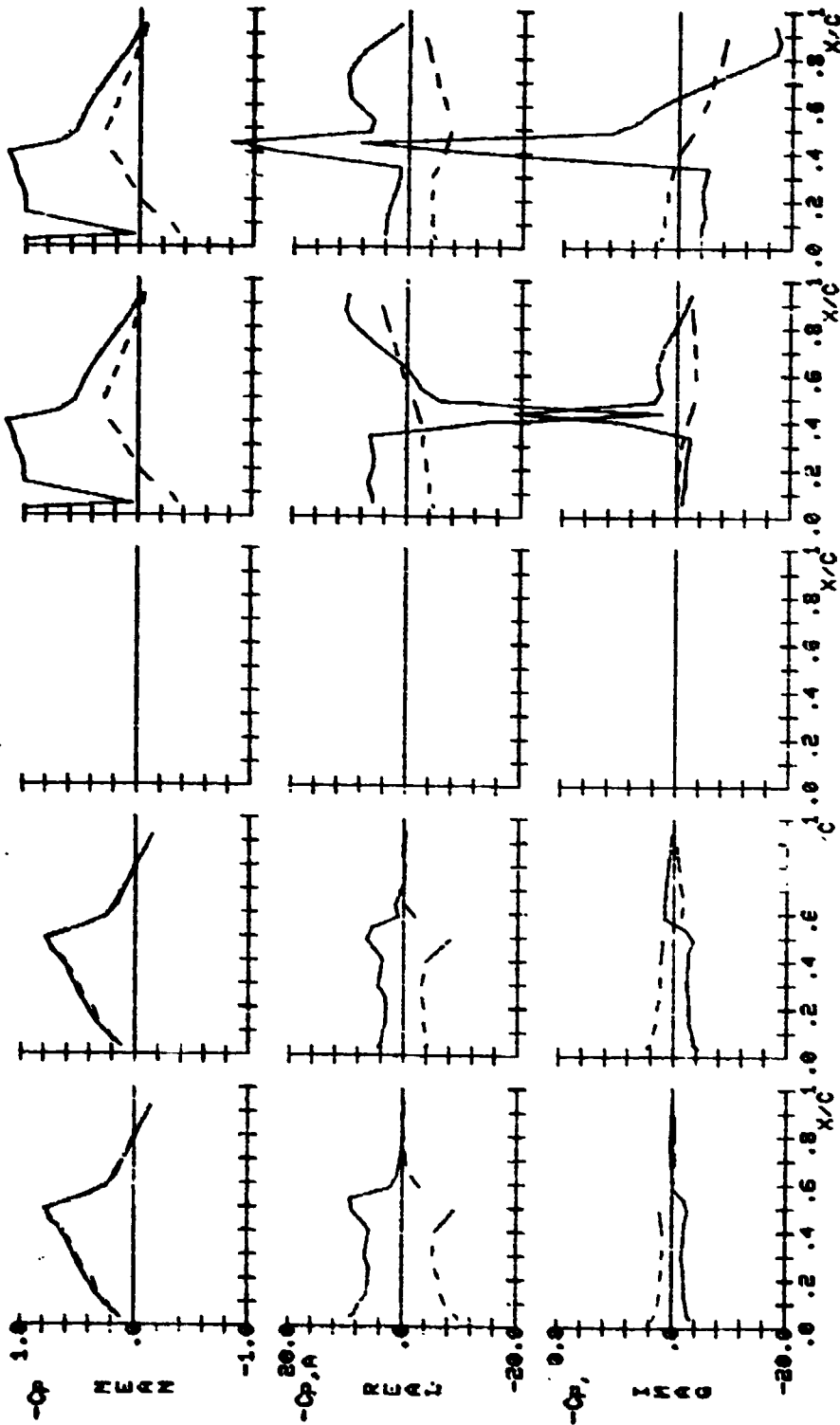
D.I. = 66 D.I. = 67 D.I. = 68 D.I. = 69 D.I. = 70

Figure 13.- Continued.



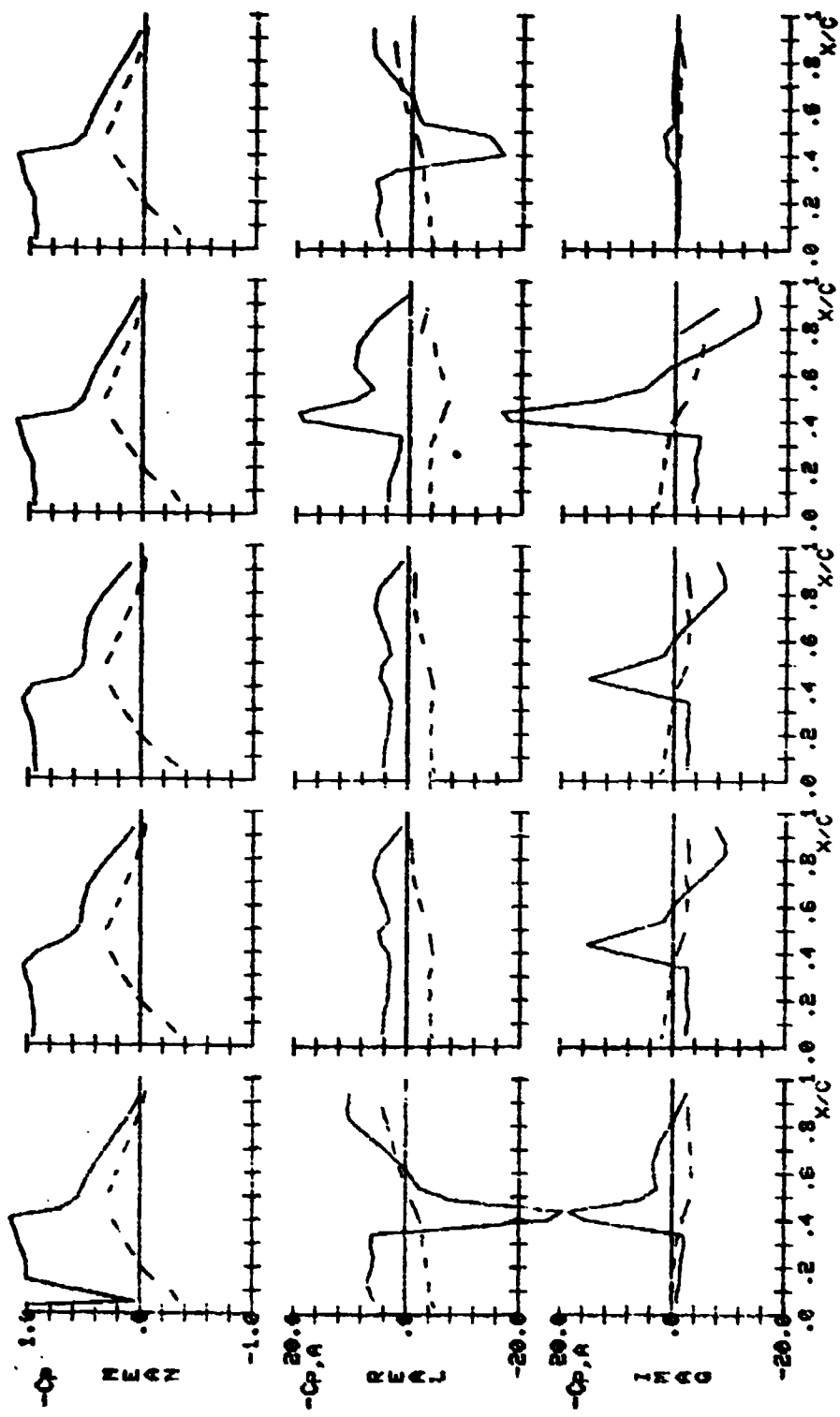
D.I. = 71 D.I. = 72 D.I. = 73 D.I. = 74 D.I. = 75

Figure 13.- Continued.



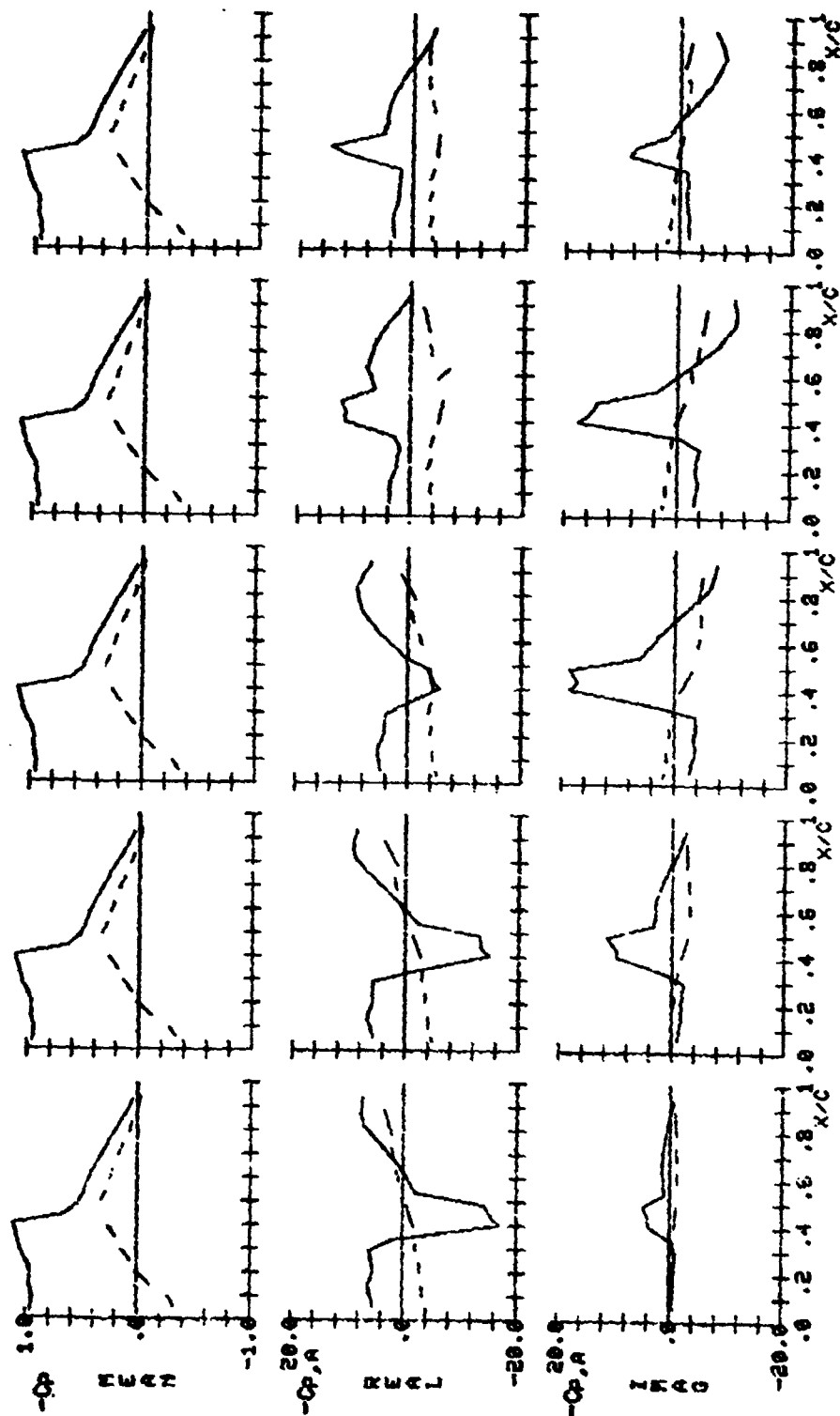
D.I. = 76 D.I. = 77 D.I. = 78 D.I. = 79 D.I. = 80

Figure 13.- Continued.



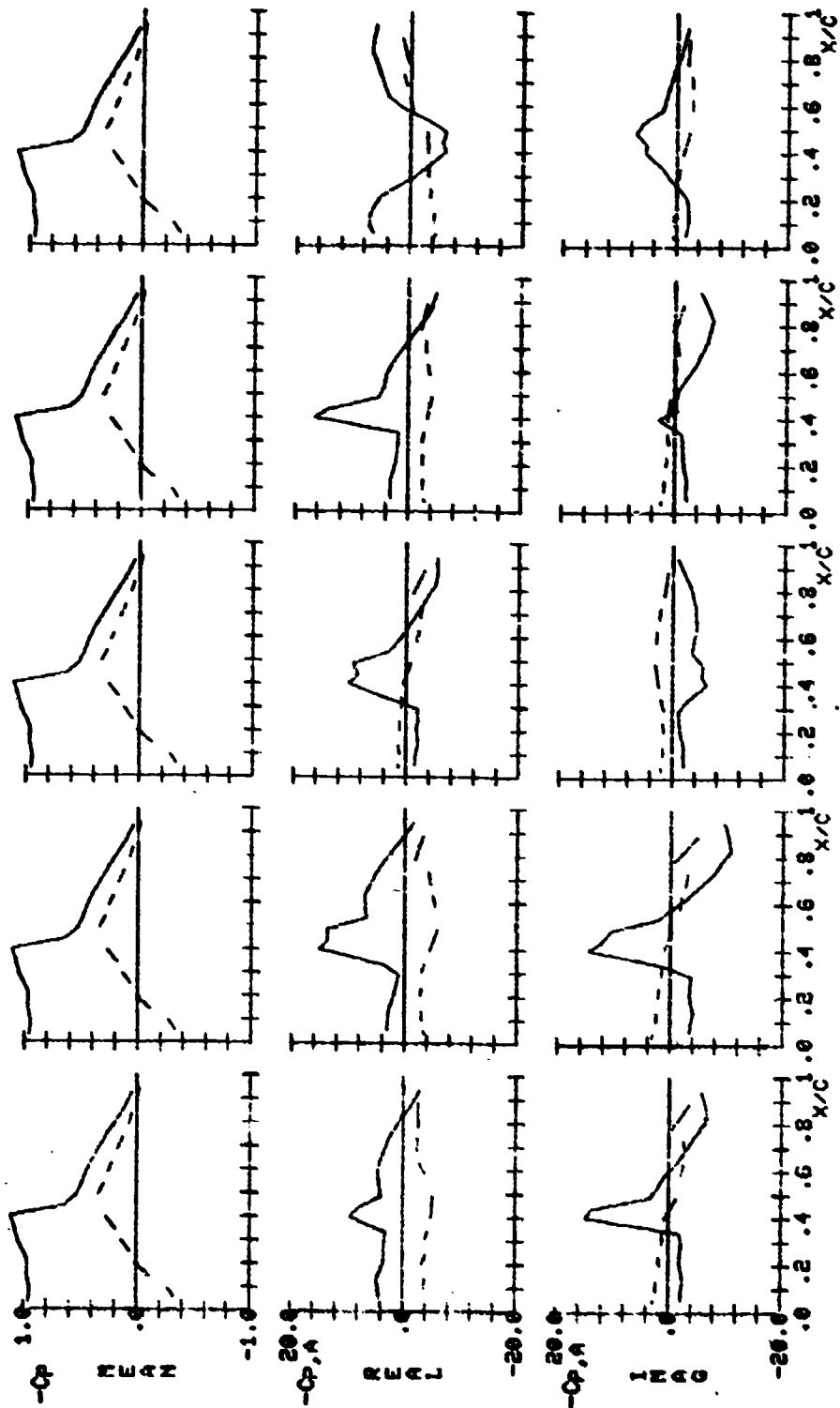
D.I. = 81 D.I. = 82 D.I. = 83 D.I. = 84 D.I. = 85

Figure 13.- Continued.



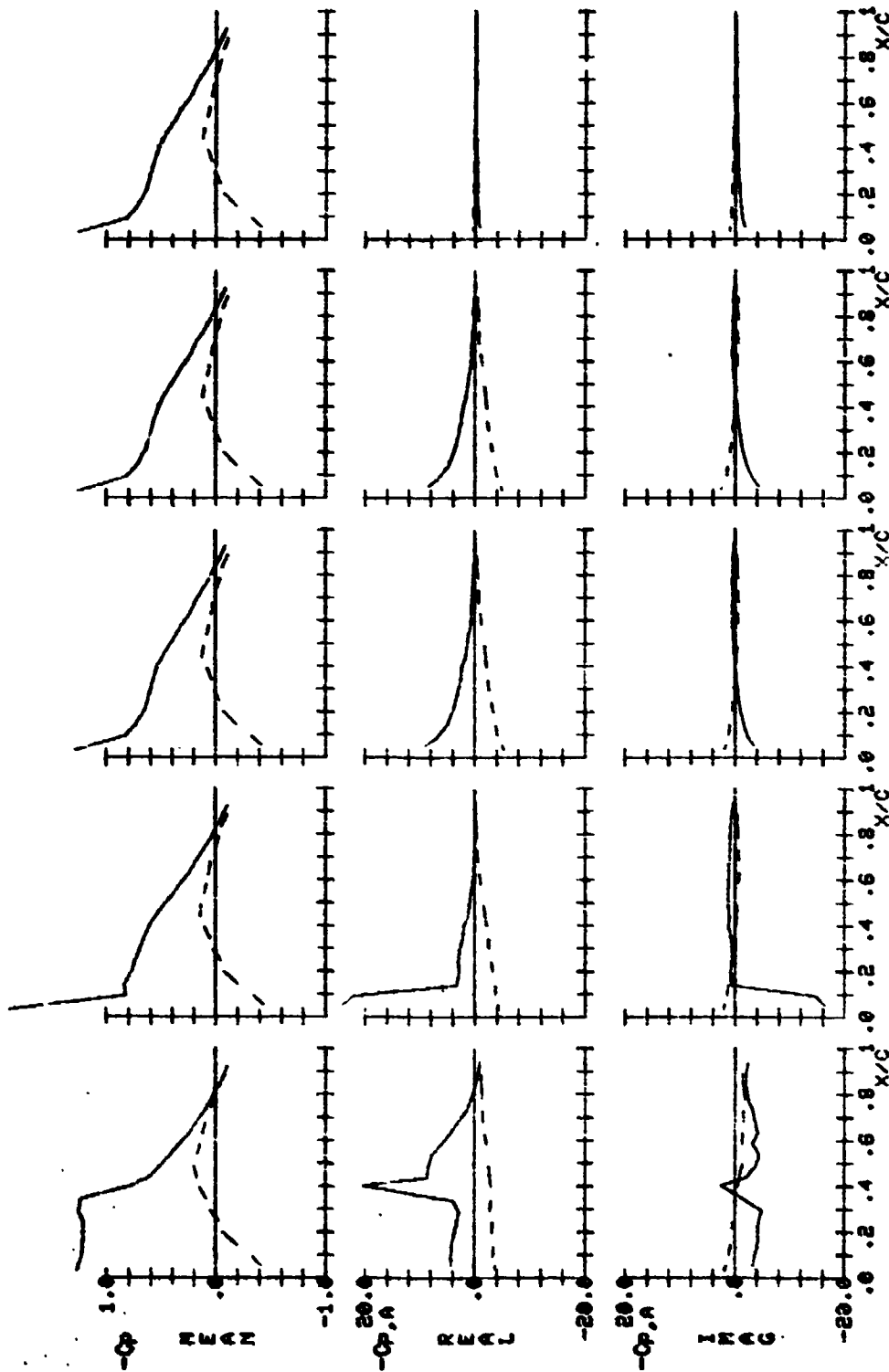
D.I. = 86 D.I. = 87 D.I. = 88 D.I. = 89 D.I. = 90

Figure 13.- Continued.



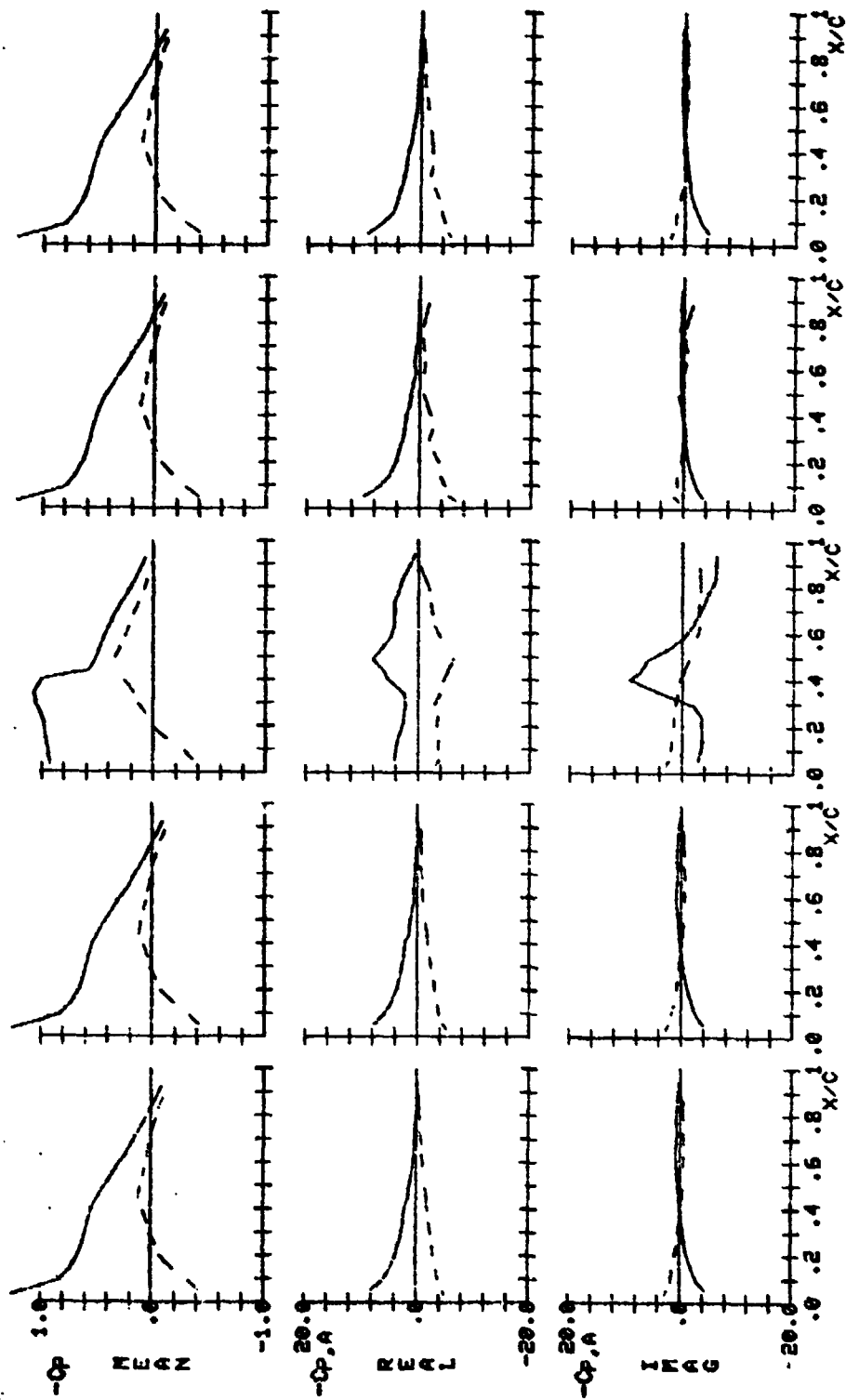
D.I. = 91 D.I. = 92 D.I. = 93 D.I. = 94 D.I. = 95

Figure 13.- Continued.



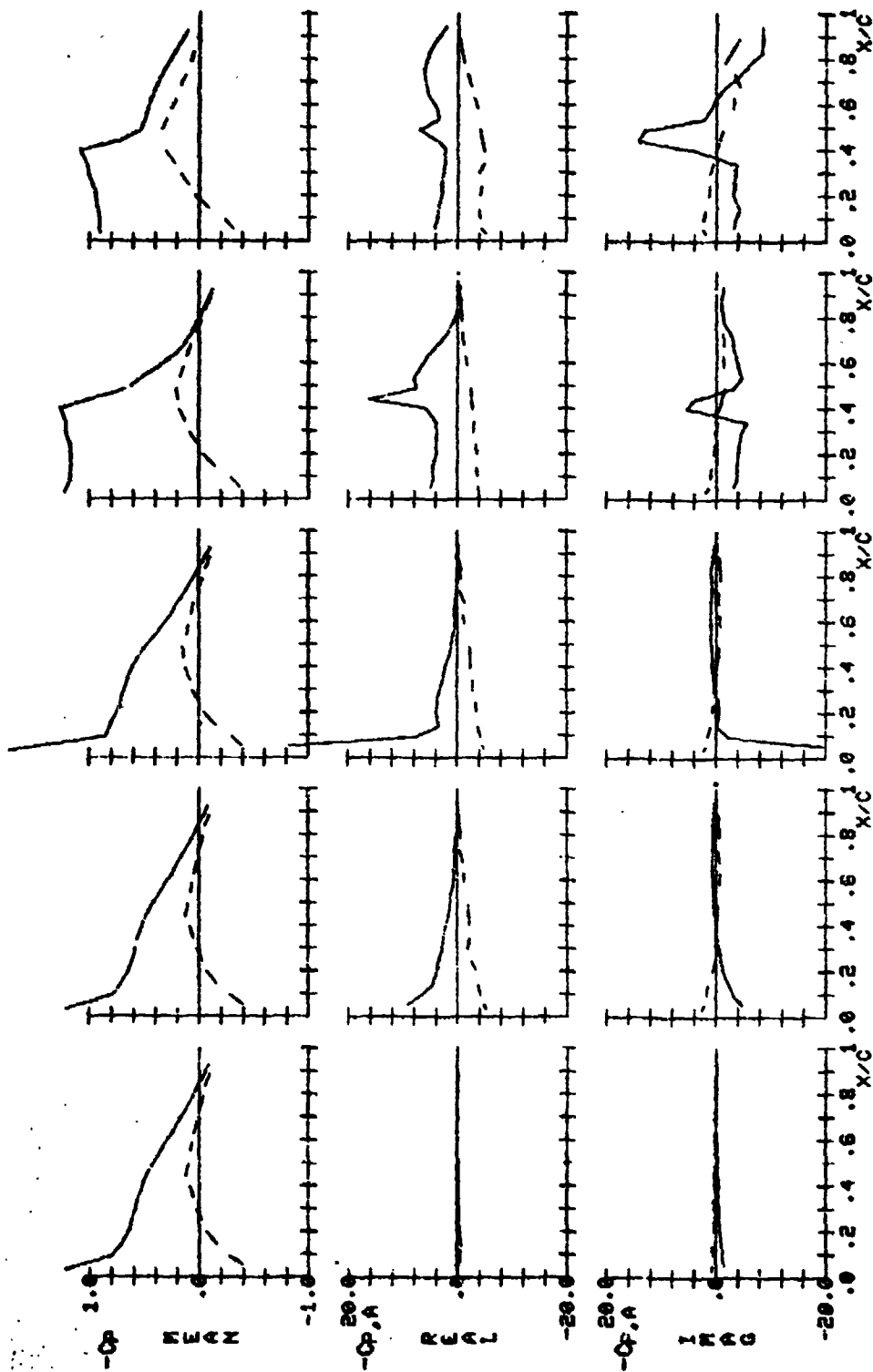
D.I. = 96 D.I. = 97 D.I. = 98 D.I. = 99 D.I. = 100

Figure 13.- Continued.



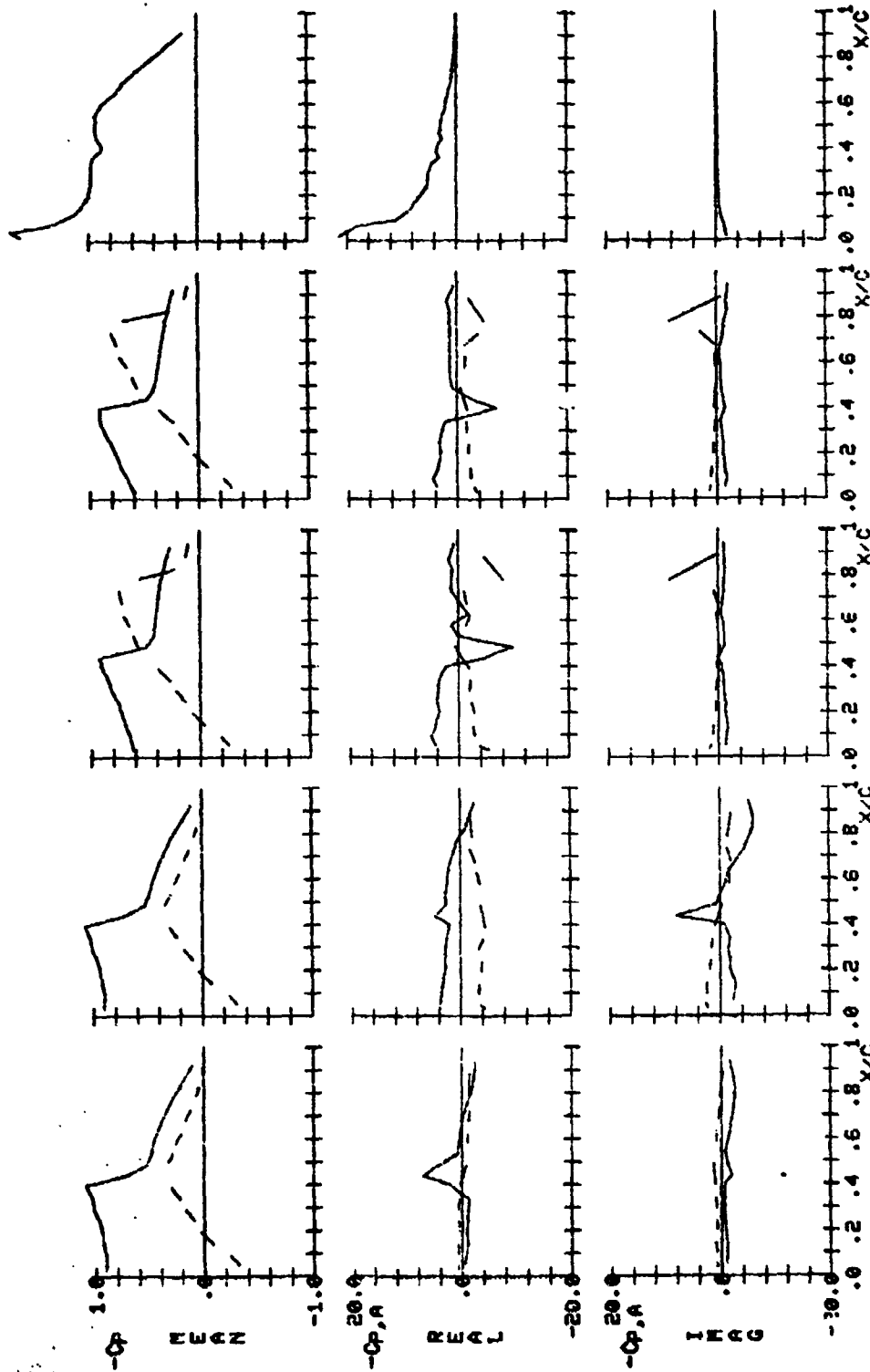
D.I.=101 D.I.=102 D.I.=103 D.I.=104 D.I.=105

Figure 13.- Continued.



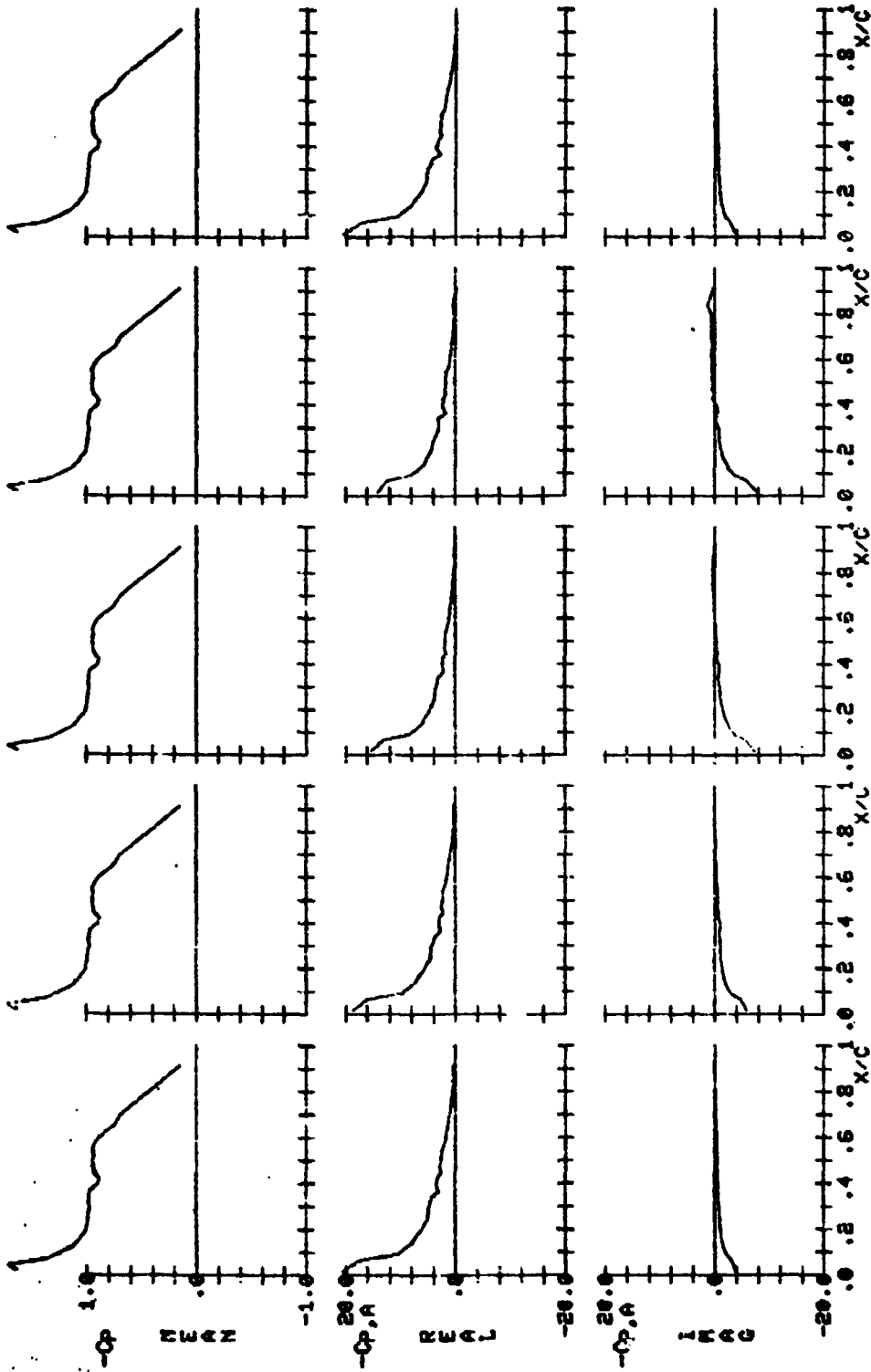
D.I.=106 D.I.=107 D.I.=108 D.I.=109 D.I.=110

Figure 13.- Continued.



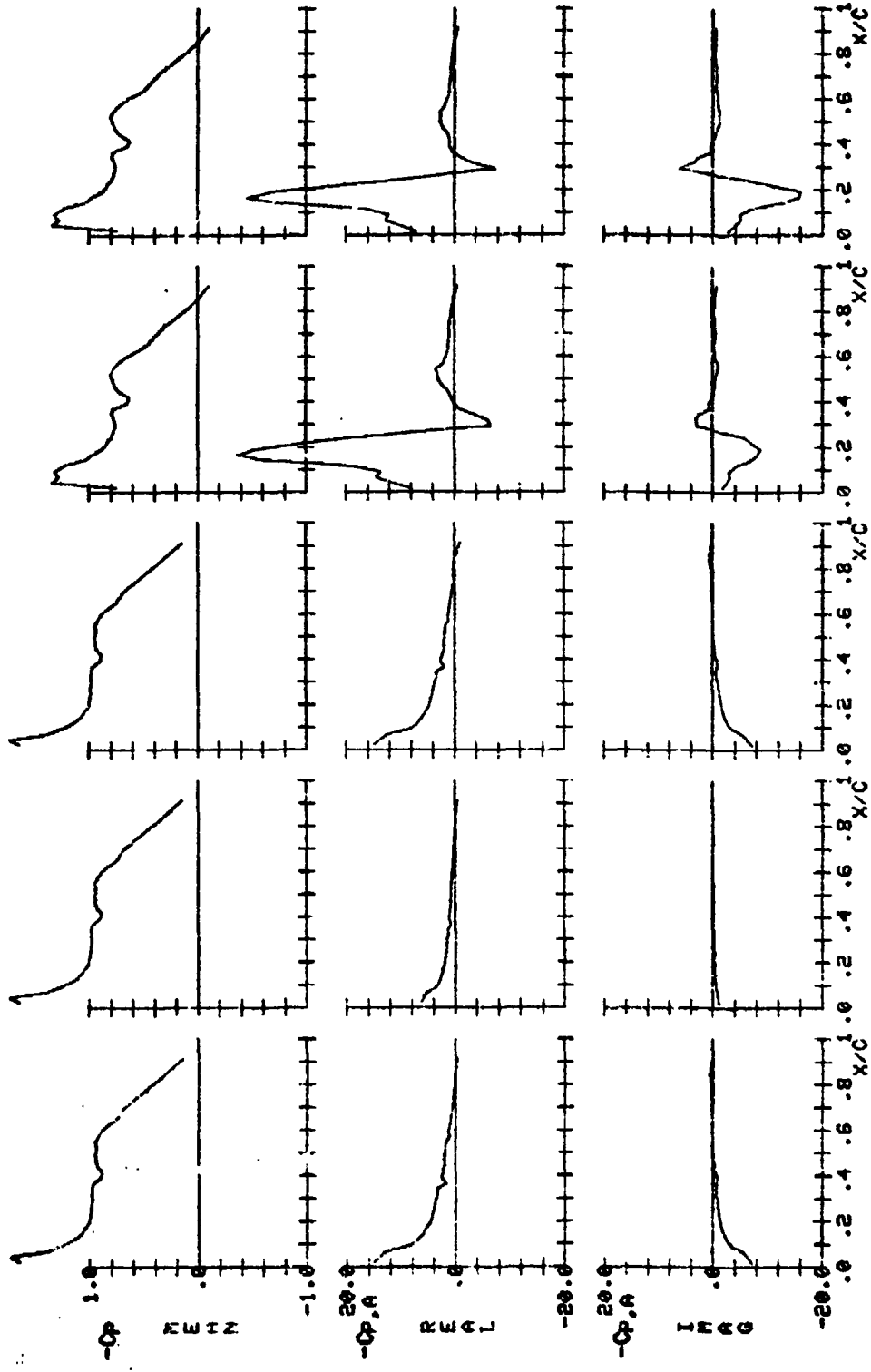
D.I.=111 D.I.=112 D.I.=113 D.I.=114 D.I.=115

Figure 13.- Continued.



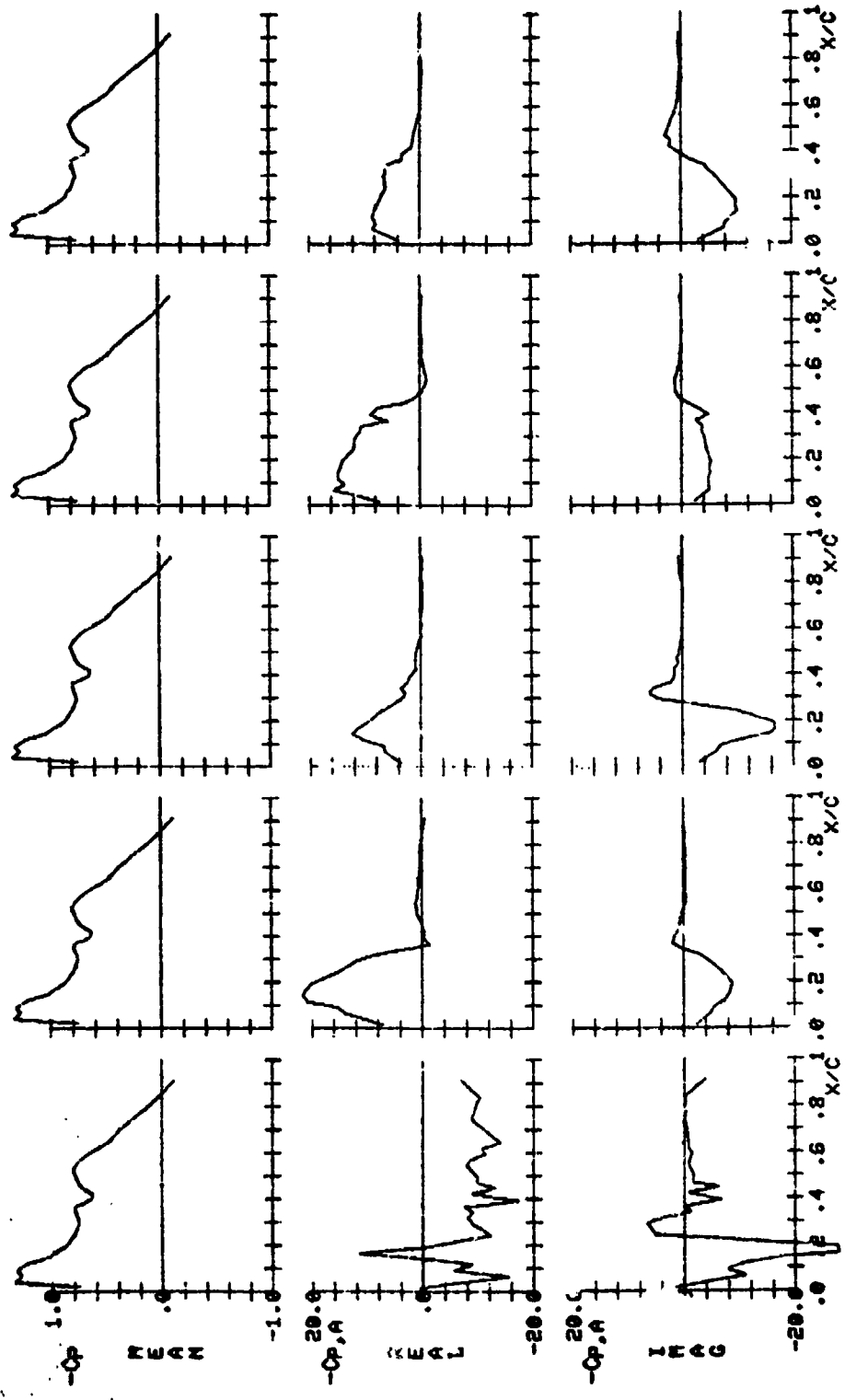
D.I.=116 D.I.=117 D.I.=118 D.I.=119 D.I.=120

Figure 13.- Continued.



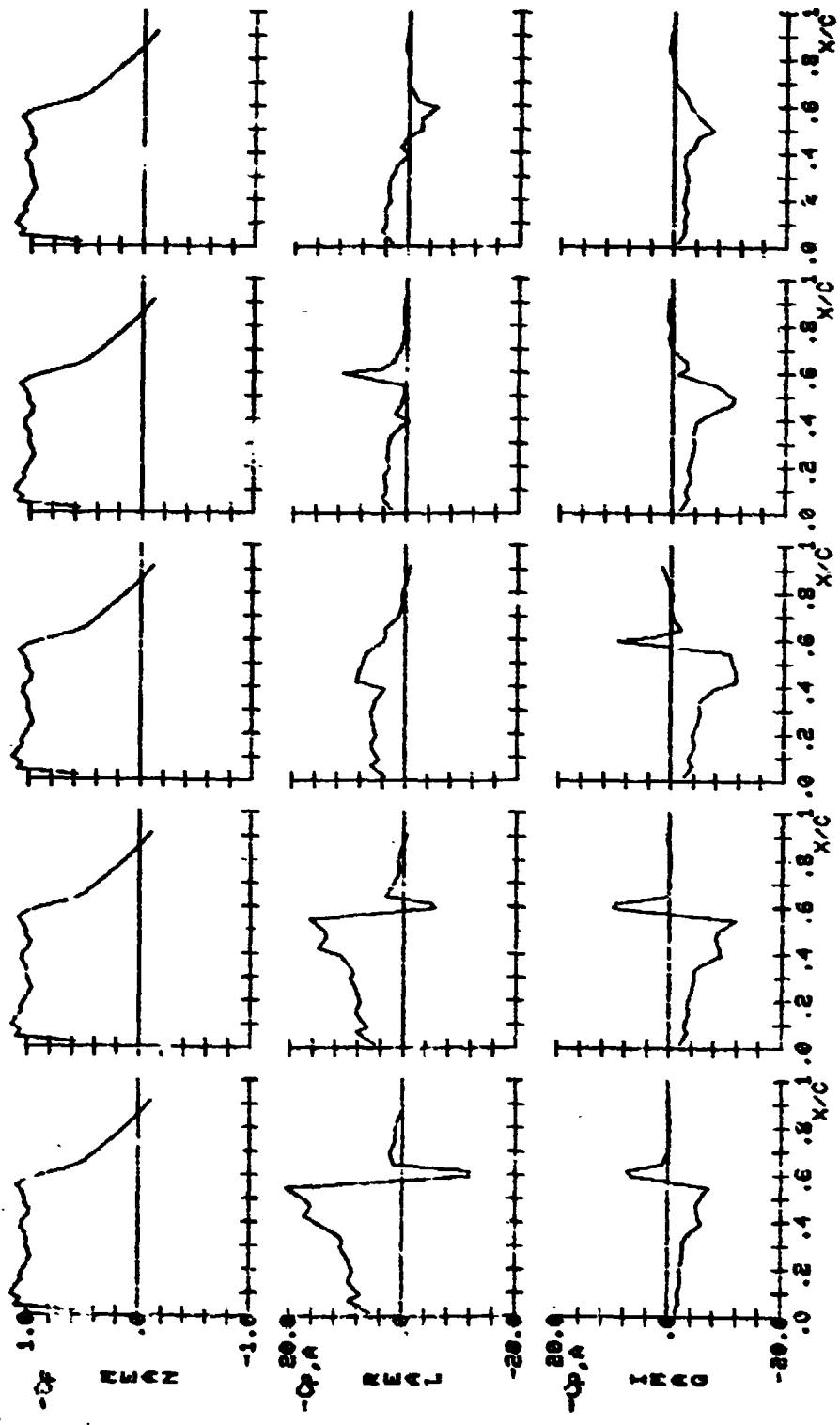
D.I.=121 D.I.=122 D.I.=123 D.I.=124 D.I.=125

Figure 13.- Continued.



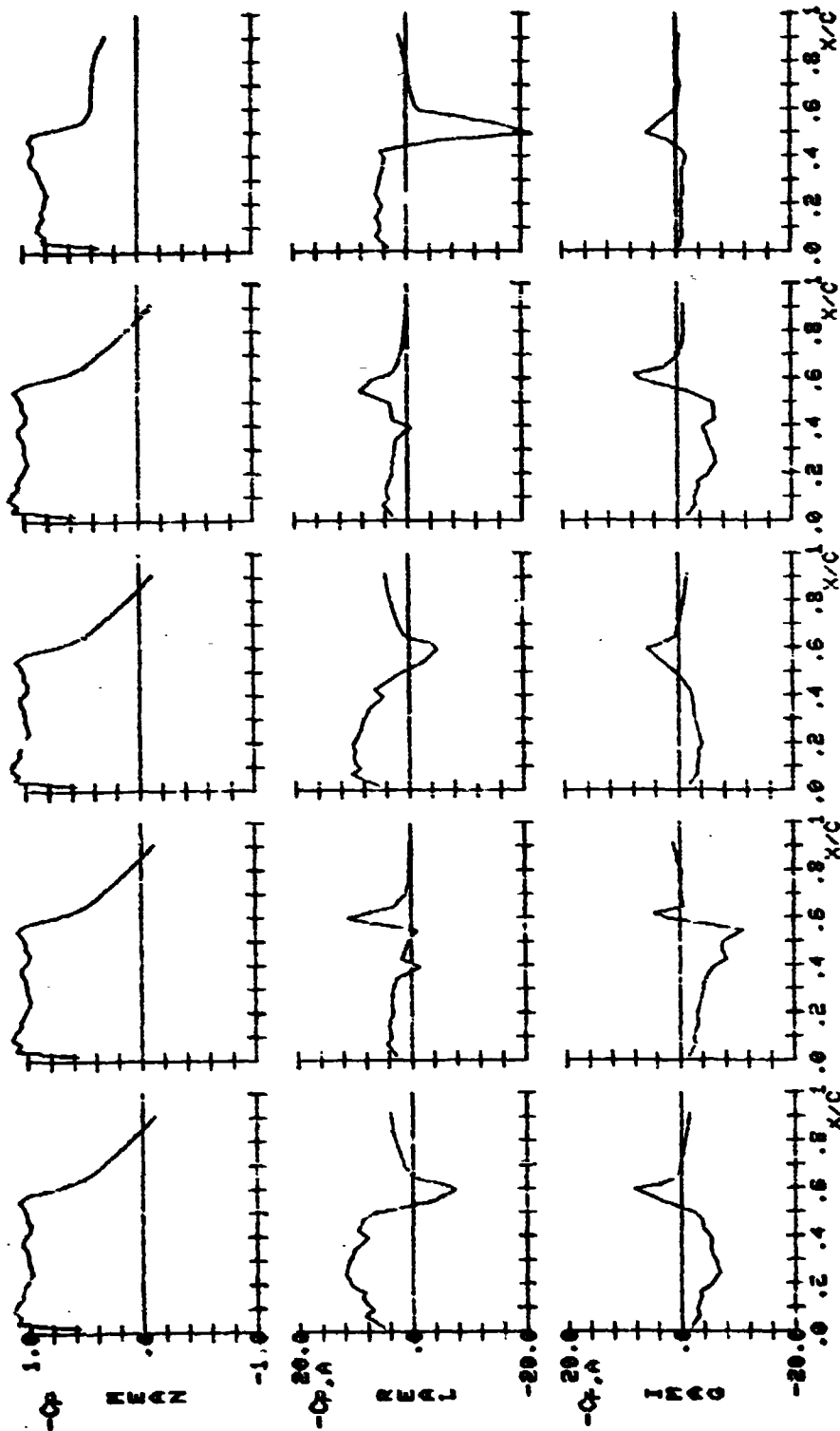
D.I. = 126 D.I. = 127 D.I. = 128 D.I. = 129 D.I. = 130

Figure 13.- Continued.



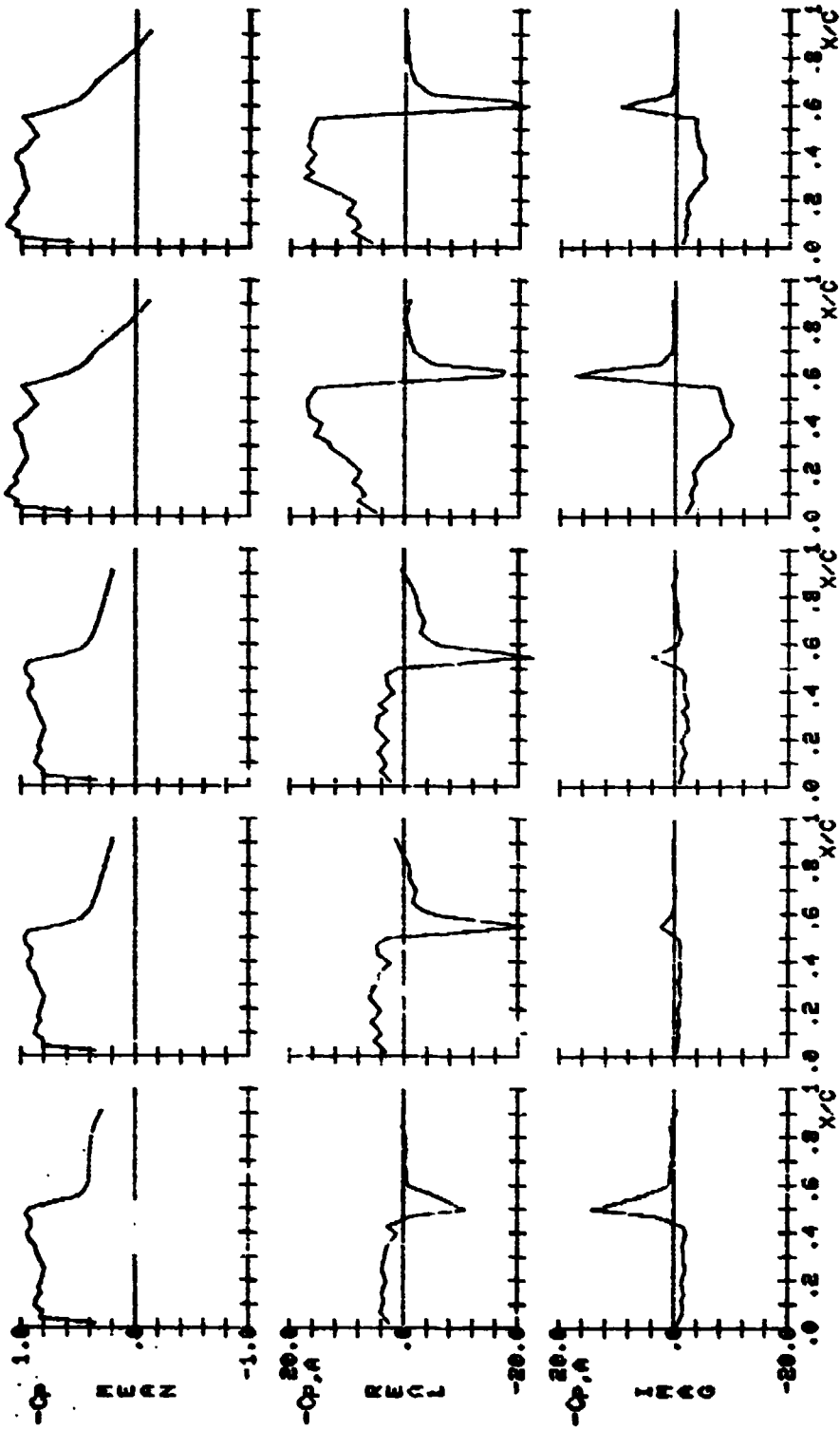
D.I.=131 D.I.=132 D.I.=133 D.I.=134 D.I.=135

Figure - Continued.



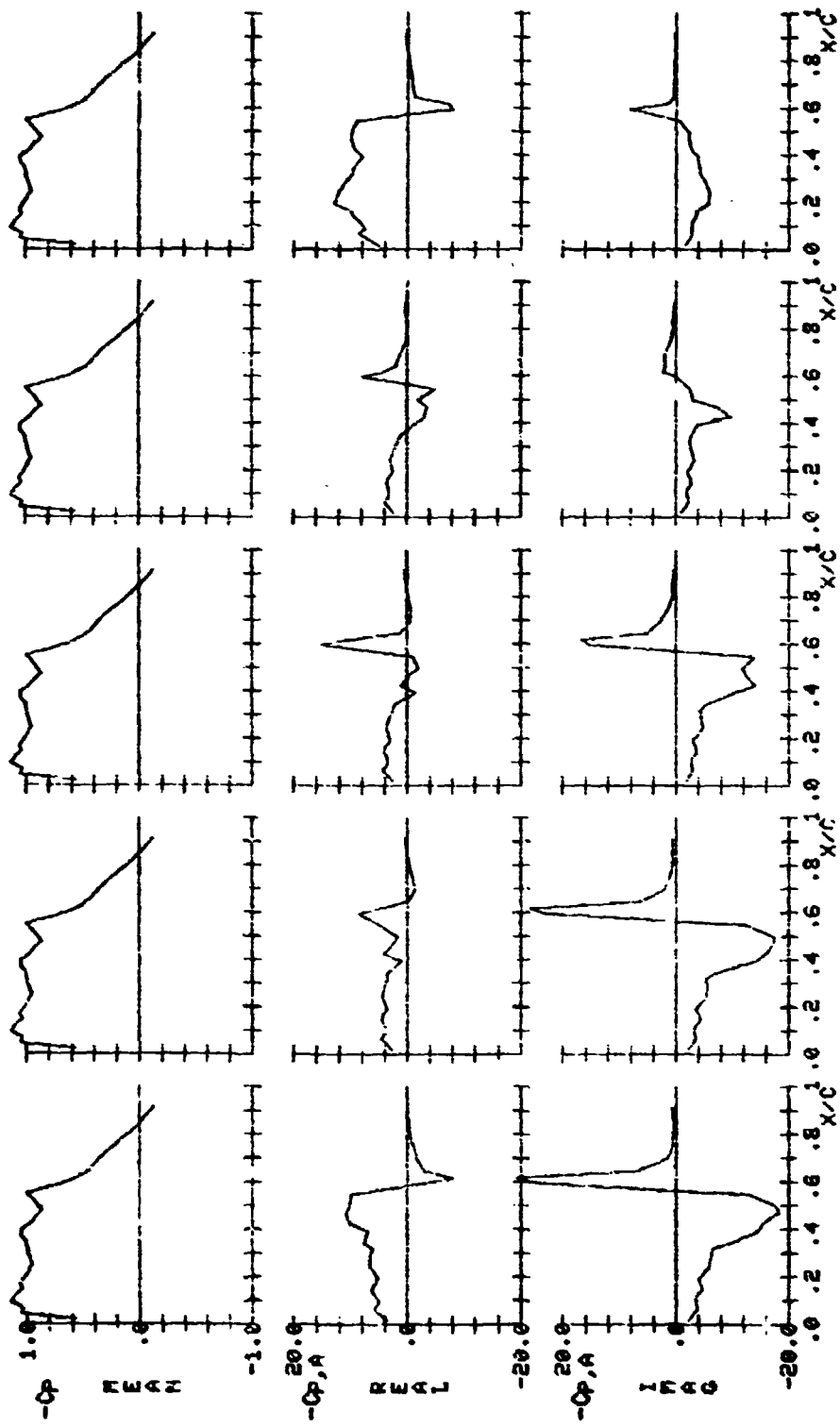
D.I.=136 D.I.=137 D.I.=138 D.I.=139 D.I.=140

Figure 13.- Continued.



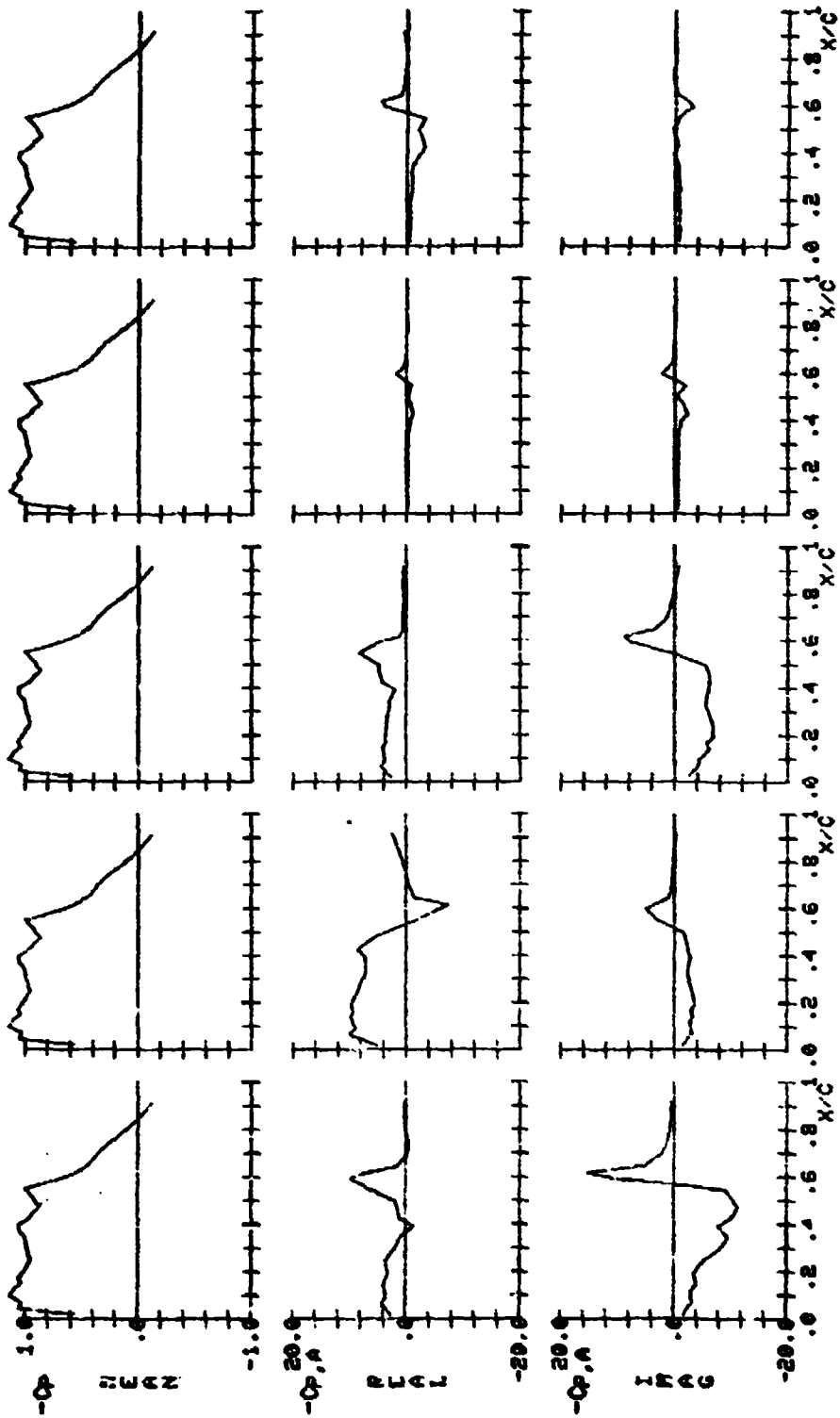
D.I.=141 D.I.=142 D.I.=143 D.I.=144 D.I.=145

Figure 13.- Continued.



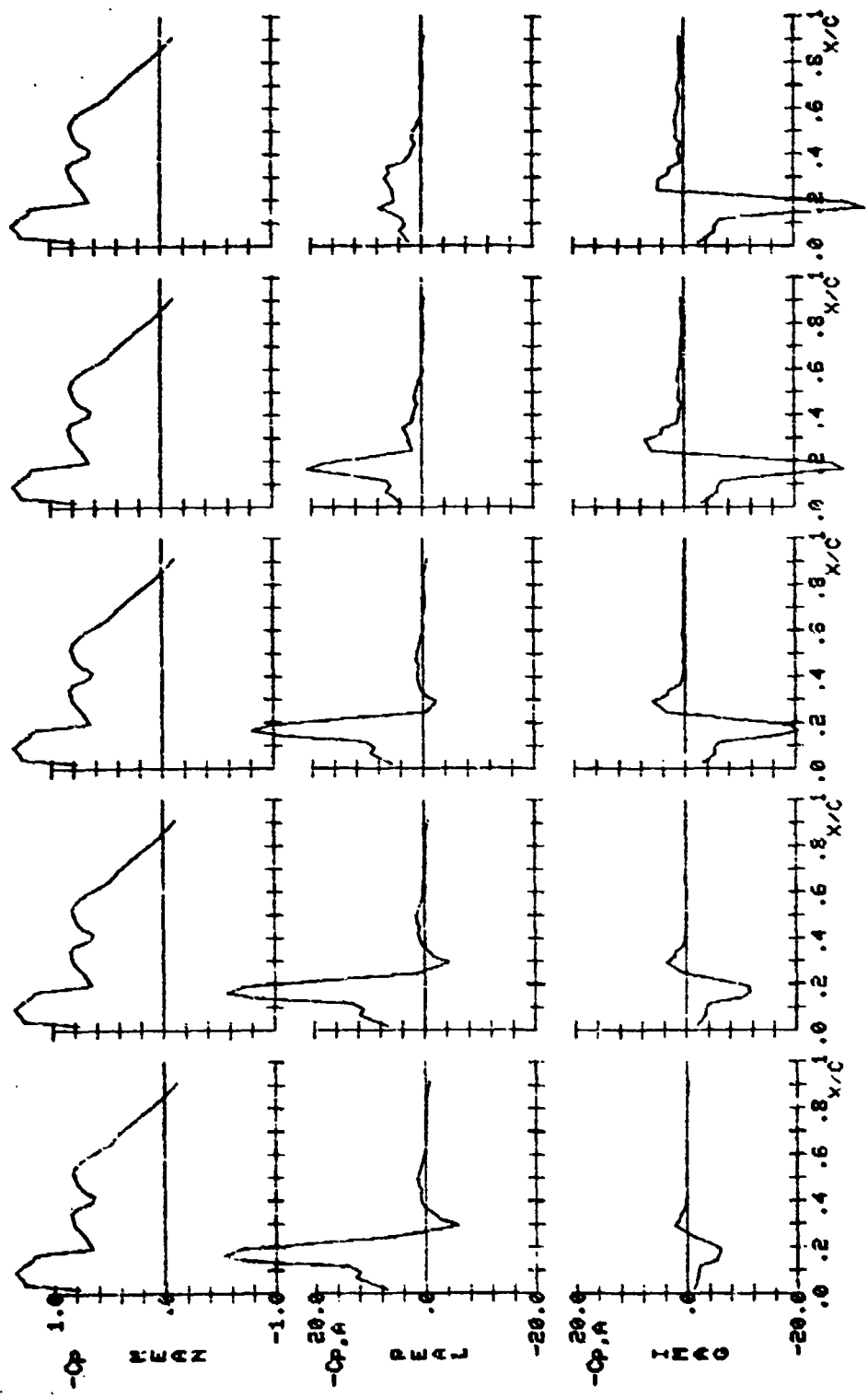
D.I.=146 D.I.=147 D.I.=148 D.I.=149 D.I.=150

Figure 13.- Continued.



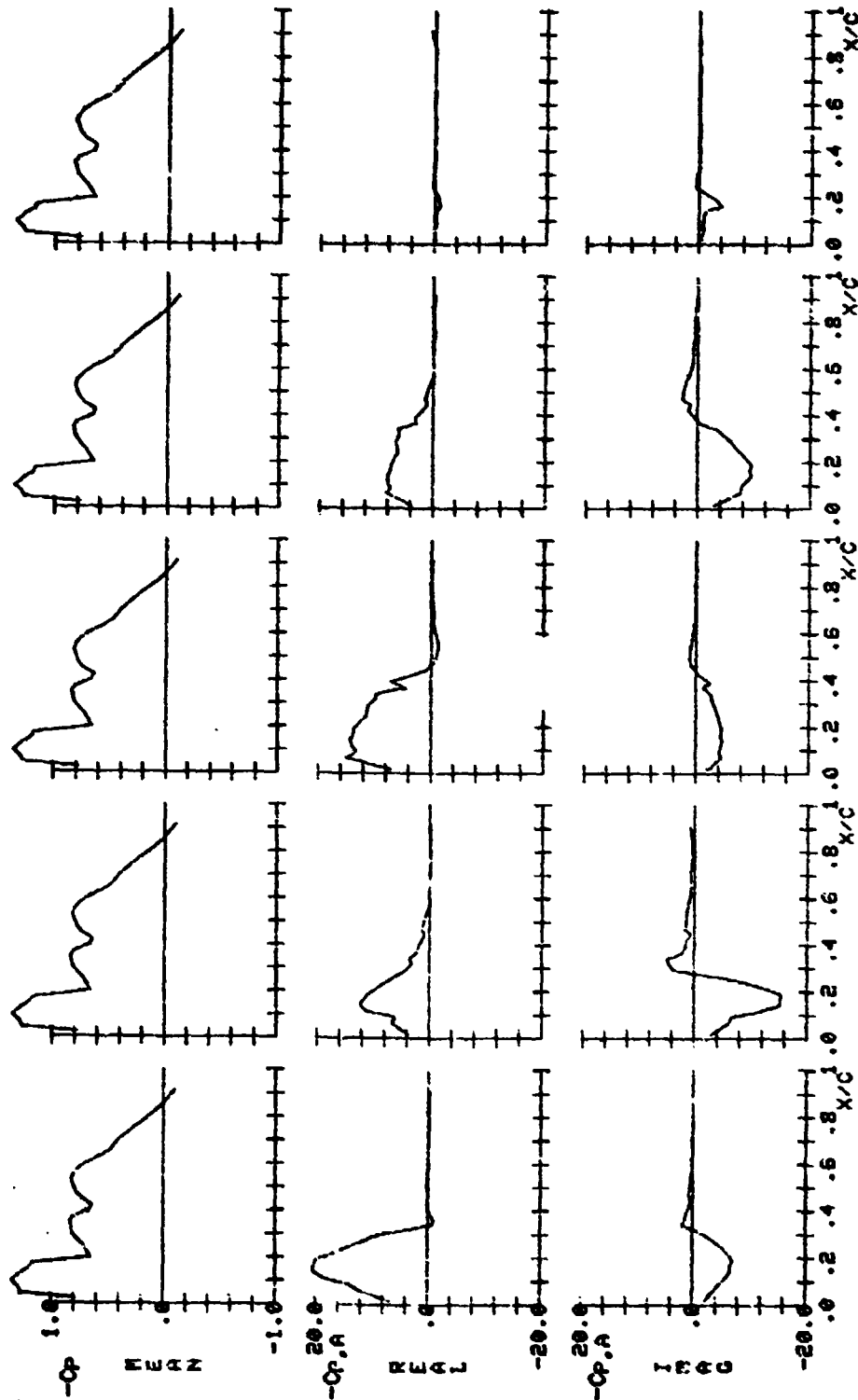
D.I.=151 D.I.=152 D.I.=153 D.I.=154 D.I.=155

Figure 13.- Continued.



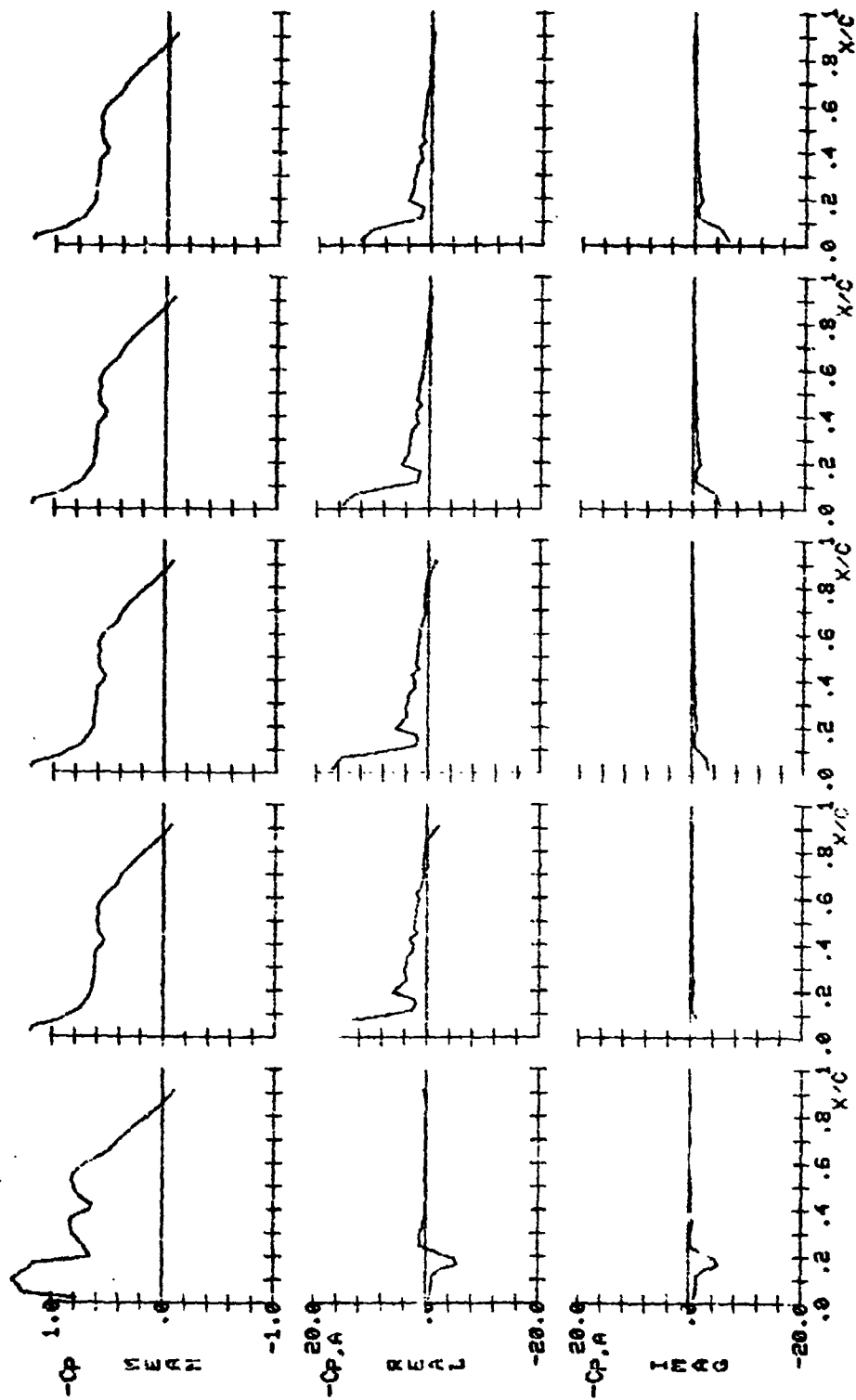
D.I.=156 D.I.=157 D.I.=158 D.I.=159 D.I.=160

Figure 13.- Continued.



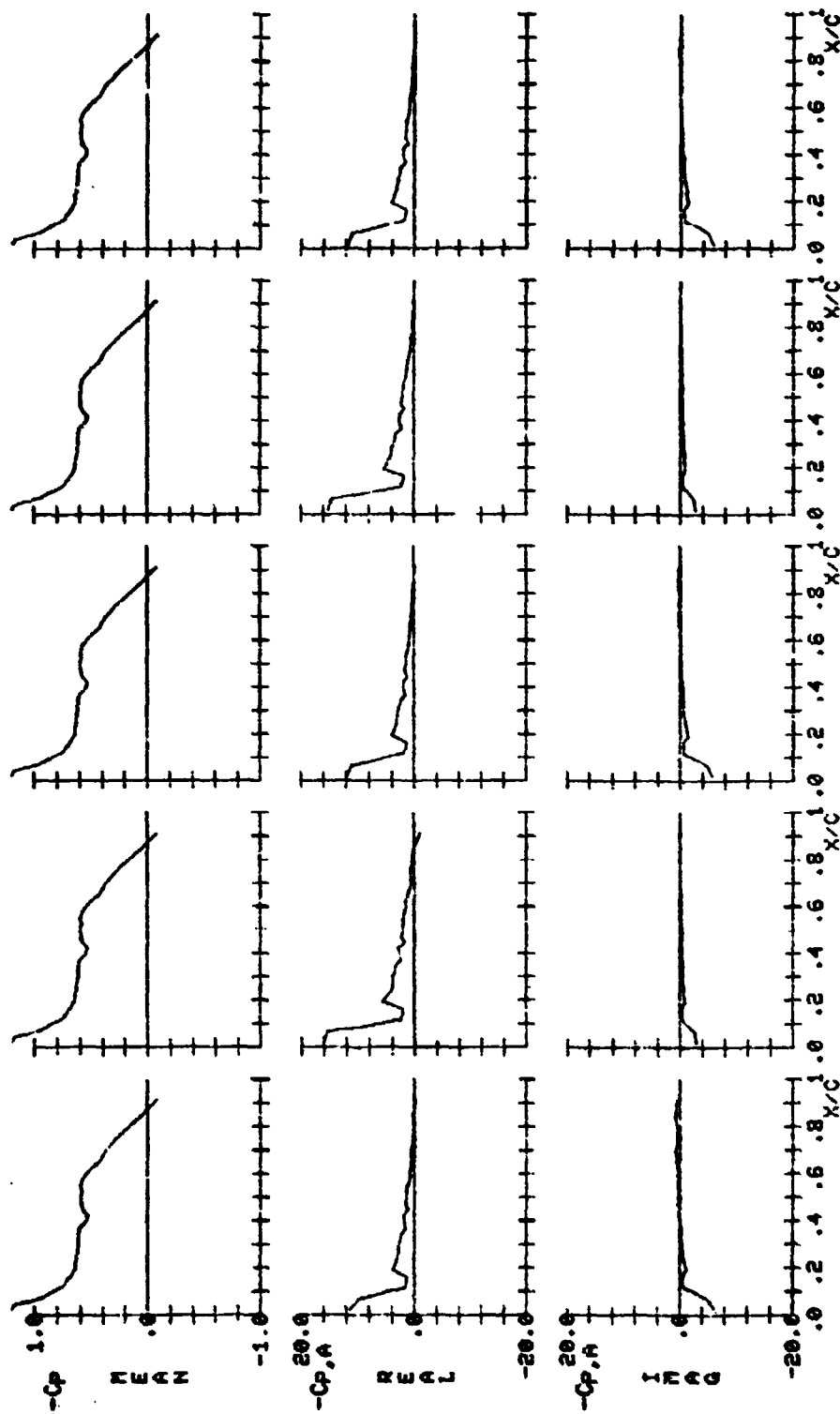
D.I.=161 D.I.=162 D.I.=163 D.I.=164 D.I.=165

Figure 13.- Continued.



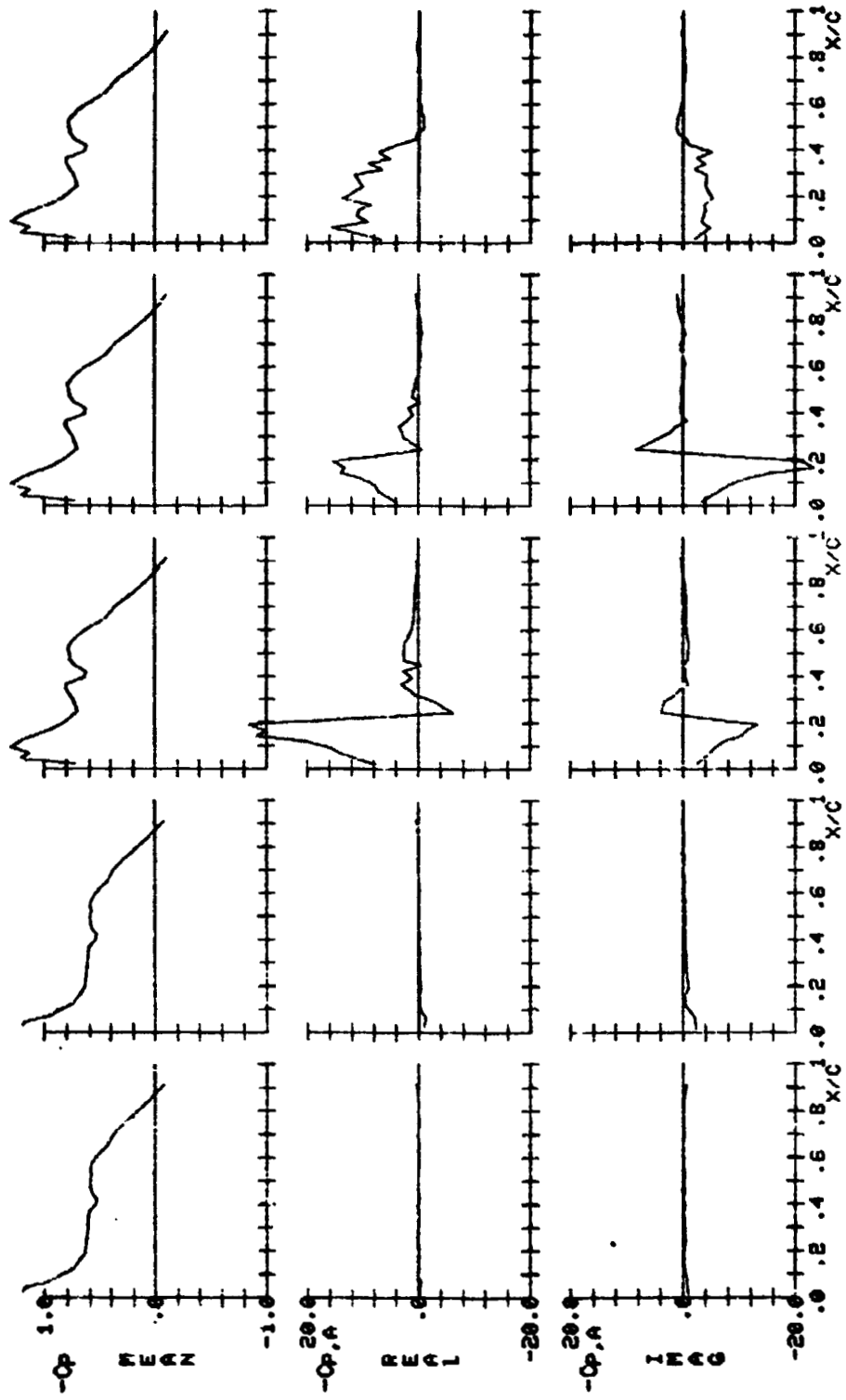
D.I.=166 D.I.=167 D.I.=168 D.I.=169 D.I.=170

Figure 13.- Continued.



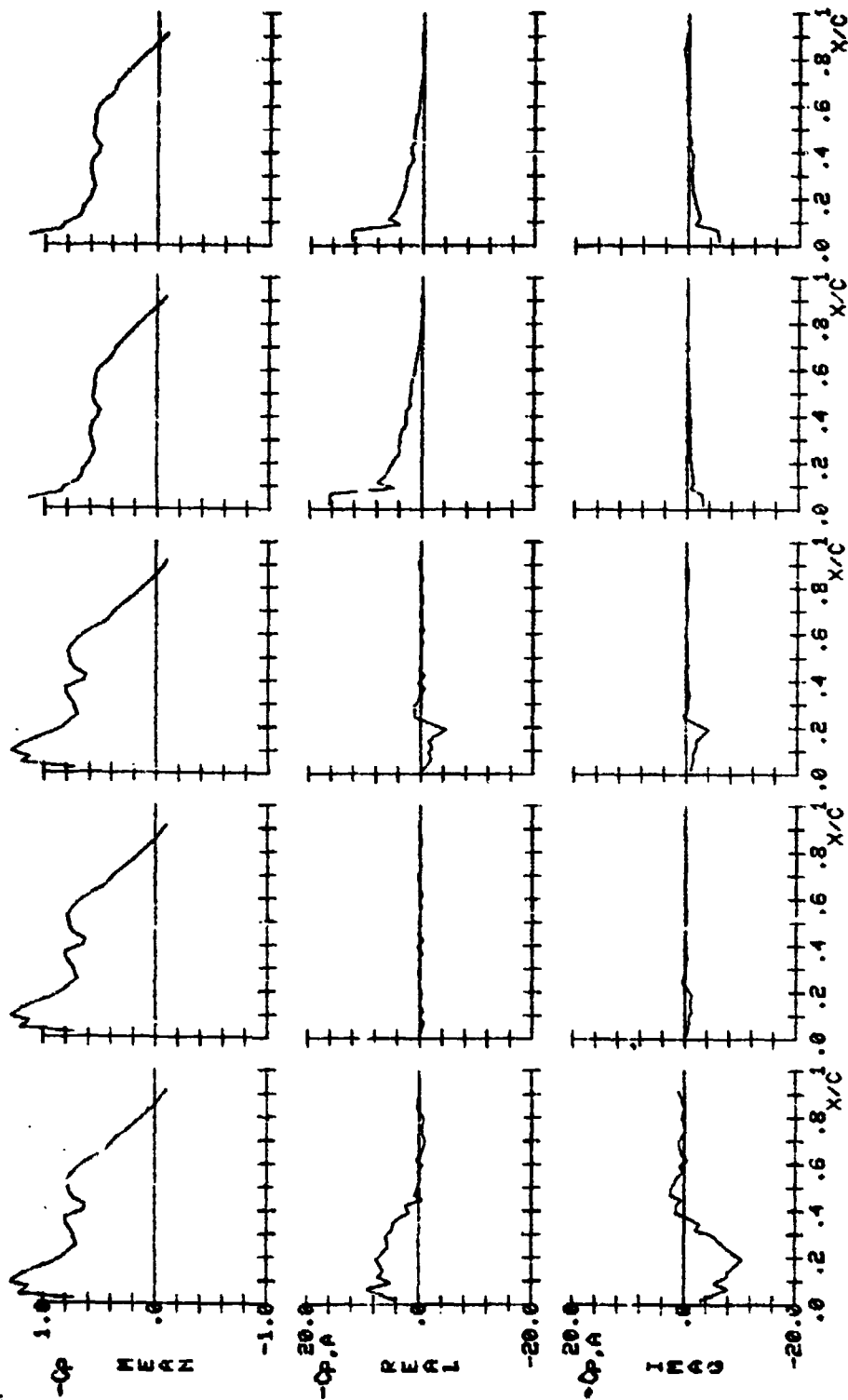
D.I.=171 D.I.=172 D.I.=173 D.I.=174 D.I.=175

Figure 13.- Continued.



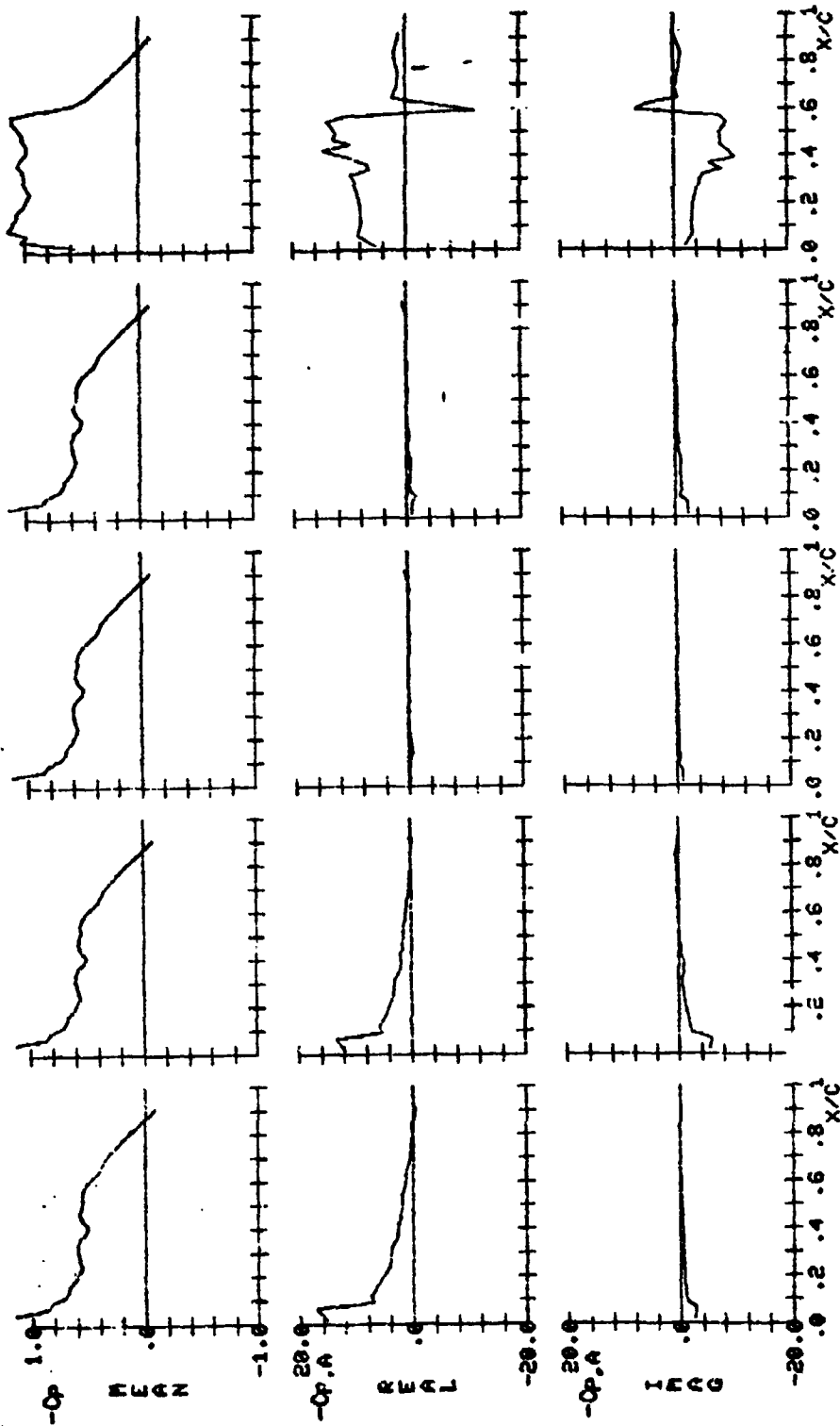
D.I.=176 D.I.=177 D.I.=178 D.I.=179 D.I.=180

Figure 13.- Continued.



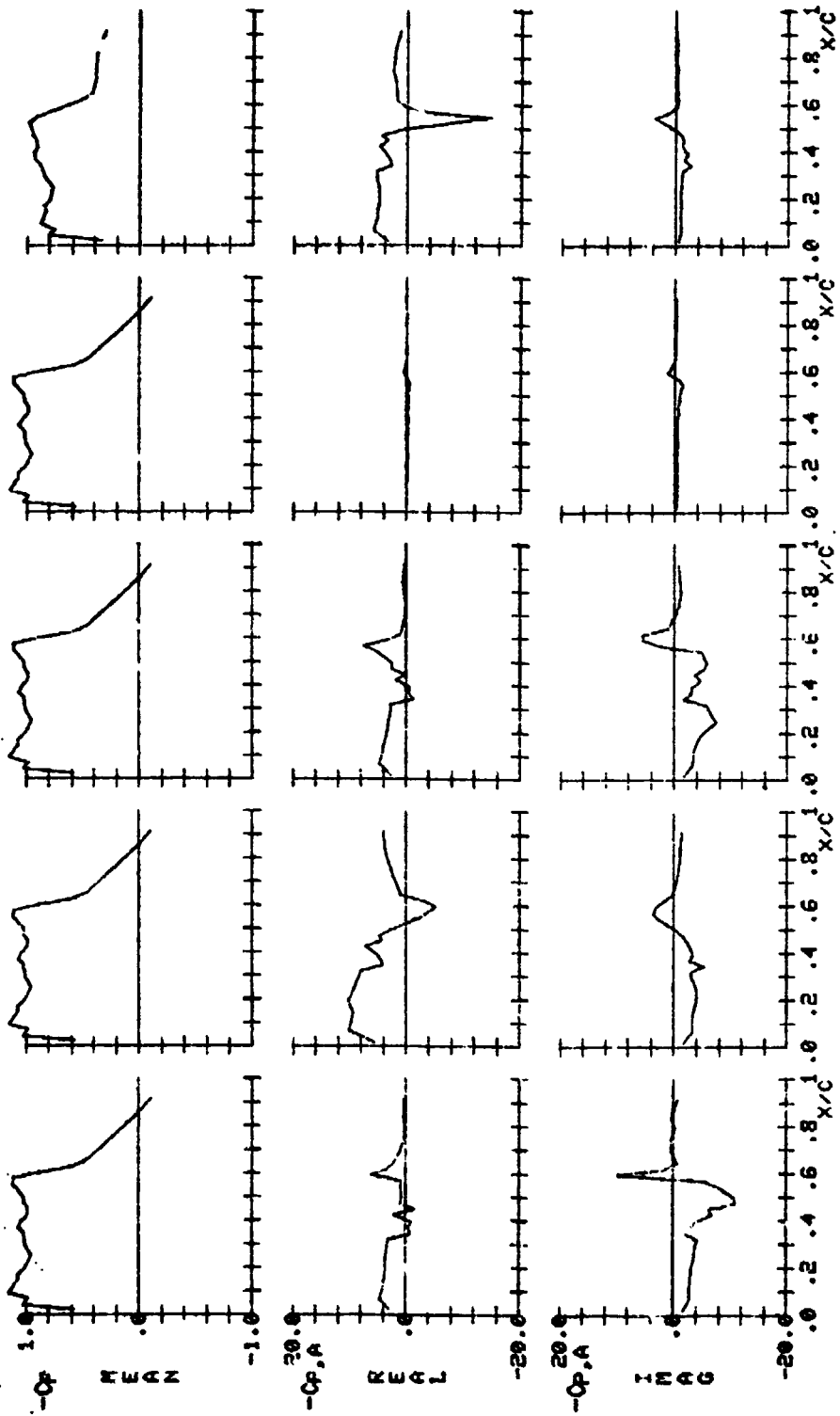
D.I. = 181 D.I. = 182 D.I. = 183 D.I. = 184 D.I. = 185

Figure 13.- Continued.



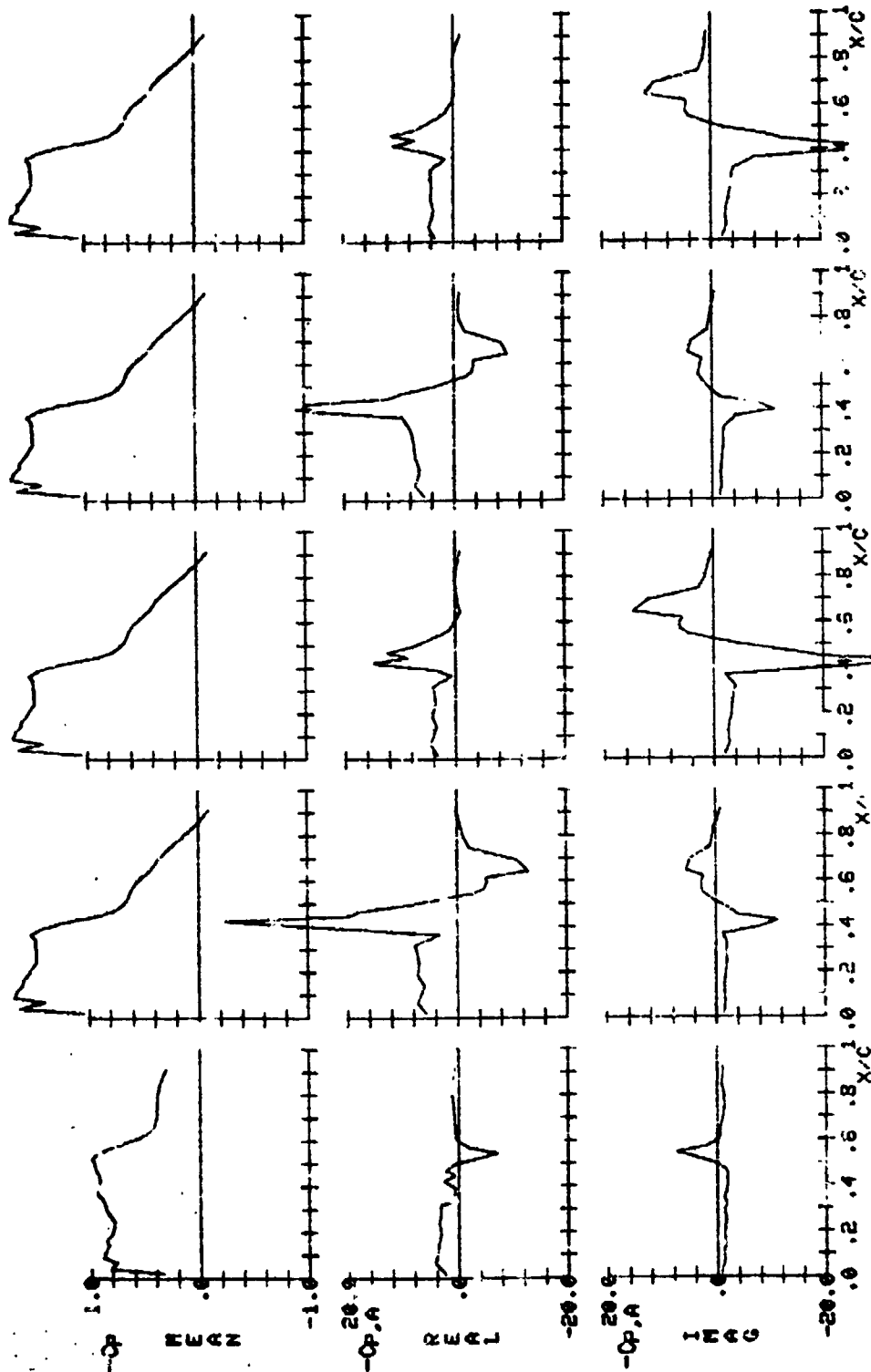
D.I.=186 D.I.=187 D.I.=188 D.I.=189 D.I.=190

Figure 13.- Continued.



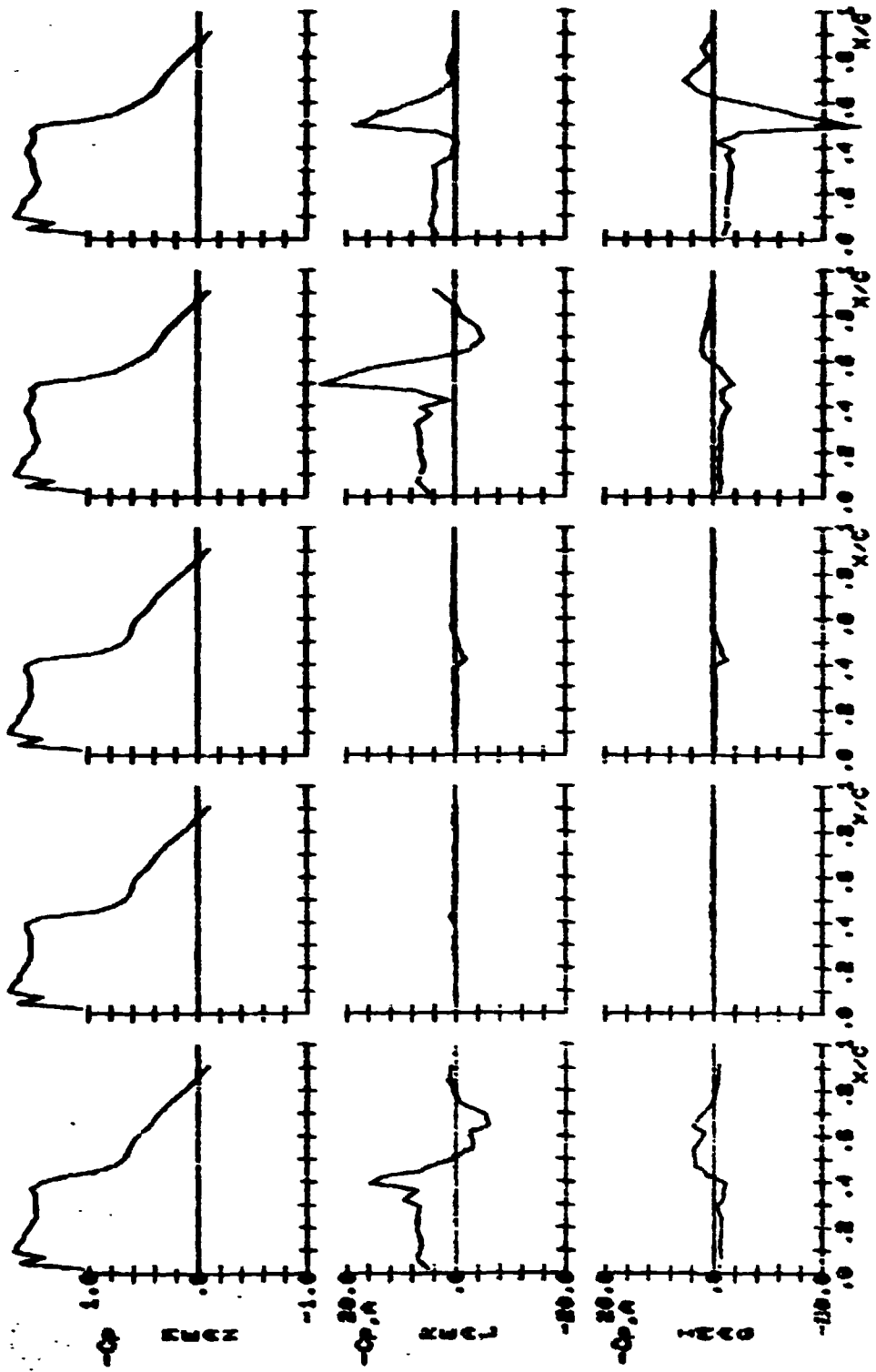
D.I.=191 D.I.=192 D.I.=193 D.I.=194 D.I.=195

Figure 13.- Continued.



D.I.=196 D.I.=197 D.I.=198 D.I.=199 D.I.=200

Figure i3.- Continued.



D.I.-201 D.I.-202 D.I.-203 D.I.-204 D.I.-205

Figure 13.- Concluded.

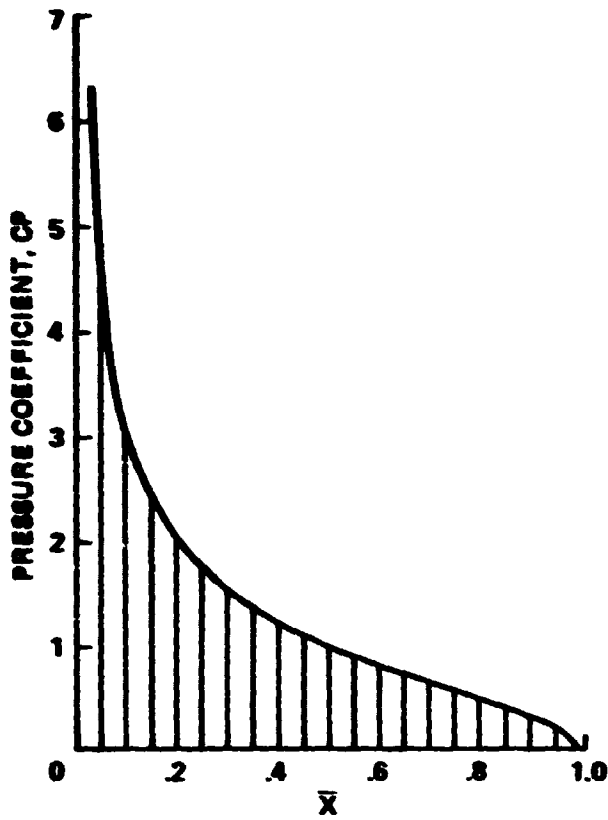


Figure 14.- Numerical integration using trapezoidal rule.

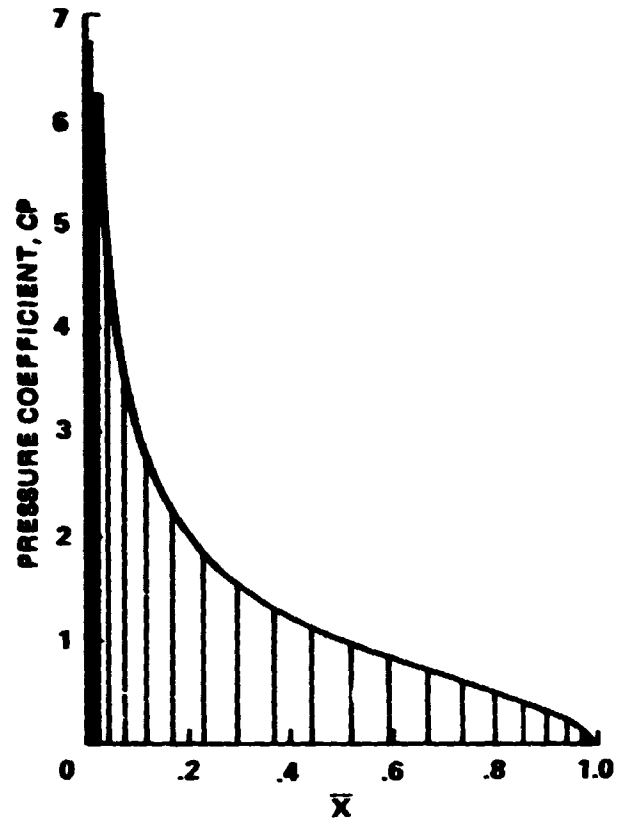


Figure 15.- Numerical integration using Gauss-Jacobi quadrature.

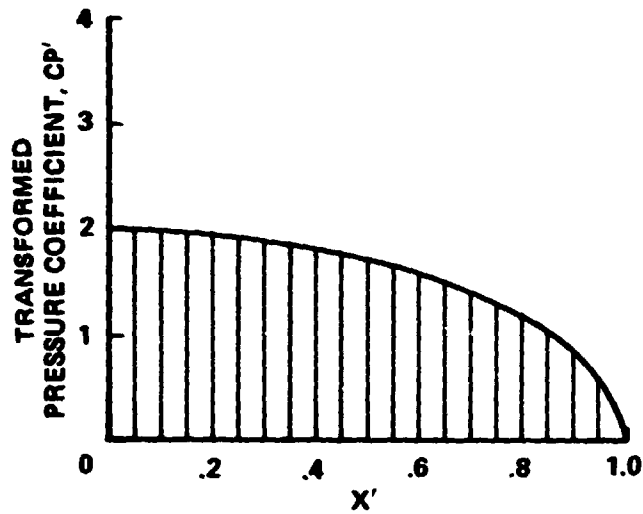


Figure 16.- Numerical integration using transformed variables and trapezoidal rule.